AN ABSTRACT OF THE THESIS OF

LESLIE ALAN BRABY (Name) for the DOCTOR OF PHILOSOPHY (Degree)

in GENERAL SCIENCE (Radiological Physics) (Major Department) presented on 10-1-71 (Date)

TITLE: IONIZATION IN MICROSCOPIC VOLUMES IRRADIATED BY ENERGETIC PHOTONS

Abstract Approved: Redacted for privacy
W. H. Ellett

The energy absorbed by microscopic volumes exposed to ionizing radiation is not well represented by the average dose due to the small number of discrete energy transfers involved. The energy deposited in a microscopic volume can be determined by measuring the ionization in a detector filled with gas at low pressure. A grid-walled spherical proportional counter suitable for making such measurements for photon irradiation is described and compared to a solid-walled counter. Measured ionization distributions are presented for ^{60}Co gamma irradiation, filtered and unfiltered 250 kVp x-rays, and for 65 kVp x-rays. Other distributions which may be of use in understanding radiation damage models are calculated from these measured distributions.

IONIZATION IN MICROSCOPIC VOLUMES IRRADIATED BY ENERGETIC PHOTONS

by

Leslie Alan Braby

A THESIS

submitted to

Oregon State University

in partial fulfillment of
the requirement for the
degree of
Doctor of Philosophy

June 1972

APPROVED:

Redacted for privacy

Associate Professor of General Science in charge of major

Redacted for privacy

Chairman of Department of General Science

Redacted for privacy

Dean of Graduate School

Date thesis is presented 1 October 1971

Typed by Barbara Braby for Leslie Alan Braby

ACKNOWLEDGEMENTS

This work was sponsored by the Office of Naval Research under Contract Number N00014-67-A-0369-006 Task Number NR105-515.

I would like to thank Dr. William H. Ellett for his guidance in this project.

TABLE OF CONTENTS

TABLE OF CONTENTS (Continued)

LIST OF TABLES

LIST OF FIGURES

LIST OF FIGURES (Continued)

LIST OF FIGURES (Continued)

IONIZATION IN MICROSCOPIC VOLUMES IRRADIATED BY ENERGETIC PHOTONS

Chapter 1

INTRODUCTION TO MICRODOSIMETRY

Microdosimetry is the name commonly given to the study of the statistical variation in absorbed energy within very small volumes exposed to ionizing radiation (Rossi, 1968). A study of microdosimetry has become necessary because the concept of absorbed dose involves an averaging operation and ignores differences in the energy absorbed by small sites within a region receiving a given average exposure. These variations can be quite large for sites within the size range of cell nuclei and other cell organelles.

1.1 Dose as an average

Soon after Roentgen discovered x-radiation in 1895 it was realized that this form of energy produced interesting effects in living material. In order to investigate the effects of radiation a technique for quantitizing the amount of radiation was needed. Ionization of a gas was among the early observed effects of x-rays, and was adopted as a means of measuring their quantity (Roesch and Attix, 1968). Originally it seemed adequate to measure radiation in terms of the amount of ionization produced in air, but as radiation's

interactions with matter became better understood it became clear that reference should be made to the amount of radiation absorbed in the particular material of interest. Finally energy was chosen as the quantity in which to express the amount of absorbed radiation, and in 1954 the International Commission on Radiological Units defined the rad, a unit of absorbed dose, in terms of energy absorbed. Specifically,

> "*Absorbed dose* of any ionizing radiation is the amount of energy imparted to matter by ionizing particles per unit mass of irradiated material at the place of interest. It shall be expressed in *rads*." "The *rad* is the unit of absorbed dose and is 100 ergs per gram."

(ICRU, 1954). A later definition (ICRU, 1968) expresses the same thing in terms of a volume element.

When applying this definition there are two problems to be overcome, first the phrase "at the point of interest" implies that a value characteristic of a point is to be found. Thus the "energy imparted" must be averaged over a region large enough that the statistical fluctuations are insignificant, but small enough that the average does not change within the region. It is generally possible to choose a region which makes this averaging possible, but in some problems, such as in the vicinity of the boundary between two different materials, the average is changing so rapidly that it is impossible. The second problem is in the conversion from the measured quantity to absorbed energy. Not even a calorimetric measurement can assure that all of the energy absorbed will be directly detected, some of it may go into endothermic chemical changes instead of heat. In

the case of ionization only about half of the energy goes to forming ions, the remainder going to produce excited states and other changes. A similar situation holds with other radiation detection devices, and a calibration factor is needed for each. In the case of ionization this factor is W, the mean energy per ionization.

1.2 Statistical Nature of Energy Deposition

The vast majority of the energy deposited in material by radiation is transferred through the interaction of fast moving charged particles (electrons, protons, or atomic nuclei) with the electrons of the material. Indirectly ionizing radiations such as photons and neutrons transfer large amounts of energy to charged particles in relatively few interactions and these charged particles then go on to have many interactions with the medium. Under normal circumstances electrons within the medium are randomly arranged with respect to the path of the charged particle. Since the amount of energy transferred by the charged particle to these electrons in a "collision" is a function of the distance between electron and charged particle as well as the particle's type and velocity, it is clear that energy losses by the charged particle will be random in both magnitude and location. The amount of energy transferred may vary from that which will produce only vibrational and rotational excited states to, in the case of two electrons, the transfer of all the energy from one particle to the other. When the energy transfer is greater than the ionization potential of the atomic or molecular orbital involved, an electron

is ejected and an ion is formed. The ejected (secondary) electron moves away from the ion with the difference between the energy transferred and the ionization potential. In many cases this electron has enough energy to ionize other atoms, and a picturesque terminology grew up out of early cloud chamber studies of ionization. Secondary electrons which cause a few additional ionizations in the immediate area are said to produce a cluster, while those with more energy are called delta rays. Classical theory of the collision between a heavy charged particle and a free electron results in the conclusion that the probability of forming a delta ray with energy between E and $E + \delta E$ is proportional to E^{-2}. Within the limits set by relativistic effects the same result is obtained for electron electron interactions. Unfortunately, this theory holds only when E is large compared to the binding energy of the orbital electrons, The information necessary to predict secondary electron spectra at low energies is not available and the approximations which have been used are not in good agreement with experimental results (Toburen and Glass, 1971). In any case the angular distribution of secondary electron paths after their formation cannot be predicted, and the energy loss rates for low energy electrons is poorly known.

The average amount of energy per micron which charged particles transfer to a material varies over a wide range depending on particle type and kinetic energy. For example 10 MeV protons in tissue lost energy at the rate of about 0.045 keV/μg cm^{-2} but have a peak energy loss rate of about 1.1 keV/μg cm^{-2} at about 100 keV (Glass and

Samski, 1967). The peak energy loss rate for electrons is on the order of 0.3 keV/μg cm^{-2} and decreases to about 0.002 at 1 MeV (ICRU, 1970: see also Cole, 1969). Since the value of W is about 0.03 keV we see that the average number of ions per μg cm^{-2} of path ranges from 10 to .06 for electrons. Since a partial ion is not possible, it is clear that high energy electrons will only occasionally form an ion in a layer of material one μg cm^{-2} thick. In thicker layers the number of ions formed will follow a Poisson distribution.

1.3 Ionization in a Small Site

From the above discussion it is clear that the normal definition of dose as a macroscopic quantity cannot be applied to objects with dimensions of a few hundred micrograms cm^{-2} or less (100 μg cm^{-2} equals one micrometer of unit density material) because the number of ionizations may be quite small and the variation in this number consequently large. In addition to statistical variation in the number of ions per unit path length there is also a distribution of path lengths within an isotropically irradiated site. This last factor is complicated by secondary electrons (delta rays) which may or may not leave the site. There are also energy depositions in the site resulting from entry of delta rays produced by particles which do not cross the site. The density function combining all of these factors is here called $f(\Delta)$, the probability of the amount of ionization, Δ, in a site per unit interval of Δ due to an event. An event is defined as the passage of a charged particle and its secondaries through the site.

This charged particle may actually be a delta ray set in motion by another particle. An event does not necessarily result in ionization within the site. In fact ionization within a 10 μg cm^{-2} site crossed by a high energy electron is unlikely. It is sometimes easier to compare energy deposition in sites of various sizes if ionization is normalized by dividing by a characteristic dimension of the site, such as its diameter, b. The quotient Δ/b is then called event size, Y (Rossi, 1968). Because an event of known energy instead of a known number of ionizations is normally used to calibrate a detector it is convenient to express ionization in terms of energy (keV) and event size in terms of energy per unit length, keV/100 μg cm^{-2}, or equivalently, for $\rho = 1$, keV/micron.

In some cases the amount of energy deposited by events of a given ionization (or size) is of interest. This can be found by multiplying the probability of an event $f(\Delta)$, by the energy Δ. This gives the density of energy per interval of ionization $d(\Delta)$. That is, the value of $d(\Delta)$ at Δ gives the fraction of the total energy which will be delivered by events of ionization between Δ and $\Delta + \delta\Delta$.

In some cases it may be reasonable to assume that only events greater than some specific ionization are effective. Then the total number of events greater than a lower limit, as a function of the value of the lower limit is of interest. This is simply one minus the distribution function, $F(\Delta)$. When this is normalized in terms of

number of events greater than Δ per 100 ergs per gram average energy absorbed it is referred to as $\Phi(\Delta)$.

If the effects of successive events in a single site are thought to be cumulative, then the successive foldings of the single event distribution with itself (Biavati, 1964; Roesch, 1969) can be made until the desired dose (or number of events) is reached. The resulting density function is called f(T) and gives the probability of a given site accumulating a total ionization T at a given mean dose (or number of events). When expressed in terms of energy per gram the quantity T becomes Z, the local energy density (Rossi, 1967). Again there are the cumulative distributions $\Psi(T)$ and $\Psi(Z)$ giving the probability of there being an accumulated energy greater than any value of T or Z at the prescribed mean dose or number of events. For the reader's convenience, Table 1.3.1 lists the symbols and nomenclature introduced in this section; details of the calculations are given in Section 5.2.

1.4 Choice of Site Size and Shape

There is some reason to believe that radiation damage to animals is initiated at the cellular or sub-cellular level (Casarett, 1968). That is, the initial effect which eventually leads to an observed end point is in the cell nucleus or other organelle. In fact much of the damage probably originates in the genetic material within the nucleus. These sub-cellular units are generally in the range of sizes where the statistical distributions of energy deposition

Table 1.3.1

NOMENCLATURE AND SYMBOLS

Single Event		Multiple Event	
site diameter	b (in 100 $\mu g/cm^2$)		
ionization	Δ (keV)	accumulated ionization	T (keV)
event size	$Y = \Delta/b$	local energy density	$Z = (30.6/b^2)\ T$
density of single events	$f(\Delta)$	density of accumulated ionization for specificed average energy transfer	$f(T)$
distribution of single events	$F(\Delta) = \int_0^{\Delta} f(\Delta)$		
density of energy	$d(\Delta) = \Delta\ f(\Delta)$		
distribution of energy	$D(\Delta) = \int_0^{\Delta} d(\Delta)$		
event frequency per rad	$\Phi(\Delta) = (b^2/30.6\ \overline{Y}_p)(1-F(\Delta))$	frequency of accumulated ionization	$\Psi(T)$

described above are quite broad, and where differences in the means of the distributions, i.e. the average energy deposited, are likely to be a poor indicator of the differences in shape. Thus it would seem that the determination of the details of these distributions, the field which has come to be known as microdosimetry, might contribute to a better understanding of the biological effect of different radiations.

With this in mind a good deal of work is being done to determine the energy deposition spectra of various radiations in sites of different sizes. A spherical site is normally used since it corresponds roughly to many significant sub-cellular structures, and because it has a particularly simple path length distribution when uniformly illuminated by straight lines. This track length distribution is simply a triangle starting with zero probability at zero length and increasing uniformly to maximum probability at path lengths equal to the diameter. This characteristic is useful when one is going to attempt to calculate the energy deposition spectrum and wants to compare it with experimental results. It has also been used occasionally to work backwards from the energy deposition spectrum to obtain the track average LET of heavy charged particles (Rossi and Rosenzweig, 1955). Kellerer has shown that the path length distribution is not, for small sites and high energy electrons, a significant consideration since the shape of the distribution is determined almost entirely by the energy loss statistics of the charged particle (Kellerer, 1968). That is, the range of energy losses for a given

path length is so broad that the variation in path length is completely lost as shown in Figure 3.1.5.

Once the site shape has been chosen, sizes to be simulated must be determined. The lower limit is set by the limitations of the detector (Rossi, 1970a). Gas proportional counters are commonly used to simulate small sites but they require a significant thickness of gas for the formation of an electron avalanche. In the usual type of detector this avalanche region is a cylinder through the center of the detector. If the detector is made to simulate too small a site, the volume taken up by the avalanche region becomes significant and the detector loses resolution or is unable to give adequate gas gain. The size at which this becomes important is open to question, but a diameter of 50 $\mu g/cm^2$ is probably safely above it. As site diameters increase the energy deposition spectra gradually become more narrow and approach the average dose. For biological purposes the size of a cell nucleus, about 400 $\mu g/cm^2$, is probably as large as would be of major interest. From a practical standpoint the upper limit of size is commonly set by the highest pressure that can conveniently be controlled and measured.

1.5 Work on Neutrons

Using well developed experimental techniques for microdosimetry (see next section) a number of typical irradiations have been studied by Dr. Rossi's group at Columbia University (Rosenzweig and Rossi, 1959; Biavati, Rossi and Boer, 1965; Rossi, 1969). These

studies and the cataloging of energy deposition spectra have been limited to neutrons and, to a much lesser extent, ^{60}Co primarily because of experimental limitations. For neutrons typical f(Y) and $\Phi(Y)$ distributions are available, and a good deal of work has gone into determining the biological significance of distributions of the type shown in Figure 1.5.1 and 2. Simultaneously other investigators have been working towards theories of energy deposition by charged particles which would allow the prediction of energy transfer distributions for various site sizes including those too small to be approached experimentally, (hopefully down to the size of macromolecules). This theoretical work has been limited primarily to heavy charged particles and to ^{60}Co gamma rays because of the lack of knowledge about the behavior of low energy electrons (Roesch and Glass, 1969; Kellerer, 1968, 1970; Berger, 1970).

The biological interpretation of microdosimetric distributions depends on the model of radiation effect it is used with. In the common hit theory models there is a parameter, k, which is defined as the probability of a hit per unit dose. In models which have a simple exponential part to the survival curve, this K is numerically equal to $1/D_{37}$. If some minimum effective energy deposition is assumed for the biological effect then $\Phi(Y)$ is equivalent to k where the value Y corresponds to that minimum energy. Rossi has applied this method to investigation of neutron induced mutation in maize seed with reasonable success (Rossi, 1969), but has found it inadequate to explain other effects such as the induction of lens opacifi-

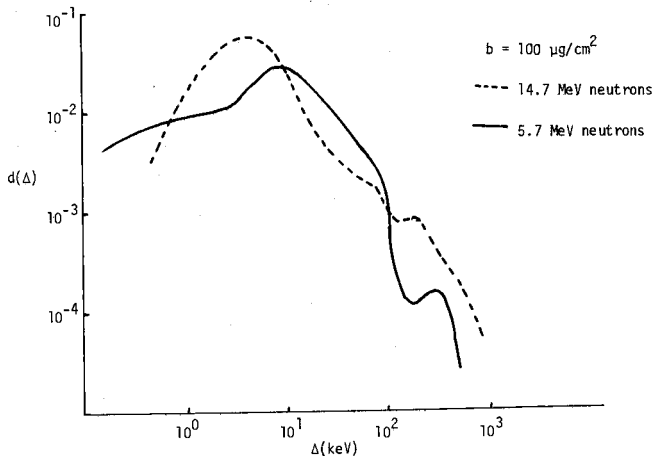

Figure 1.5.1 Typical density of energy from single events as a fraction of ionization for neutrons (Biavati, Rossi and Boer, 1965)

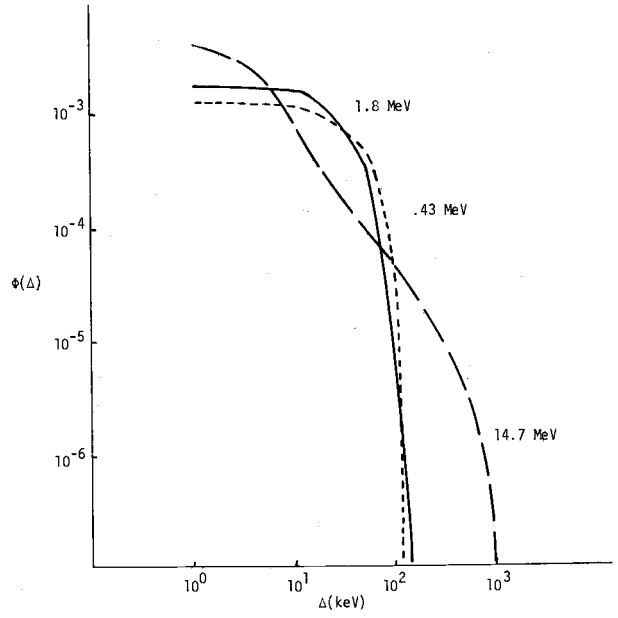

Figure 1.5.2 Typical event frequencies per rad for neutrons (Biavati, Rossi, and Boer, 1965)

cations in mice (Rossi, 1968b). Efforts to understand the effects of high and low LET irradiation in terms of a single initial effect are leading to new mathematical models which may be partially tested with microdosimetry data (Rossi, 1970b).

1.6 Motivation for This Investigation

A large fraction of the cellular radiation biology experimental work which has been done utilizes ^{60}Co gamma irradiation or x-rays between 200 and 300 kVp. These radiations also play a key part in the concept of relative biological effectiveness of other radiations since they serve as the reference radiation in most cases. This last fact alone makes it desirable to obtain microdosimetry data for x and gamma irradiation. It is expected that microdosimetry data will help in understanding the effects of high LET radiations. Since it is hoped that the RBE of various radiations will provide information useful in determining the mechanisms of radiation damage, the microdosimetry data for low LET radiations presented in this report should be of interest.

There is additional interest in the microdosimetry of low LET radiations because of the differences and similarities in biological effectiveness of these radiations. In order to use this type of data to predict biological effect in detail, it would be necessary to have an accurate model of the mechanisms which produce the biological effect. Presently available models, hit theory, etc., probably cannot do this, but they may provide a framework for some qualitative predic-

tions of the effectiveness of various irradiations. That is, the results presented here may be used with current models to make limited predictions about the relative effectiveness of various radiations. Probably a more important factor is that observed differences between biological effect and predictions based on present models and microdosimetry data will provide some of the clues necessary to improve the biological models.

The research described here was directed toward obtaining the microdosimetric data on low LET radiations necessary for physical and biological comparisons of the type discussed above.

Chapter 2

EXPERIMENTAL MICRODOSIMETRY TECHNIQUE

The investigation of the distribution of energy absorption in microscopic sites, which has come to be known as microdosimetry, is a relatively new field of endeavor. The basic technique for making measurements in simulated microscopic volumes has been worked out, but it presents experimental requirements which have not yet been fully met. The basis of this technique, the experimental requirements, and the general ways they can be met will be described here.

2.1 Simulating a Microscopic Site

Variations in energy absorption between individual sites is expected to be a major factor in determining the damage to biological entities ranging from a few microns down to hundredths of microns in diameter. It is difficult to visualize radiation detection devices being built in this size range. For this reason a technique for simulating small sites was developed. This technique, which utilizes the low density of a gas at low pressure will be described in this section.

Rossi and co-workers (Rosenzweig and Rossi, 1955; Rossi, 1967) have led in the development of a technique for experimentally determining the distribution of energy absorption events in microscopic

sites. Their method is based on replacing the microscopic site in unit density material with one several orders of magnitude larger in linear dimensions, but with correspondingly lower density. A spherical cavity 5 cm in diameter filled with a gas at around 20 torr will have a diameter of about 200 $\mu g/cm^2$, equivalent to two microns in unit density material. One type of radiation detector which can take advantage of this is the gas filled "tissue equivalent" (T.E.) proportional counter with T.E. plastic walls.

Before using a decrease in density to simulate small sites, one must first consider the effect of this change on the absorbed dose. Assuming that the mass stopping power $dE/\rho dx$ for charged particles is the same in the gaseous and solid states, Fano has shown that the average energy absorbed from charged particles per gram is independent of the density of the absorbing material of uniform atomic composition (Fano, 1954). For most detectors the assumption that $dE/\rho dx$ is the same for the gas and the wall is not strictly true for two reasons; differences in atomic composition and polarization effects. Because of the influence of the bulk properties of the medium, such as the dielectric constant, on the collision process the $dE/\rho dx$ is reduced in a solid as compared to a gas by an amount that increases with particle energy. However, for electrons at 1 MeV this effect is less than 3% in carbon (Berger and Seltzer, 1964) and is generally ignored (Roesch and Attix, 1968). This is particularly justified for ^{60}Co gamma rays and lower energy photons since the electron spectra which they produce are heavily weighted below half an MeV.

It is difficult to find mixtures of gases which have the same atomic composition as the solid material used in the detector wall. For this reason a mixture whose calculated stopping power matches that of the solid to within a few percent over the energy range of interest is chosen for most dosimetry applications. Thus, "tissue equivalent" gas mixtures containing 32.4% CO_2, 3.25% N_2, and 64.4% CH_4; or 39.6% CO_2, 5.4% N_2, and 55% C_2H_6 (Srdoc, 1970) are commonly used with a T.E. plastic consisting of 13.5% carbon black, 52.1% polyethylene, 28.22% nylon, 2.2% silica, and 4% calcium flouride (Shonka, Rose and Failla, 1958).

For the simulation of a small site by a gas-filled cavity to be useful, the distribution of energy absorption events in the cavity and the solid must be the same. If a small sphere (or other shape) is simulated by one of D times its dimensions and 1/D times its density (resulting in the same dimensions expressed in $\mu g/cm^2$) the volume of the replacement will be D^3 times that of the original. The mass of the sphere and, therefore, the total energy absorbed is equal to the density times the volume. Thus the simulated site absorbs D^2 times the energy that the original would have absorbed. The number of charged particles crossing the detector per unit time at a given flux is proportional to the cross sectional area of the detector, thus the number of events in the simulated site will be D^2 times the number in the original small site. Since the number of events and the total energy increase by the same factor it is logical to conclude that the energy per event is not changed by changing the site size and density.

It will be shown later, however, that in detectors having a solid wall, finite time resolution distorts the observed distribution of pulses.

2.2 Application of the Solid-Walled Proportional Counter

Simulation of the small site as described above is convenient in that gas at pressures of a few torr in a strong electric field will support a Townsend avalanche for which the final number of ions is proportional to, but many times greater than, the number of ions that started the avalanche. Thus the site itself can be used as a proportional counter (Rather, 1964). Customarily a smooth round wire (anode), stretched along the center of the detector, is held at a positive potential with respect at the wall. The electric field strong enough for gas multiplication is limited to a small cylinder around the wire. Gas gain depends on characteristics of the gas as well as its density and the strength and extent of the electric field. Typically with a 0.013 cm diameter wire in propane at about 14 torr a gas gain of over 2000 can be obtained.

The prime requirements for a good detector are that it collect all of the electrons formed in the prescribed volume, and that the gas multiplication be the same for all electrons irrespective of where they originate within that volume. The first requirement is easily met in a spherical volume with a collecting structure along a diameter. There are no regions which are shielded from the electric field, and at low pressures only a few volts per centimeter are necessary for ion collection (Loeb, 1955). The second requirement is more difficult.

In a sample sphere and wire arrangement the electric field would change rapidly with the distance along the anode since the distance between wall and anode decreases as one goes to the ends of the anode. The electric field and the gas gain are, therefore, much greater at the ends of the anode than at the center. Detectors designed by Rossi's group overcome this problem by surrounding the anode with a spring-like helical electrode which is at the same distance from the anode along its entire length (Figure 2.2.1). Gas multiplication is controlled by the potential difference between this helix and the anode so the gas multiplication is constant over the length of the anode. Performance of such a detector is usually checked to assure uniform gain by one or more of the following tests: by putting beams of densely ionizing particles through the detector at various points and comparing pulse height with calculated path length, by exposing the detector to monoenergetic events (photoelectric absorption of low energy photons) since gain variations will show up as poor resolution, and finally, by producing single ions or small groups of ions at various points within the detector and comparing resulting pulse heights so that the gain for electrons originating at various locations can be compared directly.

Because the helical grid structure is somewhat delicate and subject to microphonic noise, a number of people have tested detectors employing other means to get uniform gas multiplication. Several of these, including those employing field shaping electrodes at the ends of the anode have been successful (Srdoc, 1970a).

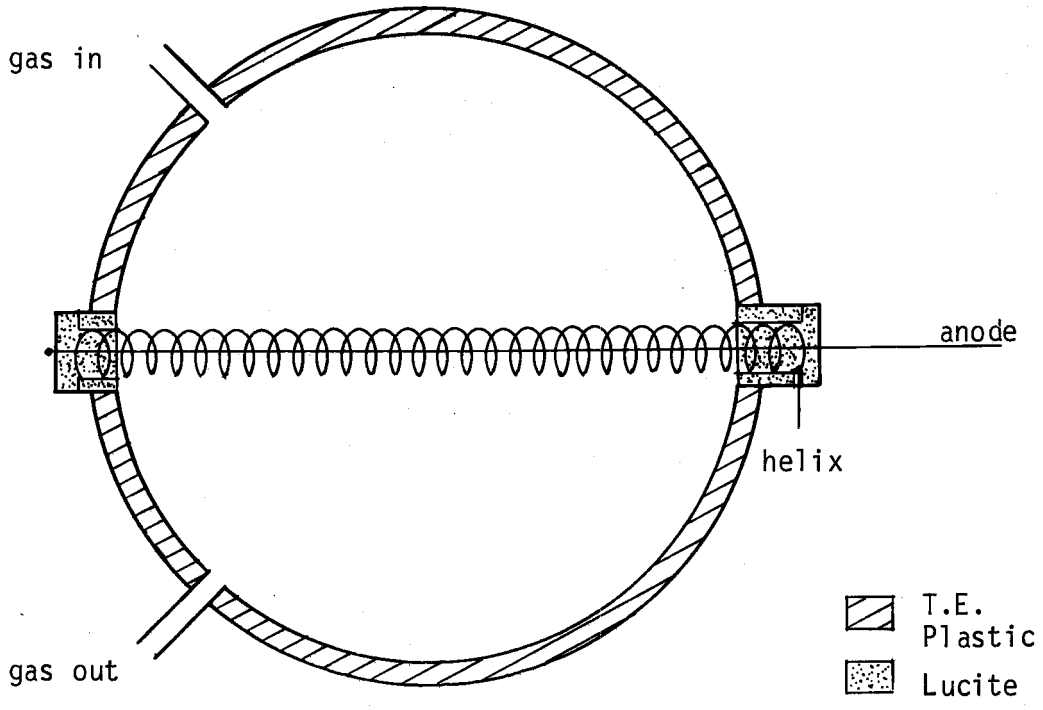

Figure 2.2.1 Schematic of a solid-walled spherical proportional counter with helical grid.

Another successful type has the spherical wall divided into segments by insulating planes perpendicular to the anode. Each of the segments is held at a potential which results in a uniform electric field along the anode (Braby, 1968). A modification of this arrangement which results in a "wall-less" detector is described in detail in Section 3.1.

2.3 Nature of the Wall Effect

Solid-walled detectors of the general type described above have been used to catalog the energy deposition spectra for neutrons and, to some extent, for gamma rays (Rossi, 1967). However, there is a problem which casts doubt on the accuracy of the results of such a detector, especially for photon irradiation. This problem is referred to as the wall effect since the presence of the solid wall at the detector boundary results in a distortion of the spectrum.

The wall effect occurs when some events which would be statistically independent in a site within a uniform medium occur almost simultaneously in the detector. These simultaneous events result from the difference in the curvature of the charged particle tracks in the gas and the more dense material making up the boundary of the detector volume. In Figure 2.3.1 part A, three types of charged particle tracks which can contribute to the wall effect are schematically represented as they cross four small sites in unit density material. The three types of tracks shown are back-scattered tracks, tracks including high energy delta rays, and V-shaped tracks from

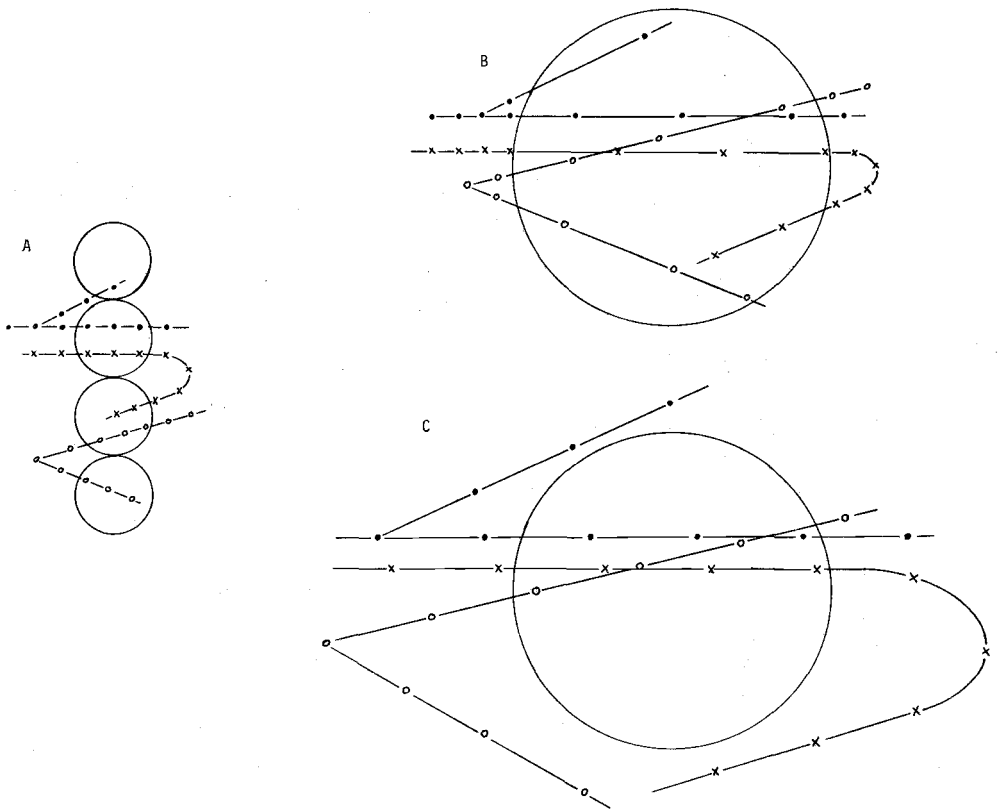

Figure 2.3.1 Schematic representation of the wall effect for delta rays (-•——•-), back-scattered tracks (-x——x-), and spallation events (-o——o-); A, in a uniform medium $\rho = 1$, B, in a cavity having $\rho = .25$, C, in a uniform medium having $\rho = .25$ (distance between points represents average spacing of ionizations).

pair production or spallation events. In part B of the figure the small sites in unit density material are simulated by a larger cavity of density 1/4 surrounded by a unit density medium. Since the figure is in two dimensions, the low density site has D times the cross section (for tracks in the plane of the paper) of the unit density site and can be thought of as representing D times as many unit density sites, i.e. 4. Comparing parts A and B of Figure 2.3.1 one can see that the change in density results in multiple segments of the same tracks occurring within the site in B, whereas in A, where the density is uniform, these segments occur in separate sites. Part C of the figure shows the same set of tracks drawn to the same scale in a uniform medium of low density. In this case the coincident events do not occur because the track curving, branching, etc. occurs in the same ratio as the increase in detector size.

Soon after the nature of the wall effect was realized (Rossi, 1967), it was deduced that for heavy charged particles, curvature and re-entry into the detector is quite unlikely. Furthermore, spallation events occur only with very high energy irradiation. Therefore, for neutron irradiation at normal energies delta rays would be the primary source of multiple events. It was assumed that the fraction of the total energy deposited by delta rays would be small enough that the spectra would not be significantly distorted. Thus, it seemed reasonable to proceed with neutron measurements with a solid-walled detector. On the other hand, electrons are frequently back scattered making the curved track wall effect important for photon irradiations.

Kellerer (1971a, 1971b) has recently worked out a semi quantitative description of the wall effect based on the fractions of the total path length which falls into the various groups, original, scattered, delta ray, etc. His treatment is not exact, but is intended to give a qualitative description of the wall effect and estimates of the fraction of the number of tracks which would be effected. His results indicate that for x-ray irradiation, the number of events per unit dose will be reduced 20-30% by a solid wall. Because of the decrease in electron back scattering with increasing energy it is anticipated that the wall effect will be less serious for gamma rays than for x-rays.

The existence of the wall effect was demonstrated (Braby, Roesch and Glass, 1970) by an experiment employing a cylindrical counter operated in a medium containing ^{14}C. The detector was centered in a large container of labeled gas, and was fitted with a partial wall with the same stopping power and specific activity as the gas. After taking a spectrum the wall was removed without changing the gas and another spectrum was taken. This experiment confirmed that a wall effect did occur, but gave no indication of its magnitude. Srdoc looked for the wall effect in long cylindrical counters by comparing ^{60}Co energy deposition spectra taken with solid-walled and wall-less chambers (Srdoc, 1970b). He found no significant difference in the spectra between the two detectors, but this may be due to the unusual path length distribution in a long cylindrical chamber.

2.4 The Wall-Less Boundary

From the above comments it is clear that in order to be reasonably confident in the results of microdosimetric measurements of photon irradiations, they should be at least checked against measurements made in a way which either eliminates or minimizes the wall effect. The approach developed for this study was to build a "wall-less" detector and operate it inside a large container of gas at low pressure. The major factors which must be considered when doing this are the relative sizes of the detector and the container, the nature of the counting gas and, of course, the design of the "wall-less" detector.

In order for a detector to be truly wall-less it must not only be free of solid material itself, but the walls of the container in which it is housed must be farther removed than the range of the most energetic charged particle. This is clearly impractical in many cases. A more practical requirement is that the solid wall be far enough away that it results in an insignificant increase in multiple events in the detector. In the case of back scatter of electrons it is clear that few will be coming back directly along their own paths, and that if the detector is several times its diameter from the wall it is not very likely to be crossed by the same particle twice. A number of estimates as to the minimum adequate ratio of the diameters have been made (Wilson, 1970; Kellerer, 1971a), but all have been quite uncertain. It appears that a ratio of chamber diameter to detector diameter between 4 and 10 should be adequate. This corre-

sponds to the detector subtending solid angles of $\pi/16$ and $\pi/100$ steradians respectively from a point on the wall.

In most detectors the counting gas needs to be matched to the wall only in terms of stopping power. However, in the case of a wall-less detector exposed to low energy photons, the photoelectric effect in the gas may be a significant source of electrons. If the photoelectric cross section of the gas and wall are not the same, the electron spectrum in the detector will be distorted due to the difference in electron production at different distances. The magnitude of this effect (and consequently how well things must be matched) cannot easily be predicted, but a particular wall and gas combination can be tested experimentally as will be shown below.

A wall-less detector must provide certain basic functions and still keep the fraction of its surface composed of solid material to a minimum. First of all it must provide a smooth boundary around the desired shape, usually spherical. There must be an adequate electric field everywhere inside this volume to collect ions without recombination. There must be an electric field outside the boundary which will sweep away the ions formed in that region before they have time to drift, by thermal diffusion, across the boundary and into the detector. On the other hand, this sweeping field should be no stronger than necessary since it may distort the paths of low energy electrons and alter the energy deposition spectra. In addition, the region of gas multiplication must be carefully controlled to give uniform gain and good energy resolution.

Several different detectors have been designed to meet these requirements. These detectors usually fall into two distinct classes: grid-walled and field line defined. The field defined detectors rely on the configuration of an electric field to determine the volume from which ions will be collected. They generally have the minimum amount of solid surface (as low as a fraction of 1%) since they normally require only two small electrodes to set the shape of the field and provide the region of strong field for multiplication. These electrodes are chosen so that there will be one set of electric field lines that follow a spherical surface. Since ions follow the field lines, those ions formed inside the sphere will remain separated from those formed outside. Guard rings or tubes are positioned around the anode so that field lines outside the spherical surface terminate on the guard rings instead of the anode, thus only ions from inside the spherical volume are detected. The ring and helix detector (Biavati, Gross, Rossi and Kellerer, 1968) and the "Martini" counter (Glass and Braby, 1969) are examples of this type.

The other major class of "wall-less" detector uses a wire or plastic grid to define the boundary of the collecting volume. This grid produces an equal potential surface which separates the electric fields of the proportional counter anode inside the volume and a set of sweeping electrodes outside it. Thus electrons formed inside the grid are multiplied and detected, and those outside are swept away. Gross's (Gross, Rodgers, Rossi and Kitzman, 1970; Gross, 1969)

spherical chamber and a number of cylindrical chambers (Glass, Roesch, and Braby, 1970; Wilson, 1970) are typical of this type.

There are significant problems associated with both of these types of detectors. The biggest problem with field line bounded detectors is in achieving a spherical shape. Shape is easily controlled with grid-walled detectors, but there are a number of difficulties in building a spherical grid. Also, the spaces between grid wires tend to be field free regions where ions drift slowly or recombine. A spherical grid-walled detector requires some means of assuring uniform gain along the anode such as the helix used in a solid-walled detector.

One means, mentioned earlier, of obtaining the uniform electric field necessary for uniform gas gain is to divide the sphere up into successive segments. The electric potential which would exist at the mean diameter of each of these segments is calculated for a cylindrical capacitor with inner and outer electrode diameters equal to the anode and sphere diameters. When each of the segments of the sphere is held at the calculated potential by a voltage divider the electric field near the anode closely resembles that in a cylindrical capacitor. This approach has been tested for a solid-walled detector (Braby, 1968) with good results. It is clear that the segments of the sphere can be replaced by wire rings of the same average radii and the electric field at the anode will be virtually unaffected. In this way the solid wall is replaced by a series of conducting rings. Adding structural support for the rings and anode one obtains a

grid-walled detector of the type illustrated schematically in Figure 2.4.1. A significant difference between this and most grid-walled detectors is that there is an electric field running along the surface of the sphere, from equator toward each pole. This electric field should greatly reduce the field free regions between grid wires, and should thus minimize the possibility of electrons drifting across the boundary. As shown in Figure 2.4.1 extra rings outside the collecting volume are used to sweep away ions formed outside the sphere.

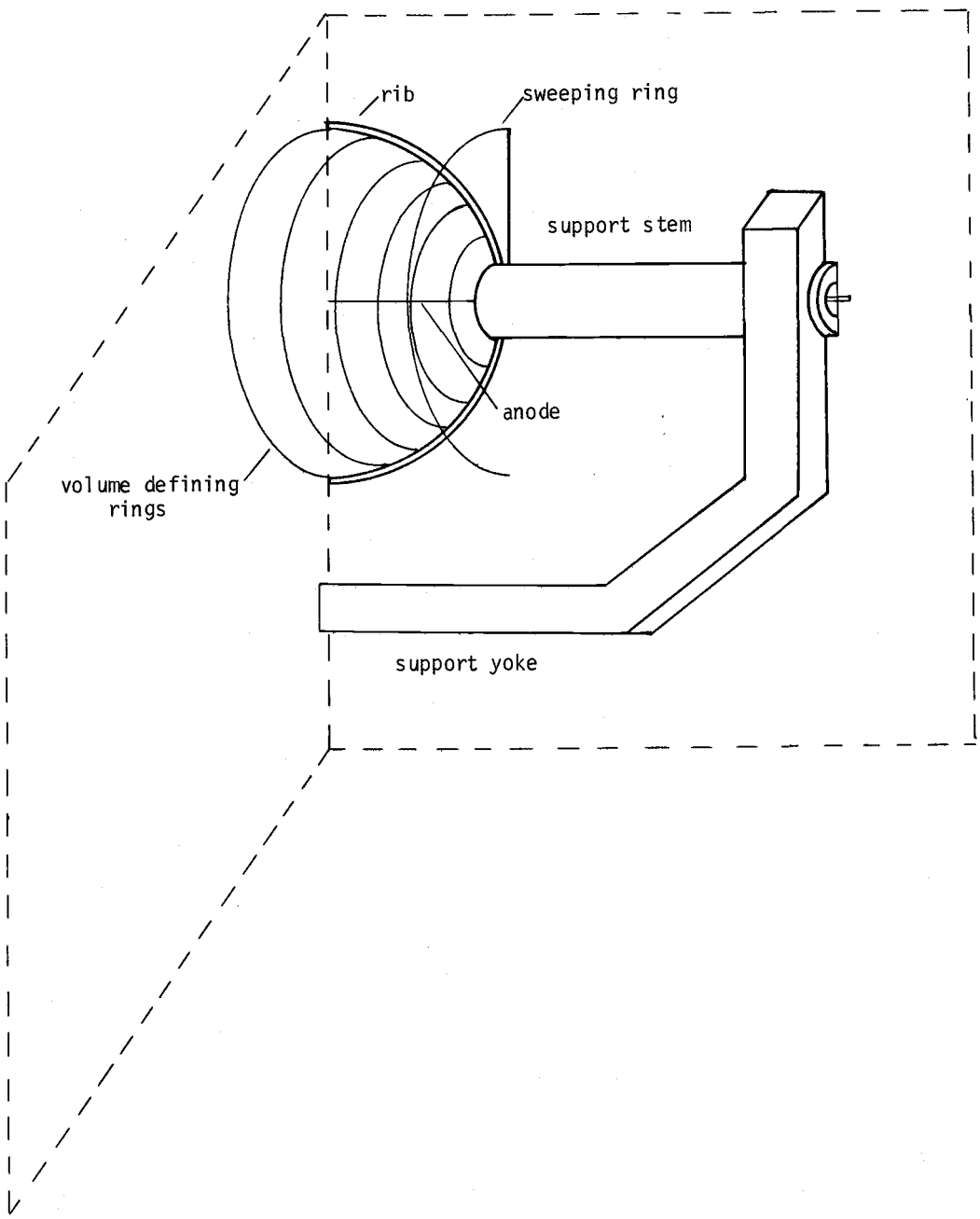

Figure 2.4.1 Schematic drawing of segmented sphere type of grid-walled detector.

Chapter 3

DESIGN AND TESTING OF APPARATUS

In order to measure the energy deposition spectra of photon irradiations a "wall-less" detector of the segmented sphere type was developed. So that the magnitude of the wall effect for various irradiations could also be measured, a solid-walled detector was obtained for comparison. In addition to the detectors, microdosimetry experiments require electronic amplifiers, gas flow apparatus, and radiation sources.

3.1 Grid-Walled Detector

The detector designed for these experiments is 5 cm in diameter. Wire rings outline the sphere and control the electric field at the anode as described in Section 2.4. This detector was designed for use in spherical T.E. plastic containers. Before placing it in the plastic spheres it was thoroughly tested to assure that it collected ions from a truly spherical volume and that it gave all ions equal multiplication. The detector was assembled as two hemispheres. The hemispheres are held together to form a sphere by a "C"-shaped aluminum yoke, as shown in Figure 3.1.1. Each hemisphere consists of eight field shaping rings, seven of them made of 0.037 cm diameter gold-plated annealed kovar wire. The eighth electrode, the smallest,

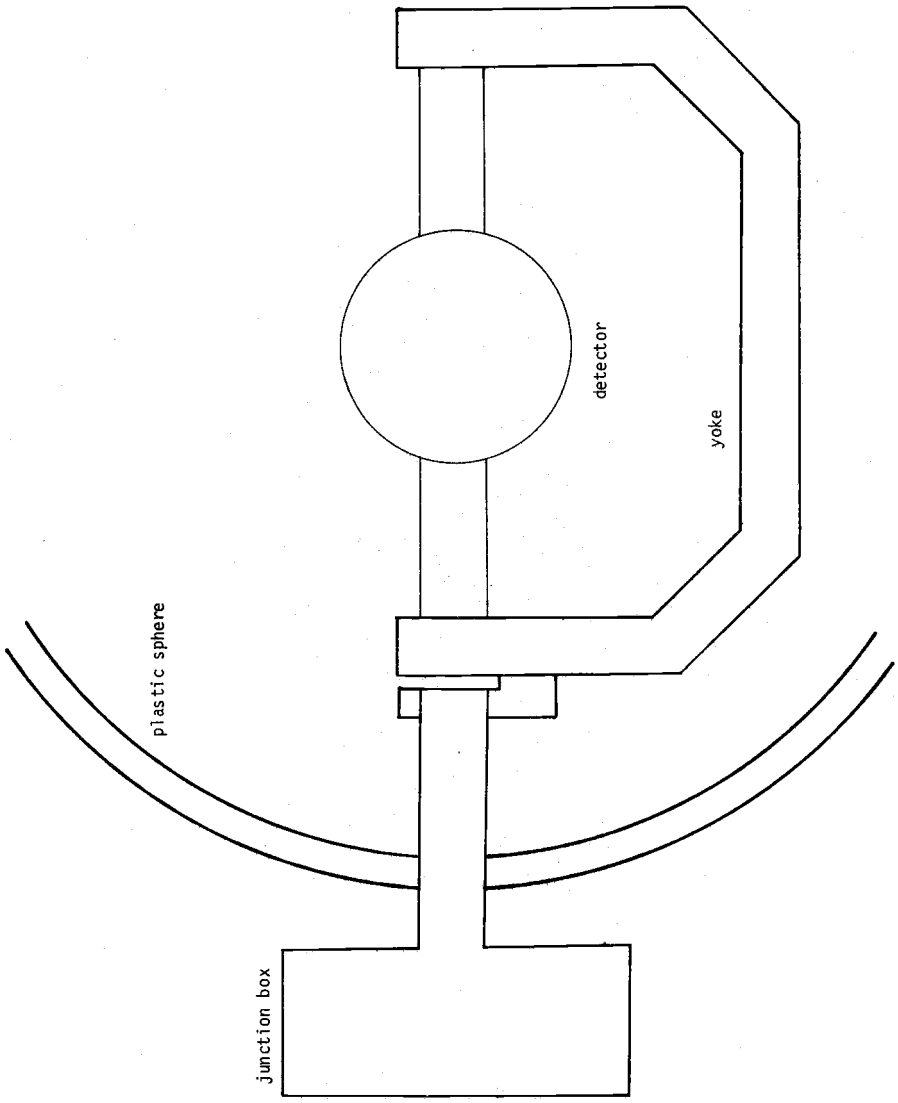

Figure 3.1.1 Grid-walled detector mounted in T. E. plastic sphere

is in the form of a short brass cylinder around the anode insulator. The wire rings are held in position by six lucite ribs 0.16 cm wide by 0.24 cm deep which in turn are supported by a lucite stem 1.75 cm in diameter held by the yoke. "Sweeping" electrodes are in the form of two wire rings, one about 1.8 cm in diameter and the other about 5 cm in diameter, concentric with the stem and 0.3 cm back from each end of the sphere. A 0.0125 cm diameter anode wire was held under spring tension, and is brought out to the end of one of the stems inside a 0.125 cm diameter kovar tube. The hemispheres were assembled by forming the rings on an hemispherical mandrel and then gluing the rib and stem assembly to them.

It is difficult to know just how much of the solid material which makes up this grid-walled detector will contribute to a wall effect. A simple estimate which should be good for comparing various detectors is the fraction of the collecting volume's surface which is covered by solid material. For this detector that is the area of the ends of the support stems plus the width times the length of the ribs plus the diameter times the length of wire used in the rings. These are respectively 6%, 4.8% and 6.2% for the detector described above. Thus, a total of 17% of the surface is made up of solid material.

Design and construction of this detector was somewhat conservative since this was the first detector of the type built. Experience indicates that ribs, rings and structural parts could be scaled down so that the amount of solid material in a detector of this size could be reduced, or a smaller detector could be built. Other methods of

supporting the rings might result in still greater reductions in solid material.

The detector was mounted successively in T.E. plastic spheres of 30 and 20 cm diameter. The same mounting was used in each sphere, with only the removal of adapter sections for the change. The detector was supported by an aluminum tube which ran from the end of the yoke through the wall of the container to a vacuum-tight junction box. This tube also served to bring electrical cables and gas tubes from the detector to feed through connectors in the junction box.

The appropriate potentials for the rings which outline the sphere can easily be calculated. The potential difference across a cylindrical capacitor is

$$V_1 - V_2 = \frac{q}{2\varepsilon_0 l} \ln \frac{r_2}{r_1}$$

where r_2 is the outer radius, that of the cathode; r_1 is the smaller radius, the anode; ε_0 is the permitivity of free space; and q/l is the charge per unit length. The potential difference between the anode and some other cylinder with radius r_x inside this capacitor is

$$V_1 - V_2 = \frac{q}{2\varepsilon_0 l} \ln \frac{r_x}{r_1}$$

Thus,
$$V_1 - V_x = (V_1 - V_2) \frac{\ln \frac{r_x}{r_1}}{\ln \frac{r_2}{r_1}}$$

In designing the detector, radii are chosen which will result in uniform spacings between rings and the fractional potential is

calculated. Then the radius is adjusted slightly if necessary to give a potential which can be obtained easily from a voltage divider.

For this detector ring radii of 2.50, 2.33, 1.96, 1.54, 1.14, 0.845, 0.626, and 0.425 cm were chosen. The corresponding potential between each and the anode is 100, 99, 96, 92, 87, 82, 77 and 77% of the maximum.

The choice of potential on the sweeping rings relative to ground is another matter. It must be optimized experimentally. It is observed that with no voltage on the sweeping rings there is a much higher count rate than expected for a given exposure. Many of these pulses, observed at the peramplifier output, show a very slow rise time. As a sweeping field is applied these slow rising pulses rapidly disappear leaving an unchanged number of fast rising pulses. In addition, it is observed that without the sweeping field many of the fast rising pulses have a slow rising component at the top, and that this too disappears with the addition of a small sweeping field. These slow rising pulses are the result of electrons slowly drifting into the detector and then being picked up and multiplied.

One test of the performance of a wall-less detector is to expose it to a broad parallel beam of alpha radiation. This would result in the triangular chord length distribution modified by straggling and by the entry of delta rays from outside the detector (Glass and Braby, 1969). Thus one expects a distribution with a large tail of small pulses, the delta rays, which rapidly decreases with increasing pulse size. For intermediate size pulses the number

should increase steadily with size, following the track length distribution, but straggling should smear out the sharp drop at the maximum pulse size. Electrons drifting into the detector from outside the spherical volume add to the delta ray tail, and extend it to larger pulse sizes. This proved to be the best test for optimizing the sweeping ring voltage. As the sweeping ring voltage was increased up to about 5/16 of the anode potential the number of small pulses decreased. Above 5/16 of the anode voltage no further change was observed. Thus it is assumed that this voltage is adequate to collect all the electrons formed outside the detector before they can drift into it, and that the remaining small pulses are due to delta rays. For this reason a sweeping ring voltage of 3/8 of the anode voltage was chosen as the normal operating point.

In order to test the detector for resolution and shape of the collecting volume it was set up in a 30 cm diameter vacuum bell jar. The detector was mounted on a slide which could be moved along one axis from outside the vacuum. A Californium source was mounted in a collimator on one end of a U-shaped bracket which crossed under the detector as shown in Figure 3.1.2. On the other end of this bracket was a silicon surface barrier detector masked down so that only about a three millimeter square could detect alphas. This bracket could be moved up and down so that the alpha beam could be made to cross the detector at any desired point. Signals from the solid state detector were used to gate a multi-channel analyzer such that only ionization events resulting from particle tracks which crossed the detector

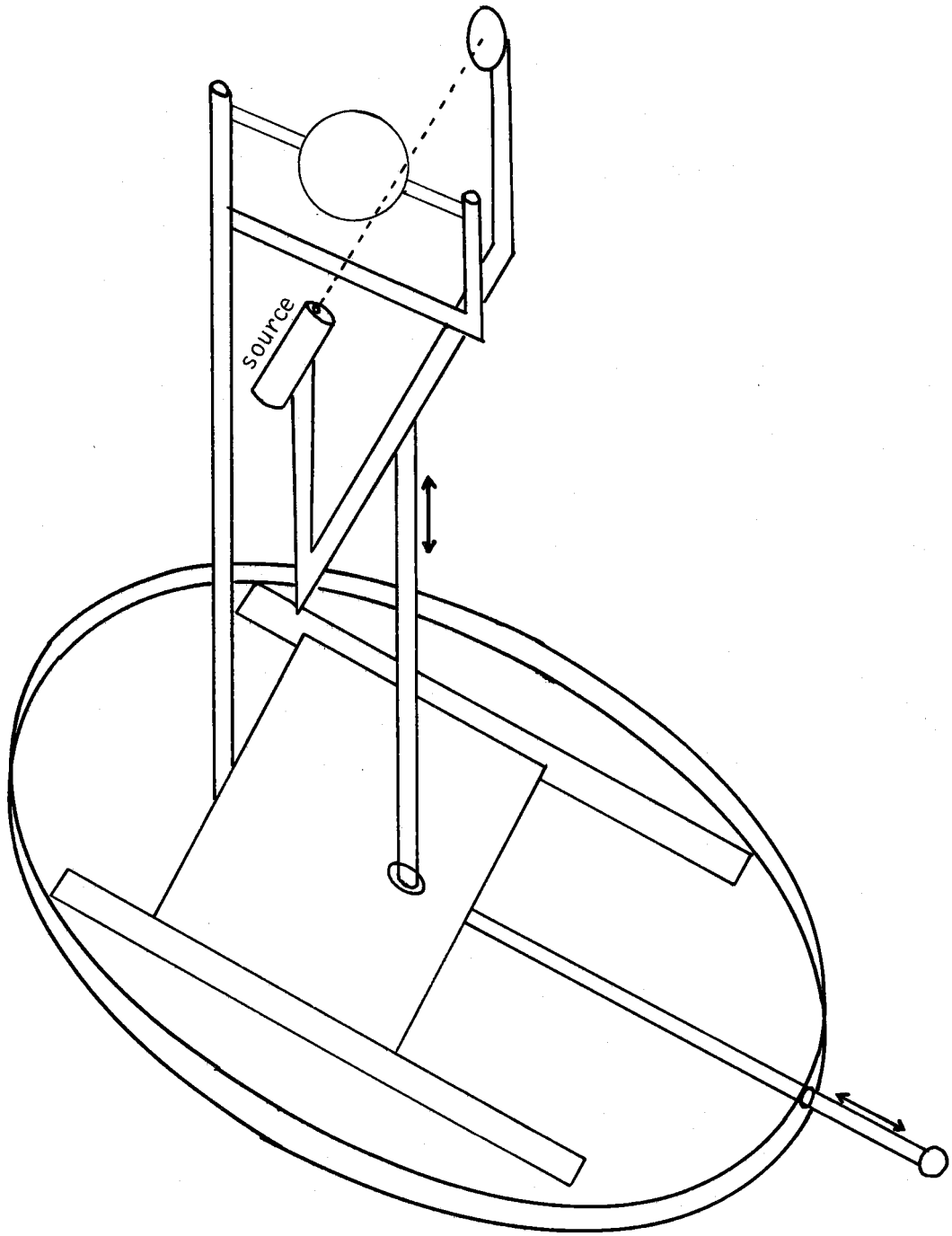

Figure 3.1.2 System for testing shape of a grid-walled detector using collimated alpha particle source

within a small cylinder reaching from the collimator opening to the solid state detector would be analyzed.

This system was used to determine effective chord length in terms of ionization for a number of chords in each of several planes perpendicular to the anode. Since 6 MeV alpha particles follow almost straight paths with nearly constant dE/dx the ionization along each chord is proportional to the actual length of that chord inside the detector. When the resulting pulse heights (actually the mean of the distribution resulting from detector resolution and straggling) are normalized in terms of the pulse height for particles traveling along a diameter, they can be plotted as shown in Figure 3.1.3. The length of the diameter was checked by determining the distance between the points at which the count rate and pulse height fell suddenly as the alpha beam is moved up and down in the detector mid-plane, the edges of the detector. This distance was equal to the physical diameter of the collecting volume, 5 cm. Chord lengths in planes parallel to the anode of the detector were also checked, and are included in Figure 3.1.3. It can be seen that in all cases the measured chord length varies from the expected chord length by no more than the radius of the alpha particle beam, as indicated by the error bars. Thus, though the detector's boundary may be slightly scalloped it is spherical to within plus or minus 6%.

Another requirement for a detector is good resolution. Resolution of this detector was checked with the Mn K_{α} x-ray (5.88 keV) resulting from electron capture decay of ^{55}Fe, and with the combined

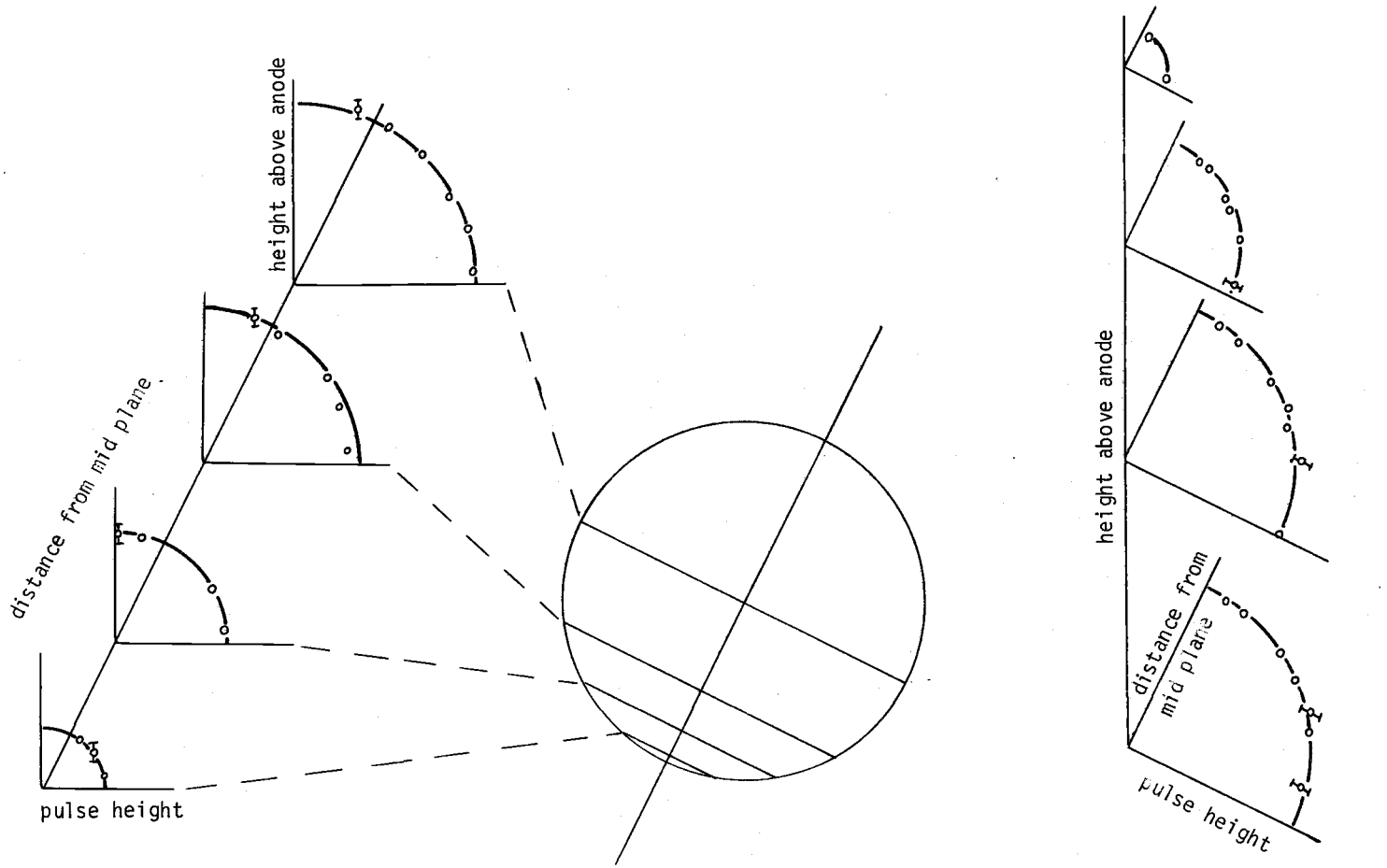

Figure 3.1.3 Effective chord lengths at various positions in the detector; lines represent lengths calculated from detector diameter.

K_α and K_β plus L x-rays and Auger electrons (2.8 keV) from Cl atoms produced in electron capture decay of ^{37}Ar. Resolution of these two peaks is about 14 and 20% full width half maximum, respectively. The resolution decreased a few percent with increasing gas gain as expected (Rossi, 1967). The L line of Cl (200 eV) can also be resolved at high gas gain with about 50% resolution. These resolutions are within a percent or two of those quoted by Rossi (1967) for conventional solid-walled detectors.

Since the detector is operated in a tissue-like plastic container, it would be appropriate to use tissue-like gas. This might be expected to be necessary for two reasons, first in order to match the stopping powers of the wall and gas to satisfy the Bragg-Gray relation, and second, to give equal photoelectric cross sections in wall and gas. This latter factor becomes significant in a wall-less detector exposed to low energy photons since a substantial fraction of the electrons reaching the detector will come from the gas instead of from the wall. A commonly used tissue-equivalent gas consists of 32.4% CO_2, 3.2% N_2 and 64.4% CH_4. Unfortunately, this is not a very good counting gas. The T.E. mixture will not give as great a gas gain before reaching breakdown as will hydrocarbons such as propane at the same density. A mixture of CO_2, N_2 and propane (Srdoc, 1970) gives better gain, but pure propane gives even higher gain. Another consideration in the choice of gas is the large flow rate necessitated by the long piping runs required in the x-ray facility used for this experiment. This would have resulted in consumption of many cylinders

of any T.E. gas mixture since they must be kept in the gas phase. This would not only have been quite expensive, but would introduce some uncertainty in successive measurements since gas mixtures commonly vary 2 or 3% in composition from bottle to bottle.

For the above reasons instrument grade propane was used in these experiments. This is reasonable since the stopping power of propane (calculated by the equation given by Bichsel (1968)) using I = 53 is less than 10% lower than that of muscle (Berger and Seltzer, 1964) from 0.01 to 1.0 MeV. The electron spectrum in the detector will probably be affected only slightly by the mis-match in photoelectric cross sections since the slowing down spectra for electrons of various initial energies are similar (Bruce, Pearson and Freedhoff, 1963). More significant than this is the fact that energy loss straggling rather than charged particle energy or path length distribution controls the energy deposition spectrum. Kellerer (1968) has shown this in the case of ^{60}Co irradiation of a 100 $\mu g/cm^2$ site (Figure 3.1.4) by calculating the energy deposition spectrum ignoring the track length and LET distributions, but including the straggling calculation. This is compared to a spectrum calculated without straggling but including dE/dx and path length distributions, and to the spectrum obtained by including all three factors. He found that there was no major difference in the spectra when just straggling or all three factors were considered, but when straggling is ignored, the spectrum is changed drastically.

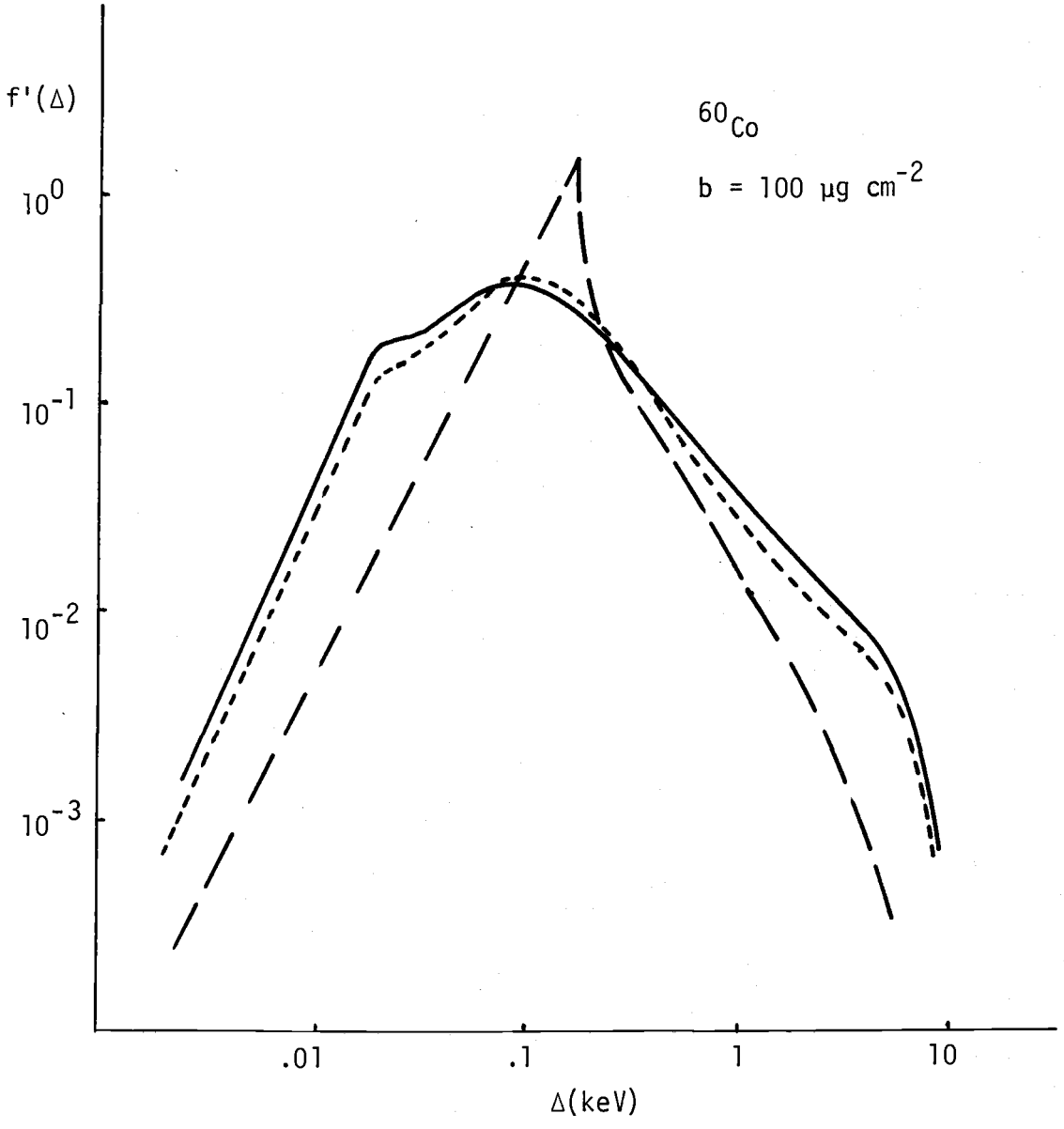

Figure 3.1.4 Calculated f'(Δ) distribution for ^{60}Co including straggling but not path length or dE/dx variations -----, including path length and dE/dx but not straggling — —, and including all three factors ——— (Kellerer, 1969).

To further assure that the use of propane as a counting gas was not distorting the results, it was compared experimentally with the methane T.E. gas mixture. The comparison was made for 65 kVp irradiation since the difference in photoelectric cross sections of the two gases would be greater than for the other radiations used in these experiments. Figure 3.1.5 shows $N(\Delta)$ spectra for the detector filled with propane and with the T.E. mixture. The only significant difference is in the number of small events which results from the poorer gas gain with the T.E. mixture. If the anode voltage is increased to the point where the same gain is obtained (not always possible because of breakdown) detector operation appears to be in a region of limited proportionality with an extreme loss of resolution.

3.2 Solid-Walled Detector

In order to compare spectra in wall-less and solid-walled detectors a commercially manufactured solid-walled proportional counter was used. This detector is basically an EGG model IC-13 LET chamber which employs a helical grid design very similar to that used by Rossi. This 5.72 cm diameter T.E. plastic sphere detector was modified for use with x-ray irradiation. These factory modifications included replacing the original aluminum vacuum chamber with one of lucite, installation of a ^{55}Fe calibration source, gas connections for continuous flow, and external connections to both the helix and the anode with a minimum of stray capacitance. The input section of the

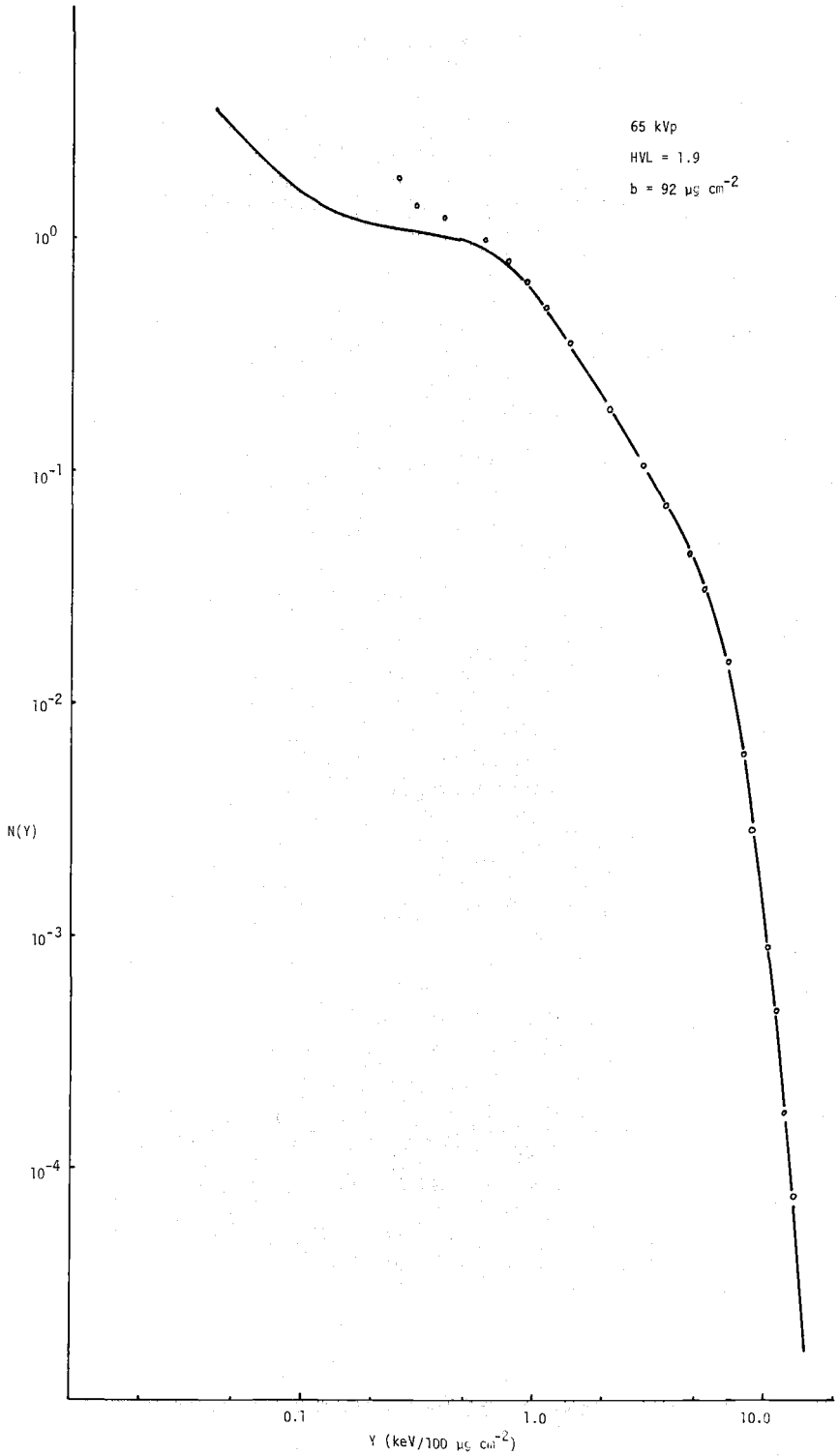

Figure 3.1.5 N(Y) distribution for 65 kVp x-ray taken with T.E. gas (o o) and propane (———).

preamplifier was screwed directly to the aluminum bulkhead of this detector and the signal connection was made without any intervening connectors or cable.

The ^{55}Fe calibration source in this detector is mounted quite near the opening into the sphere. The source emits not only photons, but also Auger electrons and photoelectrons from interactions in the source backing. Some of these electrons enter the collection volume along with the 5.9 keV x-rays. Since the electrons have passed through about 2 cm of gas they are not monoenergetic when they enter the detector. In fact their energy deposition spectrum is continuous from zero up to almost 5.9 keV. Because the thickness of the site in mass per unit area is so small and the atomic number of propane is so low, the number of photoelectric events inside the sphere is relatively small compared to the number of electrons coming from the source. The result is that for most site sizes the photoelectric peak is buried under the electron distribution. Above about 400 $\mu g/cm^2$ the gas thickness between the source and the entrance to the detector is great enough that most of the electrons are stopped, and this source can be used for calibration. At smaller site sizes a trace of ^{37}Ar in the counting gas is used for calibrations.

Since this detector is a standard design which has been used successfully by many people, the only testing necessary was to check on resolution and noise (which would indicate problems with the FET in the preamplifier). Resolution with this detector is about 18 to

20% full width half maximum, for the 2.8 keV ^{37}Ar line with the site sizes and gas gains used in these experiments.

3.3 Electronics

One of the major problems in applying microdosimetry to x-ray and gamma irradiations has been in obtaining an electronic system with low enough noise. Since a significant part of the dose delivered by electrons is in the form of small events (low numbers of ionizations), especially in small size sites, it is desirable to be able to resolve from the system noise events of one ion pair. Assuming gas gain of 1000 this means that we would like to resolve a pulse of 1000 electrons. By setting a discriminator at 5.5 times the RMS noise of an amplifier system, the background count rate can be reduced to about one count per second (Fairstein and Hahn, 1965). Thus an electronic noise level of 180 electrons RMS is required. A very good charge sensitive preamplifier with field effect transistor input will have a noise level of about 100 RMS electrons with no added input capacitance. This noise will increase with the addition of detector capacitance, and also with the addition of lossy dielectrics which generate noise in charge sensitive circuits (Radika, 1968). These two factors nearly double the noise of the preamp for most spherical proportional counters. Thus if single ion events are to be detected, both the best gas gain and low noise electronics are needed.

At the time this project was started the Canberra Model 1408 C preamp seemed to be the best available. Its specified noise level is

120 RMS electrons with two microsecond RC pulse shaping. These preamps use very high value signal and feedback resistors which protect the FET from damage due to rapid changes in the detector bias supply voltage. However, these large resistances provide no protection in the case of breakdown in the proportional counter. Replacement of the input FET is, therefore, fairly routine. It was found that the two preamps we used gave lowest noise when TI 2N4857's were used in the input and that the noise was then about 100 RMS electrons, without added input capacitance, varying a few percent depending on the individual transistor. When connected to the solid-walled detector noise was about 170 RMS electrons.

The main amplifier used in this experiment was a Tennelec TC 202 which was operated in the unipolar pulse shaping mode. This amplifier has pole zero cancellation and adjustable time constants. The shaping time constant must be adjusted to be at least as long as the proportional counter pulse rise, otherwise part of each pulse will be lost resulting in poor resolution. As the shaping time is increased further the preamplifier noise is decreased, but the chance of pulse pile up in the amplifier is increased. This becomes a limiting factor at high count rates and can result in distorted spectra. Oscilloscope observations of the proportional counter pulses indicated that 1.6 microseconds would be adequate with respect to proportional counter rise time. This was checked by taking spectra at low count rates with 1.6 and 2.4 microsecond shaping times. There was no difference in the two so it is assumed that 1.6 microseconds is

adequately long. To assure that the count rate in a given experiment was not too great, the measurement was repeated at higher and lower (when possible) dose rates. The absence of any difference in the spectra indicates that there is no distortion due to pile up. Critical adjustment of the amplifier pole zero cancellation control requires a large count rate of nearly monoenergetic pulses which is not available in this type of experiment. Thus the setting had to be based on the relatively uncritical minimization of the undershoot band observed on an oscilloscope at high count rate.

The data from these experiments were collected with a Nuclear Data 2200 series pulse height analyzer with a 50 megahertz analog-to-digital converter. The linear gate was operated in the closed position and the internal lower level discriminator was used.

Additional electronics used included an Ortec 428 detector bias supply which was modified with additional filtration to minimize noise. This power supply was occasionally supplemented with a 300 volt battery in series to give a maximum anode voltage of 1300. An oscilloscope was used to allow observation of the pulses as various conditions were changed. A Hewlett Packard Model 3400A RMS voltmeter was used to monitor preamp noise. A mercury relay tail type pulser (TC 812) was used to test the preamp and provide a basis for setting the analyzer zero position.

3.4 Gas Handling System

In a proportional counter the gas gain is a strong function of gas density. In order to get meaningful results the gas density must remain constant to better than one percent over the entire period between the initial energy calibration and the end of the experiment, commonly a period of several hours. At the same time the gas must be flowing at a rate sufficient to prevent build up of contamination from tiny air leaks and outgassing of the detector and plumbing components, any of which might affect the gas gain. In these experiments a passive flow control system was used. Flow of gas into the system was restricted by a 50 cm long section of 0.0125 cm ID kovar tubing. The flow out was controlled by a pair of needle valves in parallel (one with an 0.14 cm orifice, the other with an 0.32 cm orifice) as indicated in Figure 3.4.1. Pressure going into the capillary tube was controlled by a low pressure regulator (Matheson Model 70B) set at about 1.5 torr above atmospheric. The pressure in the detector is determined by the difference across the needle valve needed to cause the flow out to equal the flow in. Once this system has come to equilibrium it is quite stable, but due to the long time constraints involved it is very difficult to find the proper valve settings for a given pressure. The pressure in the detector was measured directly with a mercury manometer, read with a micrometer screw. The manometer was attached to the wall-less detector through a port not carrying a flow of gas.

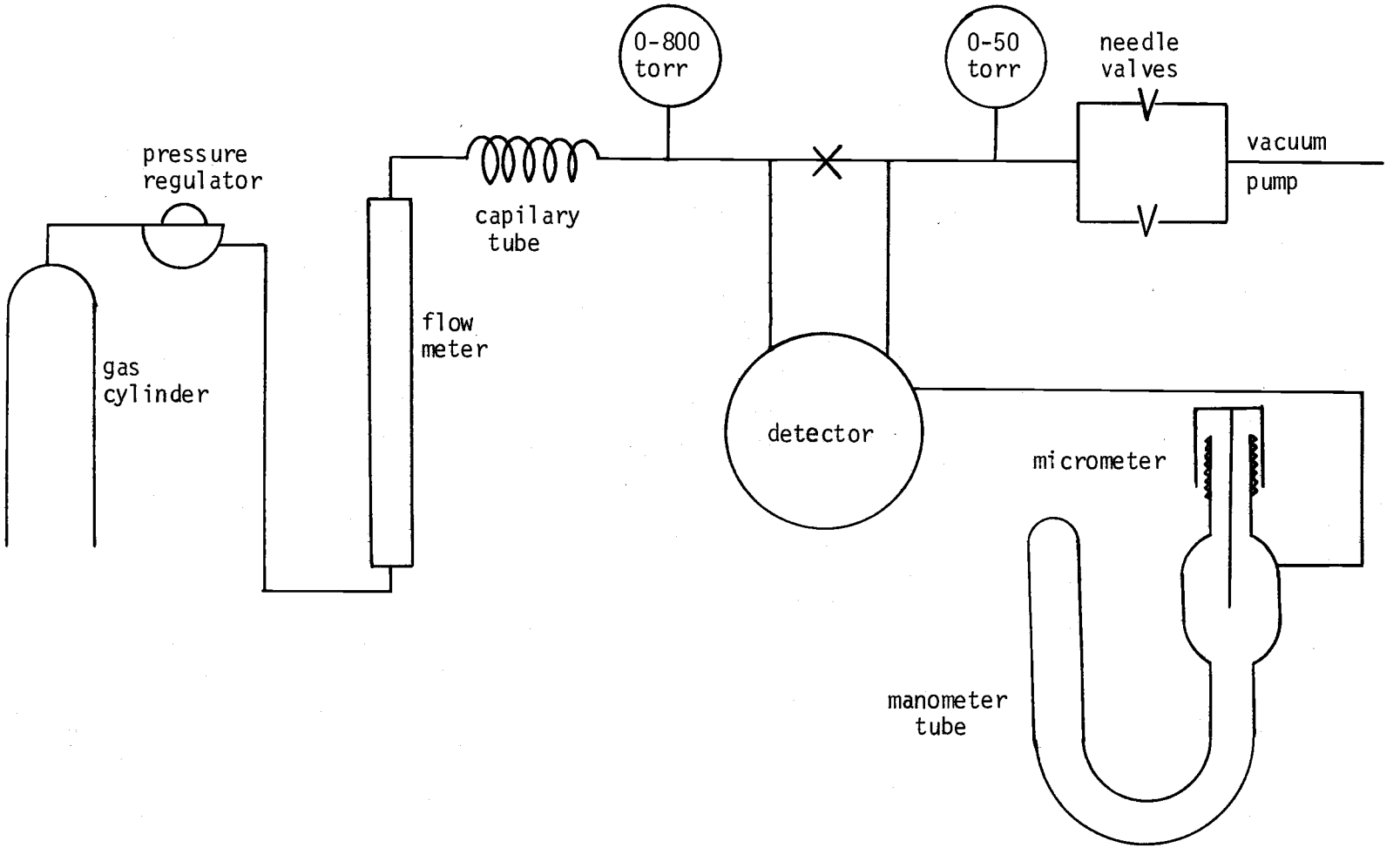

Figure 3.4.1 Gas Handling System.

3.5 X-Ray Machine

As mentioned earlier, the rate at which events occur in a simulated site as compared to an actual microscopic site is increased by the ratio of the densities squared. Density ratios on the order of 10^5 are used, so the rate at which events will be observed is increased by 10^{10}. For photon irradiation, one should expect something like one-tenth to ten events per rad in sites a few microns in diameter so there will be on the order of 10^9 and 10^{11} events in the detector per rad. Because the amplifier output pulses are several times 10^{-6} seconds it is clear that only a fraction of a rad per second can be accepted without pulse pile up. Since the output of the x-ray machine used in these experiments is bunched in short pulses at the peak of each power line cycle, the average dose rate must be even lower. Many modern x-ray machines cannot be made to operate at very low outputs. However, 60-cycle transformer machines with self-rectified tubes such as the one used in these experiments can be modified to operate at very low currents. All that is required is to substantially decrease the filament temperature. This modification along with substitution of a 300 microamp meter for the original 20 milliamp movement was made on a venerable GE Maximar III. The machine, with this modification, operates very stably in the range of currents used, 5 to 20 microamps. Exposure rates of about two roentgens per hour at 50 cm from the target can be obtained operating at 250 kVp with 1 mm Cu filtration. This was further

reduced a factor of 25 by operating the detector at 2.5 meters from the target. The resulting exposure rate was about 20 microroentgens per second at the detector.

Three operating conditions were chosen for these experiments, 250 kVp with 1 mm Cu added filter, 250 kVp with inherent filtration only, and 65 kVp with inherent filtration. The quoted kVp values are only approximate since they were obtained by extrapolation from the transformer loading tables, provided by GE, which cover 5, 10 and 15 milliamps down to 80 kVp. Half value layers were measured at more nearly conventional tube currents (either 300 μamp or 3 mamp) for each of the three conditions, measurements being made with a one R Victoreen chamber. Added absorbers in the form of 13 cm squares of copper or aluminum (commercially pure) were placed just in front of the collimator cone with the beam horizontal. The chamber was placed one meter from this with the nearest scattering material in the line of the beam another 2.5 meters away. The results of these measurements are plotted in Figure 3.5.1. The measured half value layers are 1.77 mm of Cu for filtered 250 kVp, 0.44 mm of Cu for unfiltered 250 kVp, and 1.9 mm of Al for unfiltered 65 kVp. The second half value layer for the 65 kVp irradiation is 2.9 mm of Al giving a homogeneity factor of 0.65. The unfiltered 250 kVp value was checked, using only three points, at 20 microamps (this required 2 1/3 hours of exposure time) and the half value layer determined previously was confirmed. This indicated that the low current operation is not

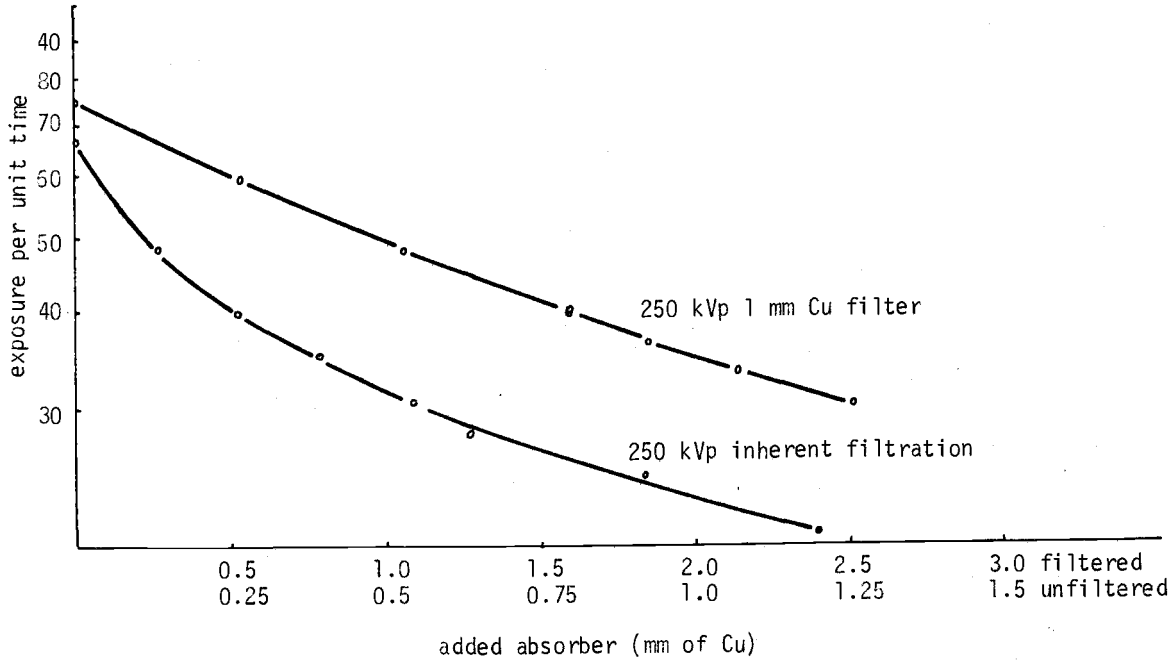

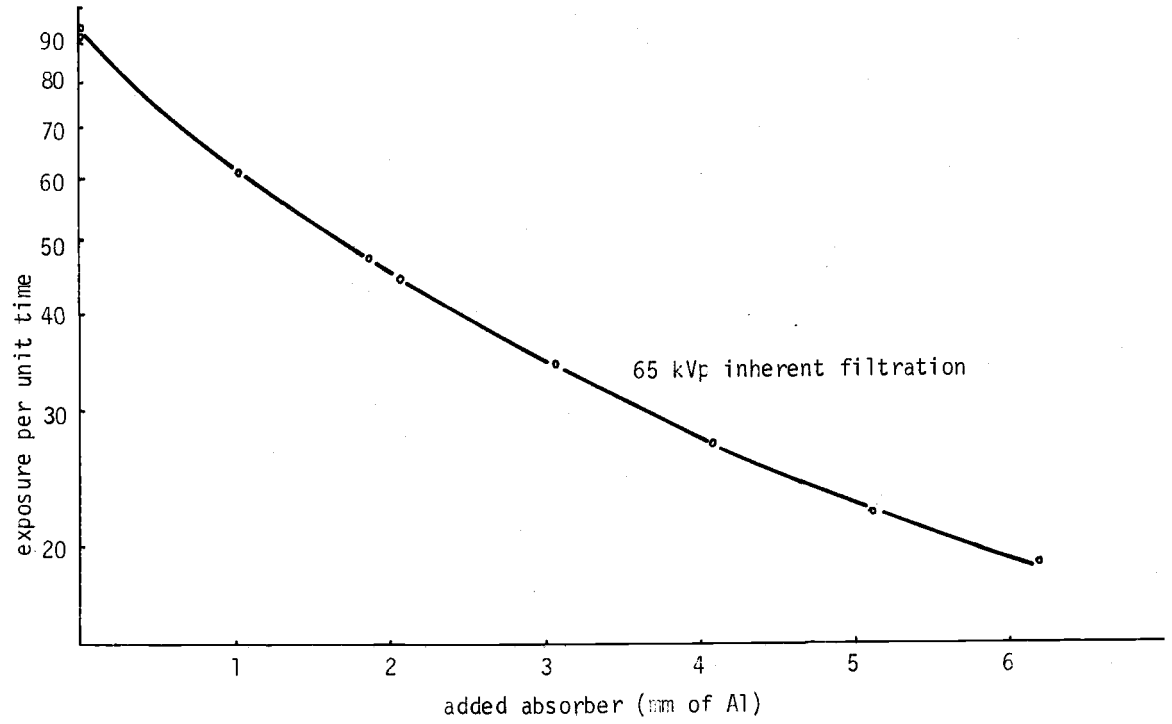

Figure 3.5.1 Attenuation curves for x-rays used in these experiments.

causing some change in electron focus or trajectory which results in a drastic change in the photon spectrum relative to normal tube currents.

Chapter 4

EXPERIMENTAL PROCEDURE

X-ray and ^{60}Co gamma ray exposures were performed in, as nearly as practical, a scatter-free environment. Experiments were repeated in such a way that equivalent measurements were independent with respect to obvious potential experiment errors.

4.1 Exposure Geometry

The x-ray machine used in this work was located in a well shielded room which also contained a 14 MeV neutron generator, The x-ray unit was positioned at one edge of the room with the beam horizontal and directed diagonally across the room. The x-ray control panel and the detector electronics and gas handling system were on the opposite side of a 60 cm concrete wall from the x-ray unit itself. The proportional counter was normally placed 2.5 meters from the x-ray source to take advantage of the inverse square reduction in dose rate. Electronic cables and gas flow tubes ran from the detector, across the room and through a maze under the floor to the instruments at the x-ray control panel, requiring a total length of about 12 meters. These great cable lengths were a potential source of both electronic and gas purity problems, but were necessitated by the shielding for the neutron generator.

An effort was made to minimize scattered radiation at the detector. The detectors and the x-ray source were operated 80 cm above the floor of the room, and there was an additional 1.5 meters beyond the detector before the beam reached the wall. Beam size was controlled by fixed rectangular collimators, giving a beam 20 by 25 or 50 by 50 cm at 2.5 meters. The larger field was used only with the grid-walled detector in the 30 cm diameter sphere.

In order to uniformly irradiate the walls of the detector it is necessary that the preamp input section and the connections between detector and preamp also be in the field. Two possible problems could result; noise in the preamp due to irradiation, and pulses due to collection of ions formed near connections of the anode cable to the detector and the vacuum feed through. In order to test these possibilities, the x-ray beam was carefully masked down so that just the potential trouble spots were irradiated. It was found that the x-ray exposure had no effect on the preamp noise or gain. Originally pulses were produced when the anode connection to the vacuum feed through was irradiated. Potting this connection with ceresin wax eliminated the pulses and no other source of spurious signals was found.

Cobalt 60 irradiations were made with a 3.4 millicurie source in a thin stainless steel holder held in the line of the x-ray beam, about 60 cm from the chamber.

4.2 Detector Operation

In order to minimize the possibility of an unrecognized systematic error in these experiments, measurements were repeated in a way which minimized the potential errors which were common to both measurements. Series of measurements involving one detector and a number of site sizes were followed by measurements with another detector, and then repeated weeks or months later. In this way the equipment had been completely disassembled, then built up again and re-calibrated between comparable measurements. Each time the equipment was set up, the electronic noise level, the gas flow rate and purity, pulse pile up, pole zero cancellation, mercury manometer zero, and numerous other factors were checked. In each case the comparable spectra obtained at separate times were in major respects identical. The only noticeable differences were in the details of the very low energy depositions. These resulted from differences in gas multiplication statistics associated with small differences in gas gain.

Each time a detector was set up a series of measurements requiring two or three days would be undertaken. Following necessary checks of the system, the gas pressure would be adjusted to establish the desired site size. After the gas pressure had come to equilibrium ^{37}Ar and ^{55}Fe calibration measurements would be made and then spectra would be taken for the three or four different irradiations. After the last spectrum was collected the calibration measurements were repeated and compared with those from the beginning of the run. If there was a

significant difference between the two calibrations the cause of the gain shift was isolated and corrected and the measurement repeated. Otherwise, work proceeded to the next site size. In each case where serious gainshift was detected it had resulted from operator error on the gas flow system.

Chapter 5

TREATMENT OF DATA

The output of a microdosimetric experiment is a pulse height spectrum which is proportional to the f(Δ) distribution. In order to be useful for comparisons with biological models this distribution must be normalized in terms of energy, and then manipulated mathematically to give those quantities and distributions, described in Chapter 1.

5.1 Data Format

Because of the wide range of pulse sizes and numbers per channel which need be recorded, the analyzer output data must be plotted on a log log scale. Pulse sizes range from Δ values of 30 eV to 12,000 eV for a one micron site and the numbers of pulses range over five decades. The range of pulse sizes makes it impractical to get the entire spectrum in a multichannel analyzer in one run. Since the first three or four channels of an analyzer cannot be relied upon, the analog to digital converter would have to be operated at about 8 eV per channel and 1500 channels would be required to include 12,000 eV. Count rate at the high energy end, where 100 eV resolution is more than adequate would then be very low. A more efficient approach is to make two measurements at different amplifier gain

settings, one immediately following the other. The first is made at approximately 5 eV per channel, then by changing only the amplifier gain control the spectrum is remeasured at 200 eV per channel. Matching these two spectra requires the electronic gain change to be accurate. Amplifier gain was checked using, sucessively, two precise voltages a factor of 40 apart as input to the preamp. The amplifier gain was changed by the same amount. When these signals were analyzed with a multichannel analyzer, pulses obtained from the two combinations of gain and input signal were within a fraction of a percent of each other.

The data, collected as two overlapping spectra, must be combined into a single curve on log log paper. To do this, the channel numbers of the low gain spectrum are first multiplied by 40 and plotted on the same scale as the high gain spectrum. Since count rate is not necessarily constant for the two measurements, the number of counts per channel does not have a predictable ratio between the two spectra; but the difference is a multiplicative constant. Since the data are plotted on a log log scale it is a simple matter to shift the axis vertically to match the two spectra. The low gain spectrum was generally plotted from channel 5 to the point where there were no more pulses. In this arrangement channels 5 through 8 of the low gain spectrum are redundant with channels 200 through 320 of the high gain. In all cases this overlap section of the two curves matched to within the statistics of the points. For convenience in subsequent processing these spectra were also normalized in terms of Y,

energy deposition per 100 μg cm^{-2}, at the same time. This normalization was based on the ^{37}Ar and ^{55}Fe calibrations. Thus the analyzer output was plotted in two sections, the number of channels per keV per 100 μg cm^{-2} calculated, and the data were traced onto identical log log paper with the horizontal axis shifted to give an energy calibration. This spectrum, normalized in terms of energy, but not in terms of number, is referred to as N(Y), the number of events versus event size.

Calculation of normalized spectra, mean values etc., was done on the basis of equal logarithmic intervals. This approach rather than linear intervals was chosen because it reduces the total number of data points required to describe the spectrum. Little is lost in resolution since at the high energy end most of the spectra are changing relatively slowly. Calculation of means and areas on a logrithmic scale is based on the observation

$$\int_0^{Y\ max} Y(N)YdY = \int_0^{Y\ max} Y^2N(Y)dY/Y$$

$$= \int_0^{Y\ max} Y^2N(Y)d\ln Y \qquad (5.1.1)$$

A primed symbol, for example f'(Y) will be used to designate functions calculated per logarithmic interval. Values of N(Y) at equal logarithmic intervals for use in the calculations were read from the smooth curve described above. This was considerably facilitated by preparing a master drawing ruled at the desired intervals and placing it on a light box under the graphed data.

The N(Y) distributions used in these calculations have been truncated at Y values corresponding to a Δ value of about 30 eV. This was done so that the results would more truly represent ionization; it makes little sense to extend results below one ion pair, the smallest allowable energy increment. Since, depending on gas gain, multiplication statistics distort the observed spectrum below two to six ion pairs, the N(Y) values in this region were determined by extrapolation. For the calculations used here, N(Y) was taken as a constant equal to the value at the first reasonably reliable point, usually two ionizations. Many other schemes for filling in this region are possible. Two reasonably extreme ones are shown in Figure 5.1.1. The resulting change in f(Y), shown in Figure 5.1.2, is not very dramatic. The mean $\overline{Y}_p$, is decreased less than 5% for the upper curve, and is increased less than 2.5% by the lower curve. The dose average value of Y is changed by less than 0.5% in either case. What little difference the choice of extrapolation makes is reduced considerably when various irradiations or detectors are compared, since for a given site size, the same extrapolation was made in each case.

5.2 Calculated Distributions

A number of different distributions can be calculated from the experimental data. The relative usefulness of each of these distributions in studying a particular biological or physical phenomenon depends on the problem which is being considered and to some extent

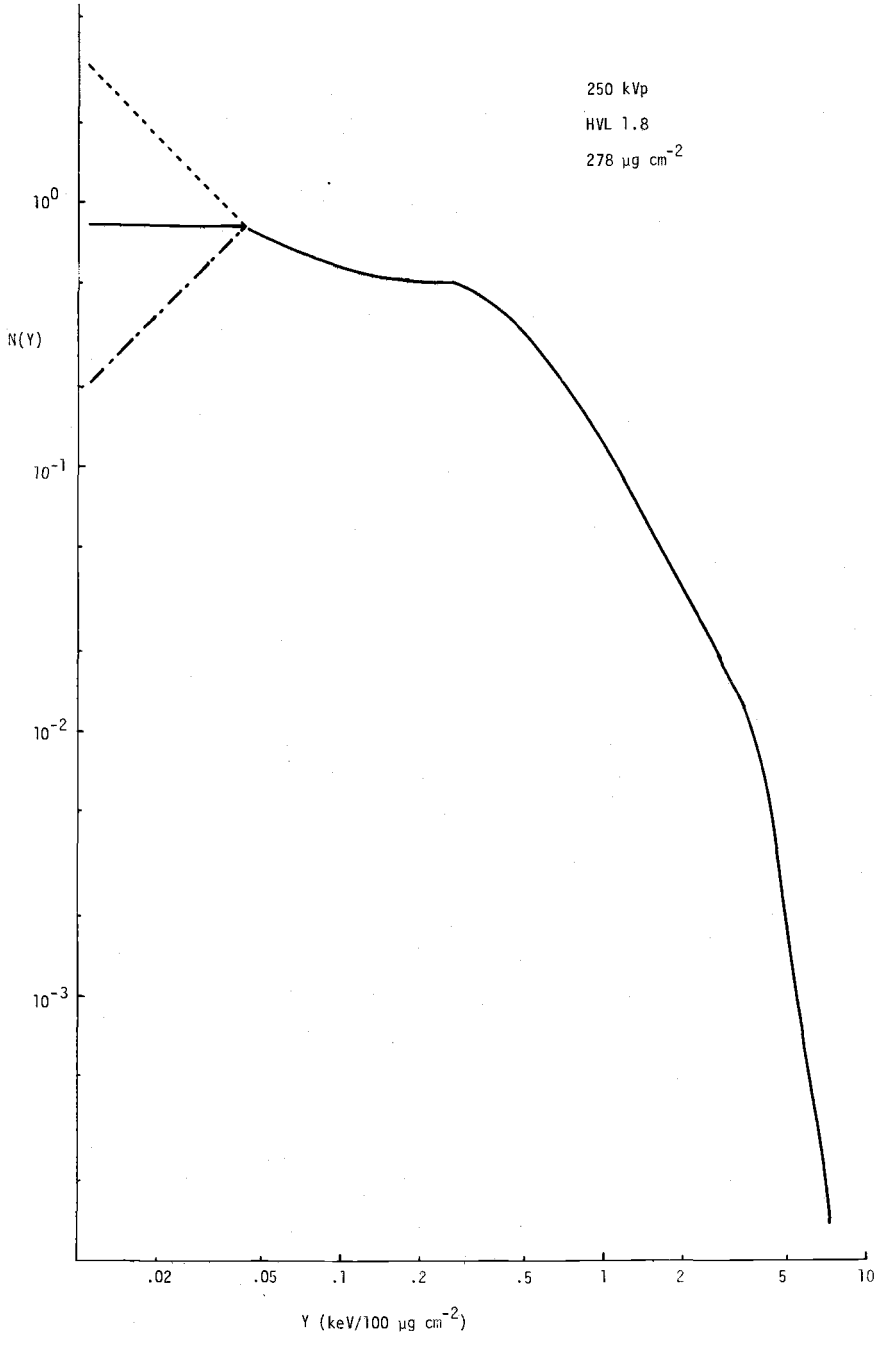

Figure 5.1.1 Possible extrapolations of N(Y) from four ion pairs to one ion pair; solid line used in this study.

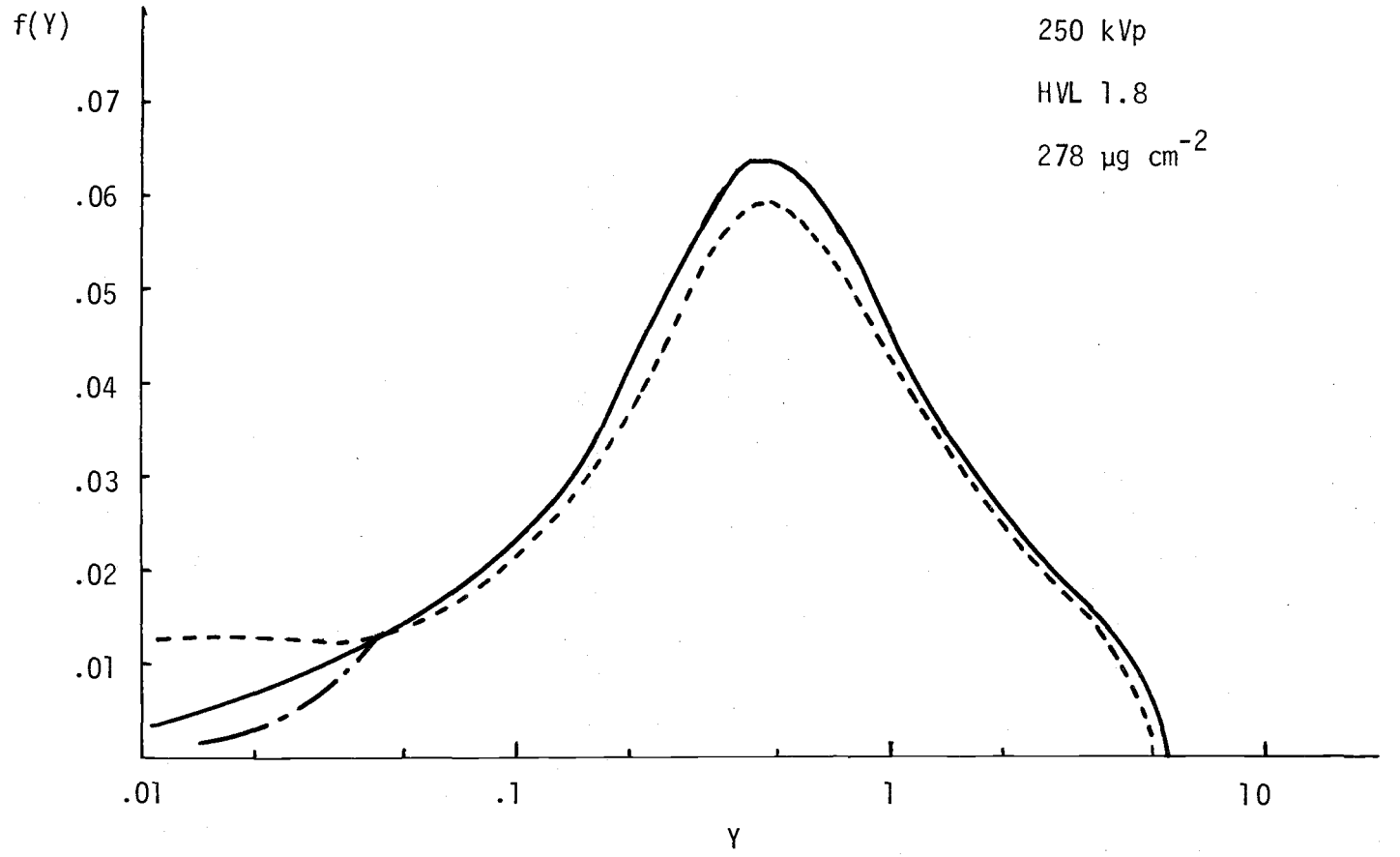

Figure 5.1.2 Effects of the extrapolations shown in Figure 5.1.1

the personal preference of the user. Thus the choice between comparing either a Y spectrum or Z spectrum to cell lethality data might be made on the basis of dose rate and whether or not a repair mechanism is expected to function. The distinction between distributions in Y and Δ is essentially one of scale change and a choice depends on whether one prefers to think in terms of total energy in the site or average energy per unit path length.

When f(Δ) is desired it is obtained by simply multiplying the values of Y by the site diameter. Since the Y scale is usually plotted logarithmically this can be done graphically by simply shifting the axis by an appropriate factor.

The following distributions are thought to be of general interest. With the exception of the T and Z distributions, they were calculated in one short program run at the OSU computer center via teletype terminal.

The density of events per log interval, f'(Y), is Y times N(Y) normalized to unit area

$$f'(Y) = \frac{Y\ N(Y)}{\Sigma Y\ N(Y)} \qquad (5.2.1)$$

On a linear interval this would be

$$f(Y) = \frac{N(Y)}{\Sigma N(Y)} \qquad (5.2.2)$$

The dose per logarithmic interval is calculated and normalized to one keV

$$d'(Y) = \frac{Y^2 N(Y)}{\Sigma Y^2 N(Y)} \qquad (5.2.3)$$

This can easily be converted to $d'(\Delta)$ by shifting the axis by a factor equal to the site diameter.

The fractions of the events greater than Y, $1 - F(Y)$; and the fraction of the dose delivered by events greater than Y, $1-D(Y)$, are calculated

$$1-F(Y) = 1 - \sum_{Y=0}^{Y} f(Y) \qquad (5.2.4)$$

and

$$1-D(Y) = 1 - \sum_{Y=0}^{Y} d(Y) \qquad (5.2.5)$$

The number of events greater than Y per unit energy, $\Phi(Y)$, is

$$\Phi(Y) = \frac{1}{\overline{Y}_p b(\text{keV})} \frac{M}{1.602 \times 10^{-9} \text{ erg/keV}} [1-F(Y)]$$

$$= \frac{1}{\overline{Y}_p b(\text{keV})} \frac{.525\ b^3 \times 10^{-12} \text{ grams}}{1.602 \times 10^{-9} \text{ erg/keV}} [1-F(Y)]$$

$$= \frac{1}{\overline{Y}_p} \frac{b^2}{3060} \frac{\text{erg}}{\text{gram}} [1-F(Y)]$$

$$= \frac{1}{\overline{Y}_p} \frac{b^2}{30.6} [1-F(Y)] \text{ per rad} \qquad (5.2.6)$$

where b is the site diameter and M, the mass of the site, is

$$M = \rho v = \rho\ 1/6\ \pi b^3$$

$$= .525\ b^3 \times 10^{-12} \qquad \text{for } \rho = 1 \text{ and } b \text{ in } \mu\text{meters.}$$

$\overline{Y}_p$ is the mean Y per event so $1/\overline{Y}_p b$ is the mean number of events per keV deposited.

$$\overline{Y}_p = Y\ F(Y) \qquad (5.2.7)$$

which on the logarithmic scale is

$$\overline{Y}_p = \sum Y \frac{YN(Y)}{\Sigma YN(Y)} \qquad (5.2.8)$$

The variance of the number mean on the logarithmic scale is

$$\text{var} = \sum Y^2 \frac{Y_p N(Y)}{\Sigma Y_p N(Y)} - \overline{Y}_p^{\,2} \qquad (5.2.9)$$

The dose average of Y and its variance are, on the logarithmic scale,

$$\overline{Y}_d = \frac{\Sigma Y^3 N(Y)}{\Sigma Y^2 N(Y)} \qquad (5.2.10)$$

$$\text{var} = \frac{Y^4 N(Y)}{\Sigma Y^2 N(Y)} - \overline{Y}_d^{\,2} \qquad (5.2.11)$$

Again, all of these distributions can be converted to functions of Δ by multiplying by the site diameter.

In addition to the single event distributions described above the multiple event distributions can be calculated. The total energy deposited in the site is the sum of that deposited by successive events. The amount of energy per event is given by $f(\Delta)$ and the occurrence of events is a Poisson process. Thus, the multiple event distributions are calculated using compound Poisson folding program such as KFOLD, prepared by Kellerer (1968). This program starts with an unnormalized distribution of event size as input and converts it

to a distribution with only a small (about 0.2%) probability of any event occuring. This distribution has the remainder of its area in a delta function at zero event size. The distribution is then folded with itself giving the compound Poisson distribution for twice the mean number of events. This is repeated successively, doubling the mean number of events (collision numbers) and the mean energy absorbed, until a specified average absorbed energy is reached. The program gives as output, the density of accumulated ionization per unit site size, $f(T/b)$, as a function of T/b on either linear or logarithmic scale for each convolution. In order to conserve computer storage the calculations are performed on a logarithmic scale. Also included in the output is the sum of $f(T/b)$ as a function of T. In order to assure that the calculations are being performed on a fine enough grid, the moments of the calculated distributions are calculated compared with the moments calculated from the initial distribution for that convolution number.

Chapter 6

COMPARISON OF SOLID AND GRID WALLED SPECTRA

As pointed out before, it is not possible to make quantitative predictions of the wall effect, though it is possible to make rough estimates of its magnitude for different types of irradiation, and of its variation as a function of the distance between detector and wall (Kellerer, 1971a). Experimental results on the wall effect will be presented and discussed here.

6.1 Type of Irradiation

The magnitude and nature of the wall effect for four different sources was investigated. These were chosen to give as wide a range of electron energies as possible and to be reasonably representative of radiations used in typical biology experiments. These selected radiations were: ^{60}Co gamma rays; 250 kVp x-rays, HVL of 1.77 mm of Cu; 250 kVp x-rays, 0.44 mm Cu HVL; and 65 kVp x-rays, HVL of 1.9 mm for Al. Figures 6.1.1 and 6.1.2 compare the energy density functions for a 92 $\mu g/cm^2$ site in grid-walled and solid-walled detectors for each of these four radiations. The general nature of the wall effect is easily observed in these curves. The wall effect produces the expected type of change in the spectrum. That is, there is a reduction in the number of small events with a corresponding increase in

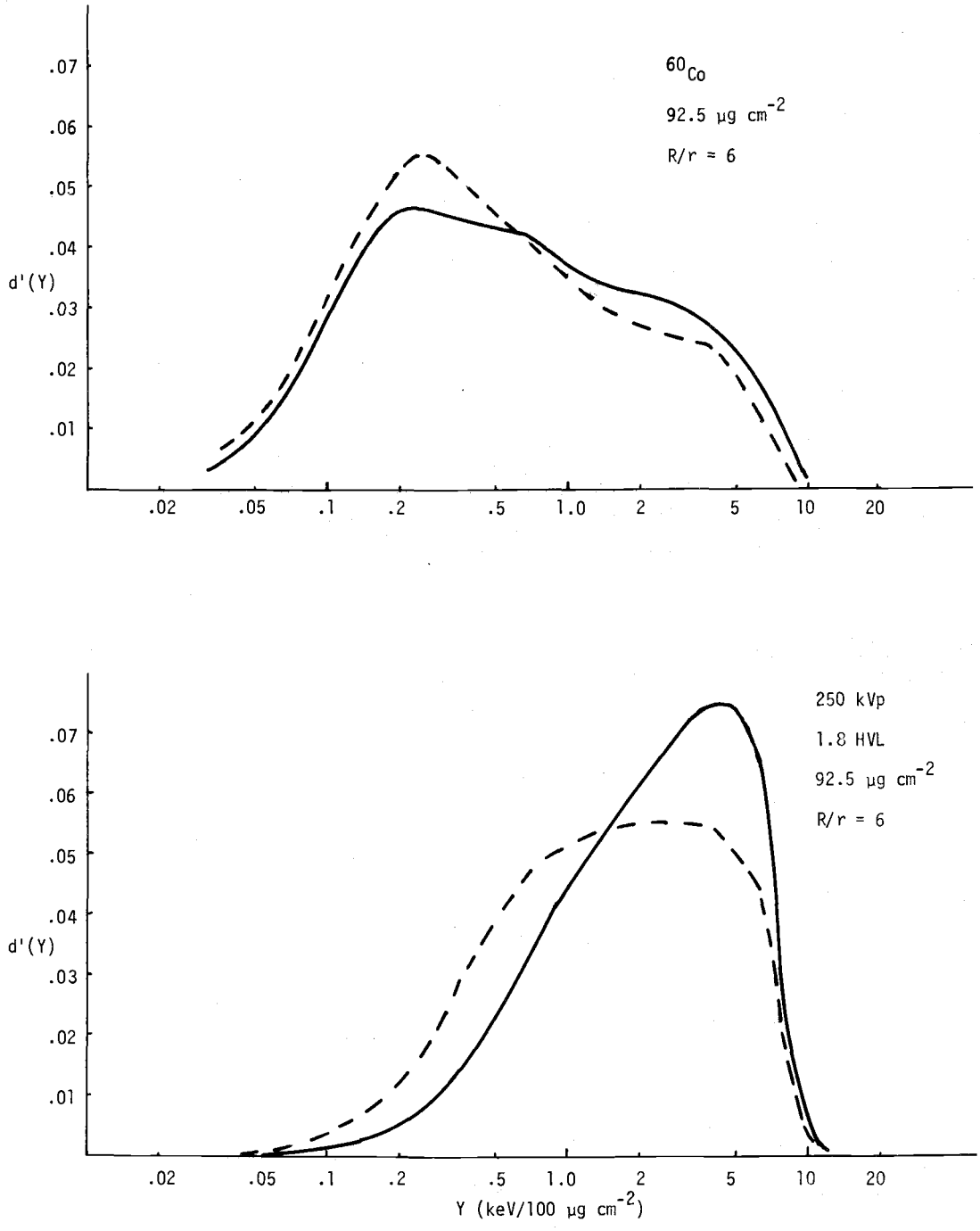

Figure 6.1.1 d'(Y) for ^{60}Co and filtered 250 kVp x-rays comparing solid- ——— and grid-walled – – – detectors.

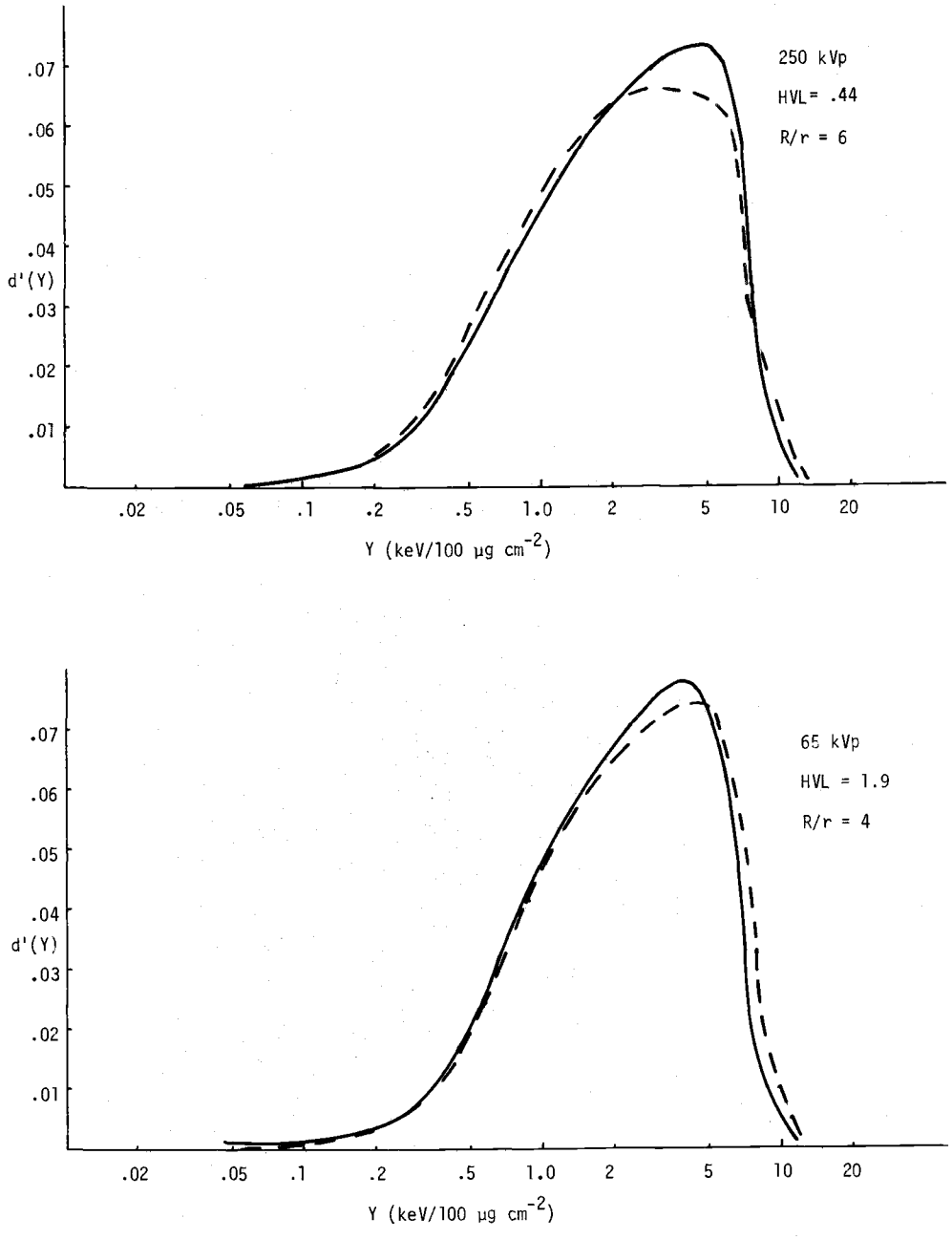

Figure 6.1.2 d'(Y) for unfiltered x-rays comparing solid wall ——— and grid wall – – –

large events. The expected increase in the magnitude of this effect for x-rays relative to ^{60}Co is also observed in the case of filtered 250 kVp x-rays. However, contrary to expectations, decreasing the half value layer of the x-ray beam resulted in a decrease in the wall effect. Irradiation with 65 kVp x-rays appears to have resulted in a reversal of the wall effect in some site sizes, as shown in Figure 6.1.2.

Plots of $d'(\Delta)$ are convenient for this comparison because they are normalized for equal doses and we expect the wall effect to alter the distribution function, but not the dose. The grid-walled detector in this comparison is, of course, not truly wall-less; 17% of its surface area is solid material, and it is housed in a plastic sphere of radius R equal to four or six times the detector radius r. Figure 6.1.3 extends this comparison to a larger site size(555 $\mu g/cm^2$) for ^{60}Co and 250 kVp (HVL 1.8 Cu) radiations. It is clear that changing site size does not bring about a basic change in the difference between solid- and grid-walled detector data. Table 6.1.1 gives the number mean and relative variance for solid- and grid-walled spectra for the four sources studied at a number of site sizes. Table 6.1.1 also gives the percent decrease in the number of events per rad which a solid wall produces.

The mean number of events per unit event size, the inverse of $\overline{Y}_p$, the mean Y per event, is plotted as a function of site diameter, b, in Figure 6.1.4. This graph shows clearly the differences in the effect of the solid wall with type of irradiation. The solid- and

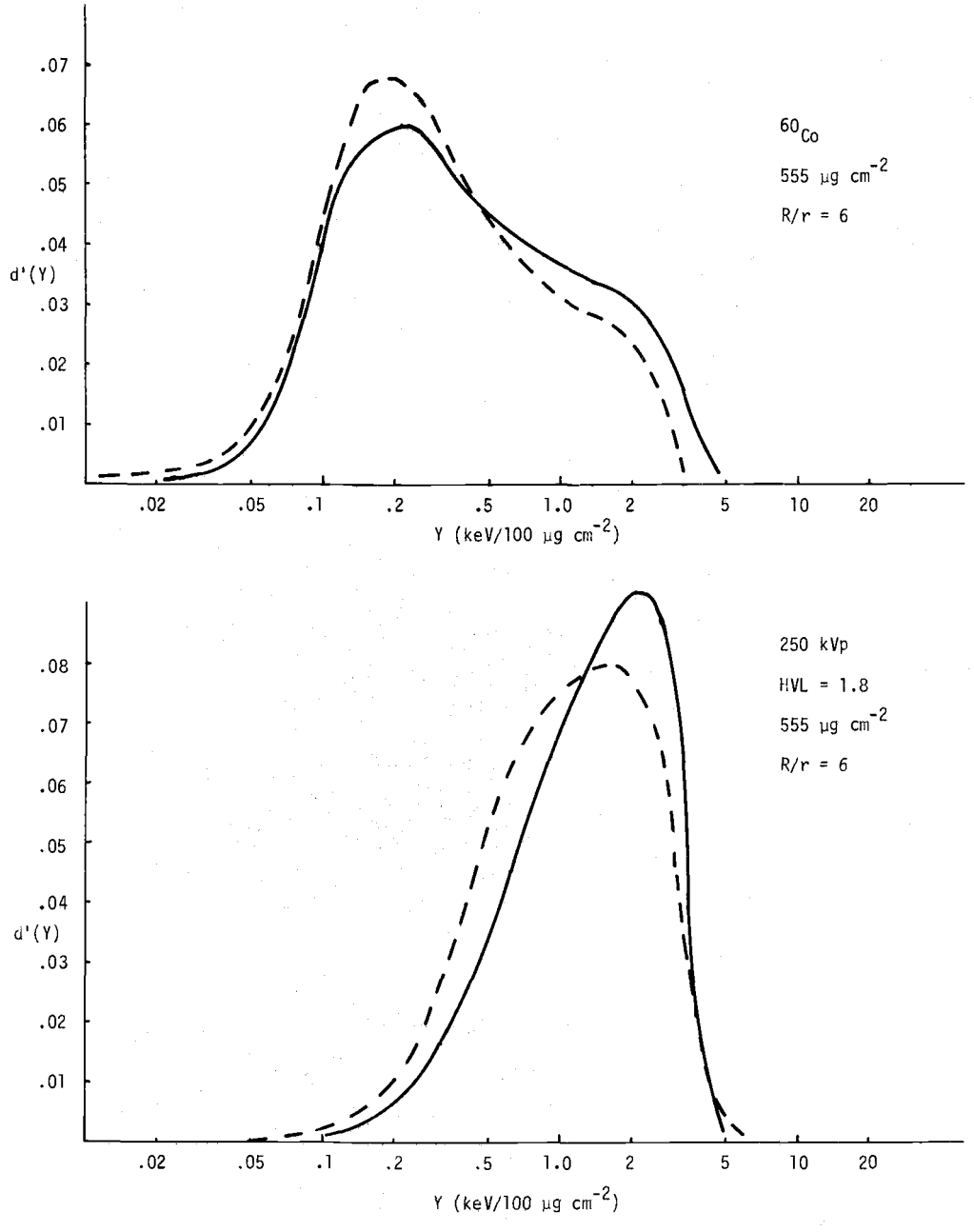

Figure 6.1.3 d'(Y) for ^{60}Co and filtered 250 kVp x-rays comparing solid- ——— and grid-walled – – – detectors at 555 µg cm^{-2}

Table 6.1.1

Wall Effect for Various Types of Radiation

Irradiation and nominal site size ($\mu g\ cm^{-2}$)	Solid Wall $\bar{Y}_p$ (keV/100 $\mu g\ cm^{-2}$)	Solid Wall Relative Variance	Grid Wall $\bar{Y}_p$ (keV/100 $\mu g\ cm^{-2}$)	Grid Wall Relative Variance	% Reduction in no of events (μ)
^{60}Co					
58	.37	3.917	.319	3.517	14
92	.295	3.697	.253	3.360	14
185	.239	3.215	.221	3.304	08
278	.244	2.873	.197	2.338	19
555	.225	2.034	.183	1.890	19
250 kVp Filtered					
58	1.262	2.063	.904	2.283	28
92	1.245	1.546	.815	2.109	34
185	1.157	1.088	.799	1.641	31
278	1.027	.977	.739	1.354	28
555	.916	.711	.678	1.030	26
250 kVp Unfiltered					
58	1.40	1.914	1.285	1.697	8
92	1.276	1.493	1.232	1.558	3
185	1.221	1.021	1.159	1.149	5
278	1.129	.858	1.094	.966	3
555	.928	.713	.928	.688	0
65 kVp Unfiltered					
58	1.664	1.447	1.68	1.409	-1
92	1.408	1.212	1.462	1.347	-4
185	1.322	.923	1.353	1.008	-2
278	1.254	.742	1.235	.817	+2

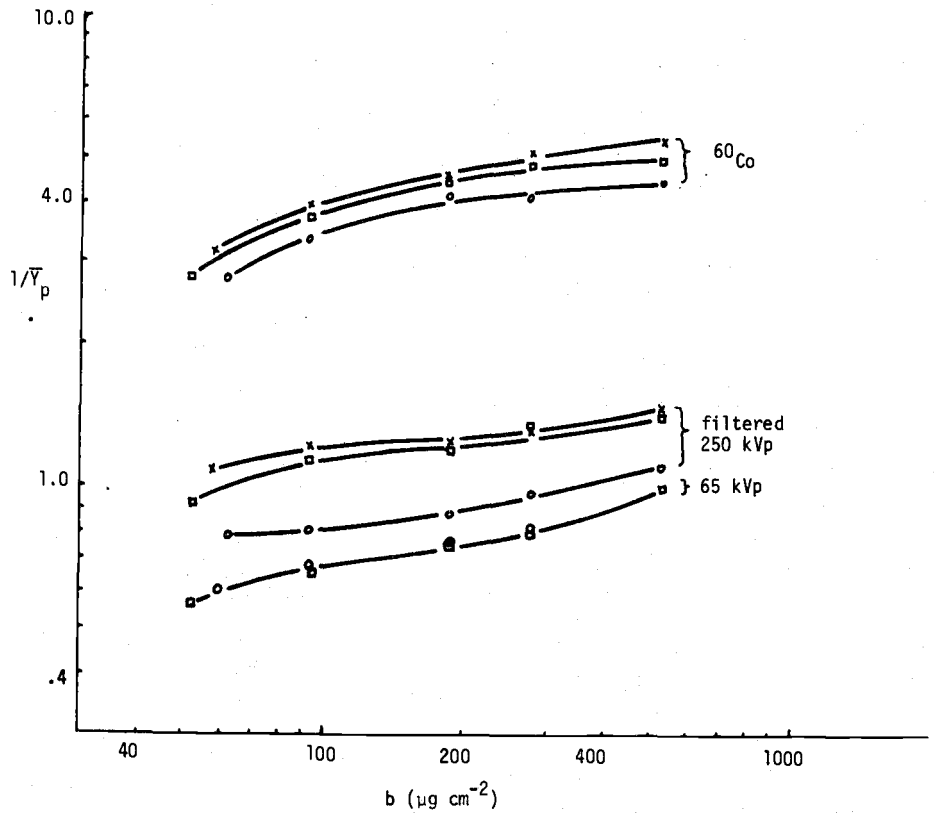

Figure 6.1.4 Number of events per unit event size (keV/100 μg cm^{-2}) as a function of site size (b) with solid wall (-o—o-), R/r = 4 (-□—□-), and R/r = 6 (-x—x-).

grid-walled curves for a given irradiation are essentially parallel. ^{60}Co shows a significantly lower number of events when the solid wall is used. Filtered x-rays show an even greater wall effect than ^{60}Co irradiation. On the other hand, for 65 kVp, there is effectively no wall effect. A single line in Figure 6.1.4 characterizes both solid- and grid-wall points. Unfiltered 250 kVp data follows very closely the 65 kVp results, i.e. no wall effect, and has been left off this graph for clarity.

Because the gas handling system did not allow the smallest site used with each chamber to be adjusted to a single value, Figure 6.1.4 was interpolated to get values of $\overline{Y}_p$ at 58 $\mu g/cm^{-2}$ diameter for Tables 6.1.1 and 6.2.1.

Since the wall effect for photon irradiations in the energy range covered here is the result almost exclusively of back-scattered electrons it should be independent of site size. That is, the number of back-scattered electrons is a constant fraction of the total number of electrons for a given electron spectrum. However, a few electrons will re-enter a site in a uniform medium. This fraction increases as the site size increases, and becomes significant for site sizes comparable to the electron range. Thus the observed wall effect may vary with site size for large sites and low energy electrons. The experimental results for the reduction in number of events with the solid wall, Table 6.1.1 and Figure 6.1.4, show no systematic variation with site size. The results vary as much as ±5% within a given kind of irradiation, but this is about the range of the estimated errors.

Errors in the calculated means of the distributions are introduced by the precision of the energy calibration which was generally about 3%, by the smoothing of the original data for large Y values where counting statistics are poor, and by errors in reading values from the smoothed graphs for use in the calculations.

Given the above errors it can be said that a solid wall increases the fraction of multiple events relative to the grid-walled detector used in these experiments by about 15% for ^{60}Co and by about 29% for filtered 250 kVp x-rays, but has little or no effect in the case of unfiltered 250 and 65 kVp irradiations.

It might be thought that differences in photoelectric cross section of propane and the T.E. plastic wall could produce the unexpected absence of wall effect for low energy photons, possibly by means of some compensating change in the spectrum. This is very unlikely since no difference in event spectra could be found when the grid-walled detector was operated using either propane or T.E. gas. In order to double check, the spectra for 65 kVp and a 100 µg site were taken with both solid- and grid-walled detectors using T.E. gas. The results are shown in Figure 6.1.5 in terms of N(Y). It is seen that there is virtually no difference in the energy absorption spectra for a solid-walled detector and this grid-walled detector.

6.2 Effect of Container Size

It is not possible to accurately predict the amount of wall effect which will be produced by a container whose diameter is a

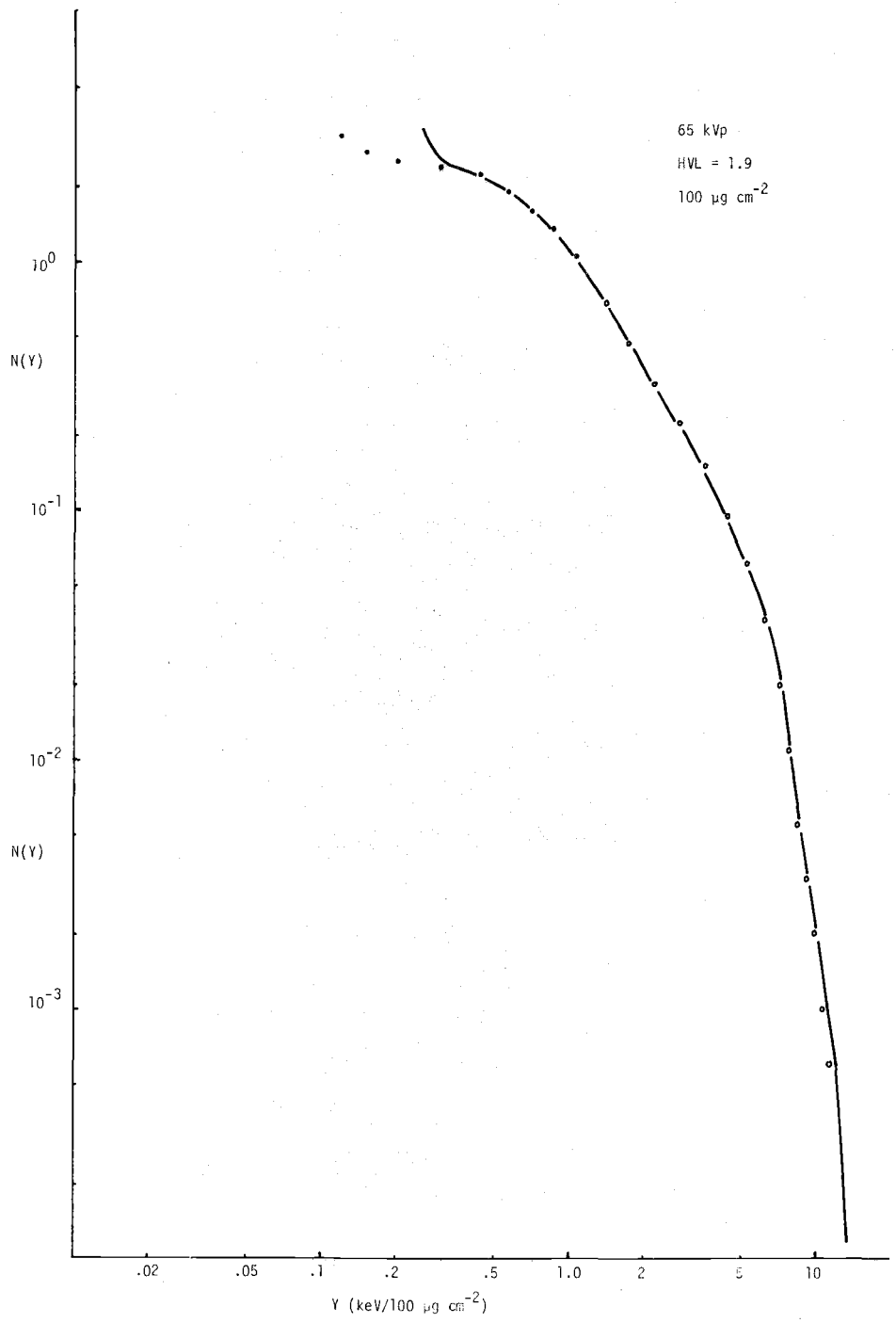

Figure 6.1.5 Wall effect in detectors filled with T.E. gas and exposed to unfiltered 65 kVp x-rays: solid line, grid-walled detector; points, solid-walled detector.

given factor larger than the detector. In order to experimentally test the effects of container diameter the detector was operated in two containers, one whose diameter (R) was four times the detector diameter (r), and one with R/r = 6. The results for ^{60}Co and filtered 250 kVp x-rays when R/r = 4 are given in Table 6.2.1. As expected the smaller container, R/r = 4, produces more re-entry events than the container with R/r = 6. Consequently, the solid wall makes a smaller change when compared to the grid-walled detector in the smaller sphere. The average reduction in number of events per unit dose for the solid wall relative to R/r = 4 when exposed to ^{60}Co is 8%, whereas relative to R/r = 6, it is 14%. However, for the lower energy electrons resulting from 250 kVp filtered irradiation the wall effect relative to R/r = 4 is 24% while relative to R/r = 6 it is 29%. An alternate way to express these results is to compare the change in the number of events in the grid-walled chamber with R/r = 4 relative to R/r = 6. In the case of ^{60}Co irradiation use of the smaller container gives a 7% decrease, and for filtered x-rays it gives a 6% decrease.

Another way to consider the importance of the wall effect is to determine the change in the fraction of events larger than some value of event size Y. That is, if one is interested in the number of events larger than a given value of Y, how large an error is introduced by the wall? Table 6.2.2 shows this for Y values of 0.173 keV/100 $\mu g/cm^{-2}$ for ^{60}Co and 0.581 keV/100 $\mu g/cm^{-2}$ for the other sources. It can be seen that when evaluated in this way the wall effect is even more serious than would be indicated by change in total number of

Table 6.2.1

Wall Effect for R/r = 4

Irradiation and nominal site size (g cm^{-2})	Solid Wall $\bar{Y}_p$ (keV/100 µg cm^{-2})	Solid Wall Relative Variance	R/r = 4 $\bar{Y}_p$ (keV/100 µg cm^{-2})	R/r = 4 Relative Variance	% reduction in no of events (ω)
^{60}Co					
58	.370	3.917	.335	3.866	9
92	.295	3.697	.267	3.651	10
185	.239	3.215	.226	3.30	5
278	.244	2.813	.207	2.860	15
555	.225	2.034	.206	1.931	8
250 kVp Filtered					
58	1.262	2.023	.99	2.169	21
92	1.245	1.546	.887	1.903	28
185	1.157	1.088	.835	1.487	28
278	1.027	.977	.731	1.216	28
555	.916	.735	.694	.949	24

Table 6.2.2

Effect of Solid Wall

Irradiation and Nominal Site Size	Solid Wall		R/r = 4		R/r = 6
	1 - F(Y)	% Increase Relative to R/r = 6	1 - F(Y)	% Increase Relative to R/r = 6	1 - F(Y)
^{60}Co(1)					
60	.455	7	.456	0	.427
90	.380	9	.348	-1	.350
180	.323	7	.309	2	.303
280	.335	16	.283	-2	.288
560	.329	19			.277
250 kVp Filtered(2)					
60	.476	29	.417	13	.368
90	.515	47	.382	9	.351
180	.545	45	.395	4	.377
280	.513	37	.368	-2	.374
560	.523	41	.376	1	.372
250 kVp Unfiltered(2)					
60	.513	-3			.526
90	.535	1			.529
180	.582	4			.559
280	.578	2			.565
560	.531	-4			.552
65 kVp(2)					
60	.634	-3	.654		
90	.639	0	.639		
180	.644	2	.629		
280	.656	1	.647		

(1) $Y_{min} = 0.173$

(2) $Y_{min} = 0.581$

events. Errors as large as 40% for filtered 250 kVp x-rays (averaged for all site sizes) are indicated.

6.3 Discussion

The experimental results show a wall effect of the general type expected, but variations with photon energy and distance to the wall were not quite what was expected. Kellerer indicates that the wall effect for x and gamma radiation will be primarily from re-entry of electrons and should be proportional to the albedo for electrons. He gives the properly averaged albedo values as ranging from 25% at 2 keV down to 20% at 1 MeV. Thus wall effect reduction in events per unit dose would be expected to decrease gradually with increasing photon energy. Instead, a rather large increase (from 14 to 29%) was found going from ^{60}Co to filtered 250 kVp x-rays, but for lower energy photons the wall effect disappeared. One requirement of Kellerer's treatment is that re-entry of electrons be unlikely in the case of the uniform medium. This is the case only if the electron range is considerably larger than the dimensions of the site. If this condition is not met there will be re-entry events in the wall-less detector and the difference between it and the solid-walled detector is reduced. For 50 kVp x-rays the majority of electrons have energies of less than 6 keV (ICRU, 1970). Over half of the electrons with 6 keV have a range of less than 50 $\mu g/cm^2$ (Cole, 1969). Thus it is reasonable to assume that re-entry events in the wall-less detector

contribute to the lack of difference between solid- and grid-walled spectra for both 65 kVp irradiation and unfiltered 250 kVp x-rays.

Another possible contribution to the disappearance of the wall effect is the reduced energy of the re-entering electron. Multiple events may be occurring which produce such a small increase in the energy of large events that they are not resolveable. Specifically, the albedos which Kellerer refers to are in terms of the number of re-entering electrons, with no reference to the energy they carry. It is likely that when electrons with rather low initial energy (a few keV) are back-scattered from a solid boundary, they have only a few hundred eV to deposit in the gas. It can be seen in Figure 6.1.2, for example, that removing events of a few hundred eV and adding that energy to the larger events would be difficult to detect given the resolution of this instrument and the logarithmic nature of the calculations. At a Y value of 6 keV/100 $\mu g\ cm^{-2}$, the interval used in the calculations is 1 keV/100 $\mu g\ cm^{-2}$ wide. Use of a linear interval for the calculations would not improve this much because the resolution at 6 keV is only 14% (Section 3.1).

A final, and rather unlikely, possibility is that the grid of the grid-walled detector is distorting the spectrum in such a way as to hide the wall effect. About 6% of the surface area of the detector used in these experiments is kovar wire. The photoelectric coefficient of this wire is quite different than that of tissue-like material, and it will be producing more than its share of photoelectrons. However, it is not the number of electrons which might affect these results.

The critical question is whether the mean of the energy deposition spectrum of the electrons from the grid differs significantly from that of the walls. If the mean of the distribution is higher than that for a truly wall-less detector, then the mean Y values for this detector will be shifted so that the number of events per unit dose will be decreased. Such a decrease would reduce the difference between solid- and grid-walled detector results. Because of the slowing down of photoelectrons in the kovar wire, it appears to be impossible to predict the energy deposition spectra of these electrons. It may be that the best way to resolve this problem would be to build a more nearly wall-less detector, preferably making all of the structure out of tissue-like materials.

Kellerer (1971a) indicates that the wall effect should decrease by a factor $(R/r)^{-2}$ as R, the container radius, increases. This prediction is based on the distribution of random chords inside a volume and the assumption that the initial track and the re-entry track are uncorrelated with respect to direction. No doubt this overestimates the number of re-entries for electrons since, in general back scatter becomes less probable with increasing angle. Kellerer estimated that $R/r = 4$ would result in considerably less than 1/16 of the number of re-entering events produced by a solid wall, and, therefore, stated that less than one percent of the total number of events should be affected in this case. Another factor which reduces the wall effect with increasing R/r is the stopping of low energy scattered electrons in the increasing thickness of gas between the scattering point and

the detector. For larger R/r ratios fewer scattered electrons will reach the detector to re-enter. The conditions necessary for the $(R/r)^{-2}$ relation to hold are most nearly met for high energy electrons where the scattering may be nearly isotropic, and a few scattered electrons will be absorbed before reaching the detector. Of the sources used in these experiments the ^{60}Co irradiation would be most likely to approach the $(R/r)^{-2}$ relationship.

If the fraction of the tracks which re-enter a solid-walled detector, a'; and the fraction of tracks which re-cross a detector inside a larger volume, x, are known the reduction in number of events per unit dose produced by a solid-walled detector relative to a grid-walled detector can be calculated. The number of events in a solid-walled detector is proportional to 1-a'; and the number in a wall-less detector inside a larger container is proportional to 1-xa'. Thus there are 1-a'/1-xa' times as many events in the solid-walled detector as in the grid-walled detector. The percent reduction in number of events as a result of the solid wall, ω, is then

$$\omega = 100\left(1 - \frac{1-a'}{1-xa'}\right) \qquad (6.1.1)$$

If a functional relationship between x and R/r is assumed, then an experimental value of ω from Table 6.1.1 or 6.2.1 can be used to determine a', and ω for another value of R/r can be calculated. If x is assumed to be $(R/r)^{-2}$ it is equal to 0.0625 for R/r = 4 and 0.0278 for R/r = 6. Applying Equation 6.1.1 to the ^{60}Co data for R/r = 4, where ω = 0.09, a' is found to be 0.096. Using this value

of a' to calculate the expected value of ω for R/r = 6 one gets 0.095. This value of ω is significantly less than the experimental value of 0.14 shown in Table 6.1.1. It seems unlikely that this difference would be due to error in the experiment considering the consistency of the ^{60}Co data in Figure 6.1.4. This would seem to indicate that $(R/r)^{-2}$ is not a good estimate of the way the wall effect varies with container size.

It might appear that the partial wall of the grid-walled detector could distort these results and cause the above discrepancy in the variation of the wall effect with R/r. The 17% solid surface on the grid-walled detector can be taken into account by subtracting 0.17a' events from the number previously given for the grid-walled case.

$$\omega = 100 \left(1 - \frac{1 - a'}{1 - 0.17a' - xa'}\right) \qquad (6.4.2)$$

This gives a correction in the right direction, but it is quite small. For the ^{60}Co example above, a' would be 0.103 based on R/r = 4 data, and the recalculated ω for R/r = 6 would be 0.096 rather than 0.095. Equation (6.4.2) indicates that the correction for a partial wall will not change the ratio of ω's for R/r = 4 to R/r = 6 appreciably until considerably more than half of the wall is solid.

No complete explanation of the discrepancy between observation and predicted change in the wall effect with container size can be given at this time. The production of energetic delta rays with their relatively high degree of angular correlation could contribute to a

slower decrease in the wall effect, but they should account for only a small fraction of the total wall effect observed for high energy electrons (Kellerer, 1971b). The ω values (Table 6.1.1) for filtered 250 kVp x-rays more nearly fit the $(R/r)^{-2}$ model, but this is probably due to electrons stopping in the gas before reaching the detector.

Chapter 7

ENERGY DEPOSITION SPECTRA FOR PHOTON IRRADIATIONS

There are a number of factors to consider when the deposition of energy is compared to models of biological injury or physical effects. Chief among these is the variation in energy deposition with two parameters, site size and type of irradiation. Within each of these factors one may want to make comparisons on the basis of several different types of distributions. Among these are the distribution of number of events, the distribution of dose for single events, the distribution of accumulated ionization for multiple event irradiations, and the number of events larger than various threshold energy transfers for a given dose. These factors and the effect of scattered photons will be considered in the following sections.

7.1 Site Size

Variation of microdosimetric parameters with site size is of interest when considering the size of the biological or chemical system which serves as the sensitive unit for the initiation of damage. Which particular parameter, $f(\Delta)$, $d(Y)$, etc. will be of interest depends on the damage model being considered.

The curves at the top of Figure 7.1.1 show the variation in the number of events per logarithmic interval for filtered 250 kVp

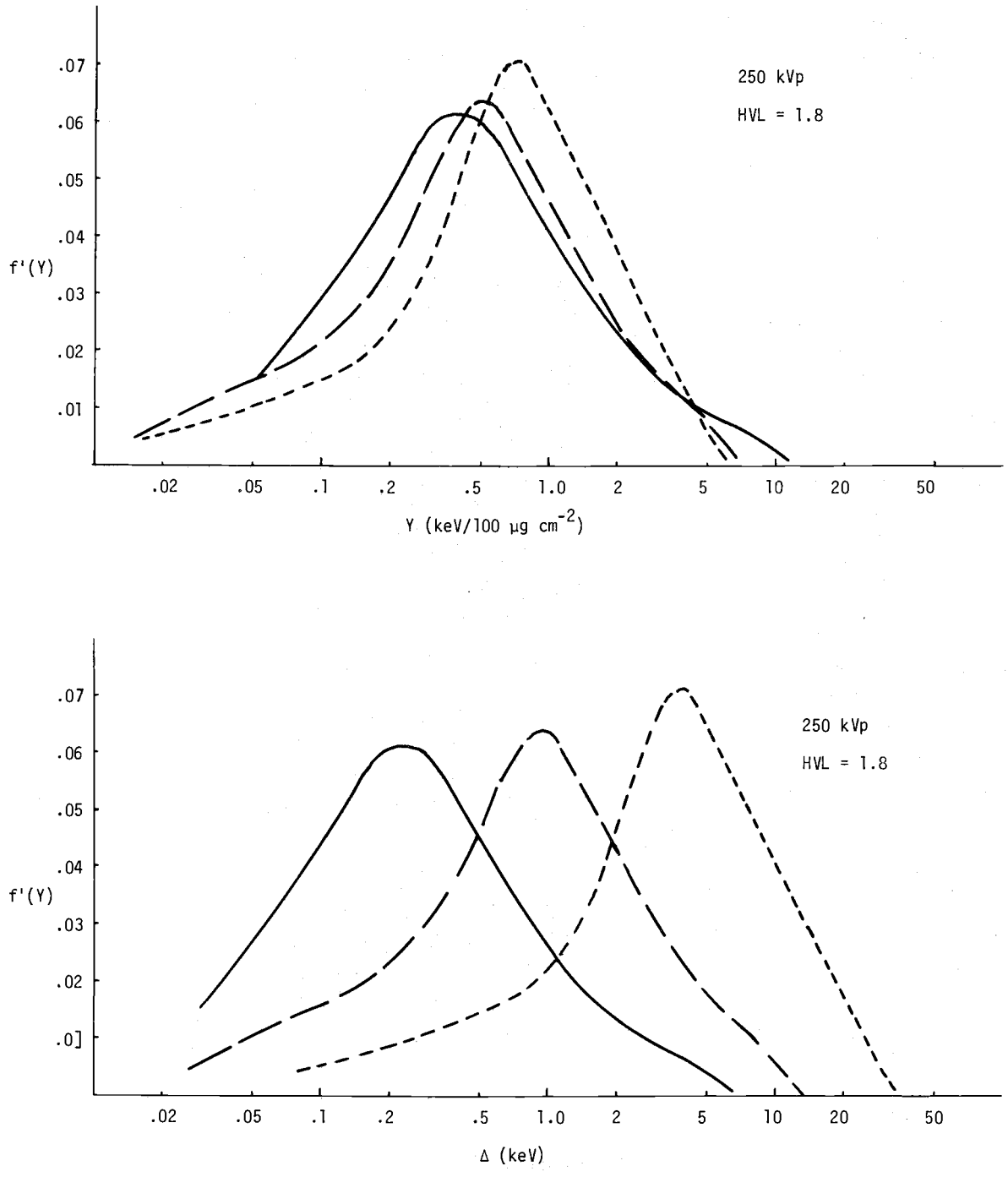

Figure 7.1.1 Variation of f'(Y) and f'(Δ) with site size; 58 µg cm^{-2} ———, 185 µg cm^{-2} — — —, 555 µg cm^{-2} - - - -.

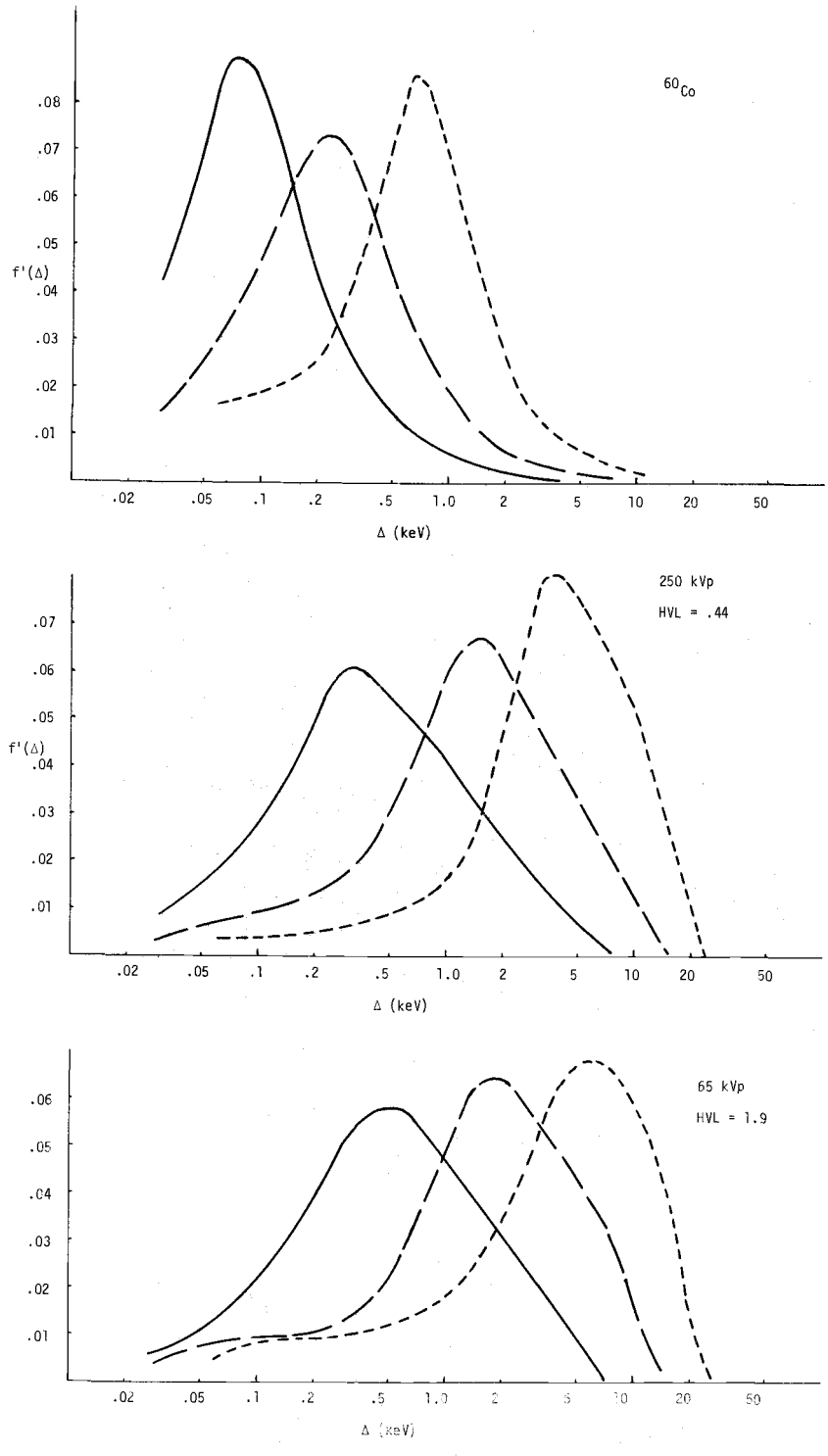

Figure 7.1.2 Variation of f'(Δ) with site size; 58 μg cm^{-2} ———, 185 μg cm^{-2} — —, 555 μg cm^{-2} - - - -.

radiation as a function of event size, f'(Y), for several site sizes. These results and those that follow are for the grid-walled detector in the large plastic sphere where R/r = 6, except for the 65 kVp data where R/r = 4. In either case wall effects are minimal. The second part of Figure 7.1.1 shows the same data in terms of ionization Δ. Differences between these two sets of curves is more apparent than real. The f'(Y) distribution stresses the average rate of energy deposition along the tracks which make up the events. It is particularly convenient when comparing spectra in different size sites. The f'(Δ) distribution emphasizes the total energy absorbed in the event. This is probably more useful when considering models of biological damage since these normally refer to the energy absorbed.
Figure 7.1.2 gives the equivalent Δ distributions for the three other irradiation sources used in this study.

The means and variances in these distributions expressed in terms of Y are given in Table 6.1.1. In the case of each radiation the expected tendency of the mean event size and its relative variance to decrease with increasing site size is shown. The mean event size decreases because the maximum dE/dx is maintained for only a short segment of an electron's track so that in the larger sites a relatively larger fraction of each track is at less than the maximum dE/dx. The variance decreases since for longer tracks the number of collisions along the track increases and the straggling becomes less important.

It may also be useful to consider the fraction of the dose in the single event spectrum per interval of Y or Δ. This density function is given in Figure 7.1.3 for filtered 250 kVp x-rays and in Figures 7.1.4 and 7.1.5 for the other irradiation sources. Tables listing the means and variances of these density functions can be found in Appendix I. Again, the mean (and the maximum) of the Δ distribution increases with the site diameter but is not quite proportional to it.

7.2 Differences Between Various Types of Radiations

One of the factors which can be varied when studying the response of a system to ionizing radiation, and thus can be used to provide information about it is the type of irradiation. It is known that at least for some systems 250 kVp x-rays are more effective than ^{60}Co gammas (Sinclair, Gunter and Cole, 1959; Hall, 1961; Humphrey and Sinclair, 1963). Since there are significant differences in the microdosimetric distributions of x and gamma radiations, it is natural to expect that at least some of the difference in biological effect might be related to differences in energy deposition.

Figures 7.2.1 and 7.2.2 compare some of the data given in Figures 7.1.1 through 7.1.5 for different radiation sources. It is immediately clear that the differences in the distribution of both the number of events and energy transfer with Δ are quite large. Table 7.2.1 compares the vaules of $\overline{Y}_p$ of the other radiations used in this study to those of ^{60}Co as a function of the site size. These

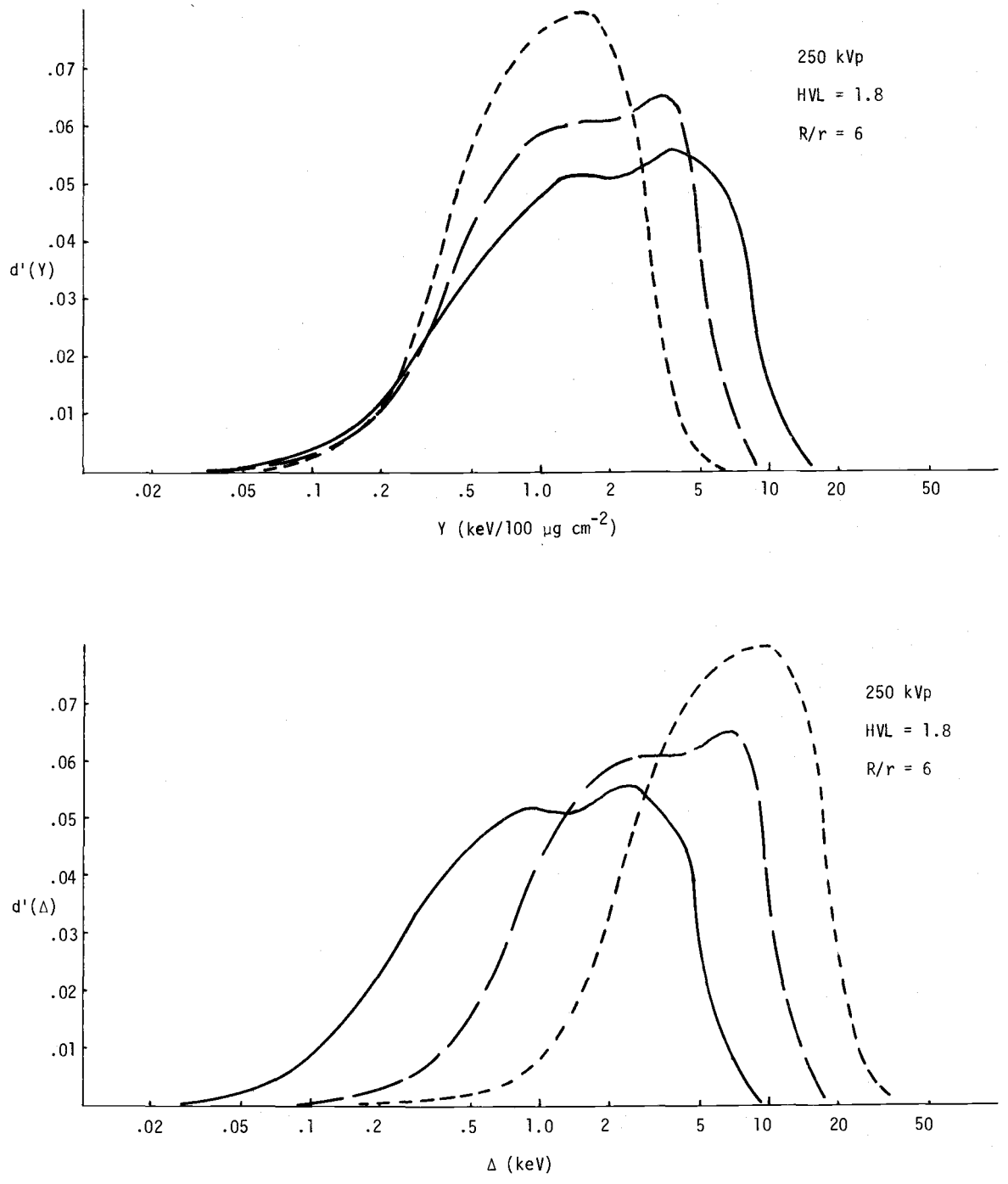

Figure 7.1.3 Effect of site size on d'(Y) and d'(Δ); 58 μg cm^{-2} ———, 185 μg cm^{-2} — —, 555 μg cm^{-2} - - - -.

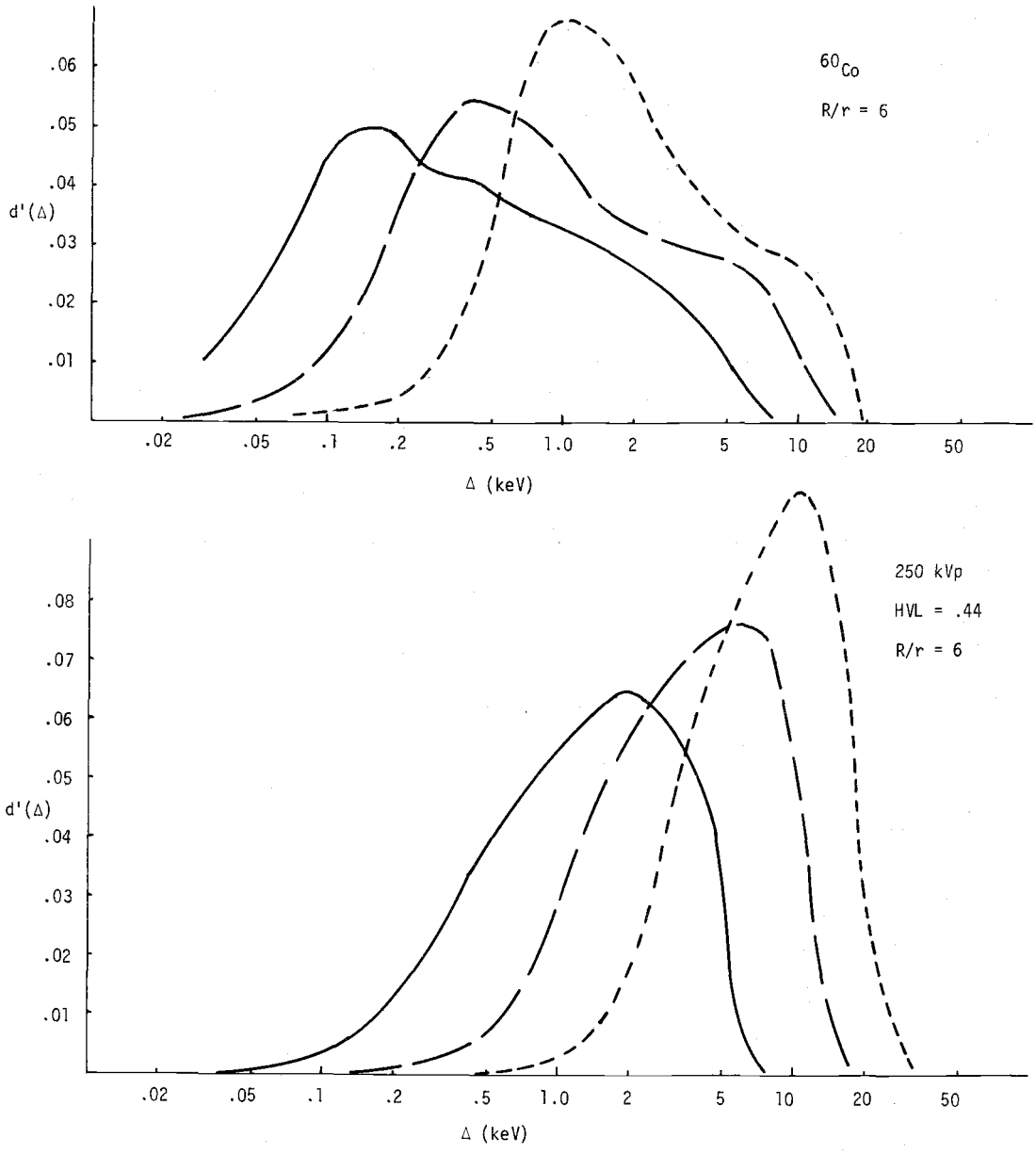

Figure 7.1.4 Effect of site size on d'(Δ); 58 μg cm^{-2} ———, 185 μg cm^{-2} — —, 555 μg cm^{-2} - - - -.

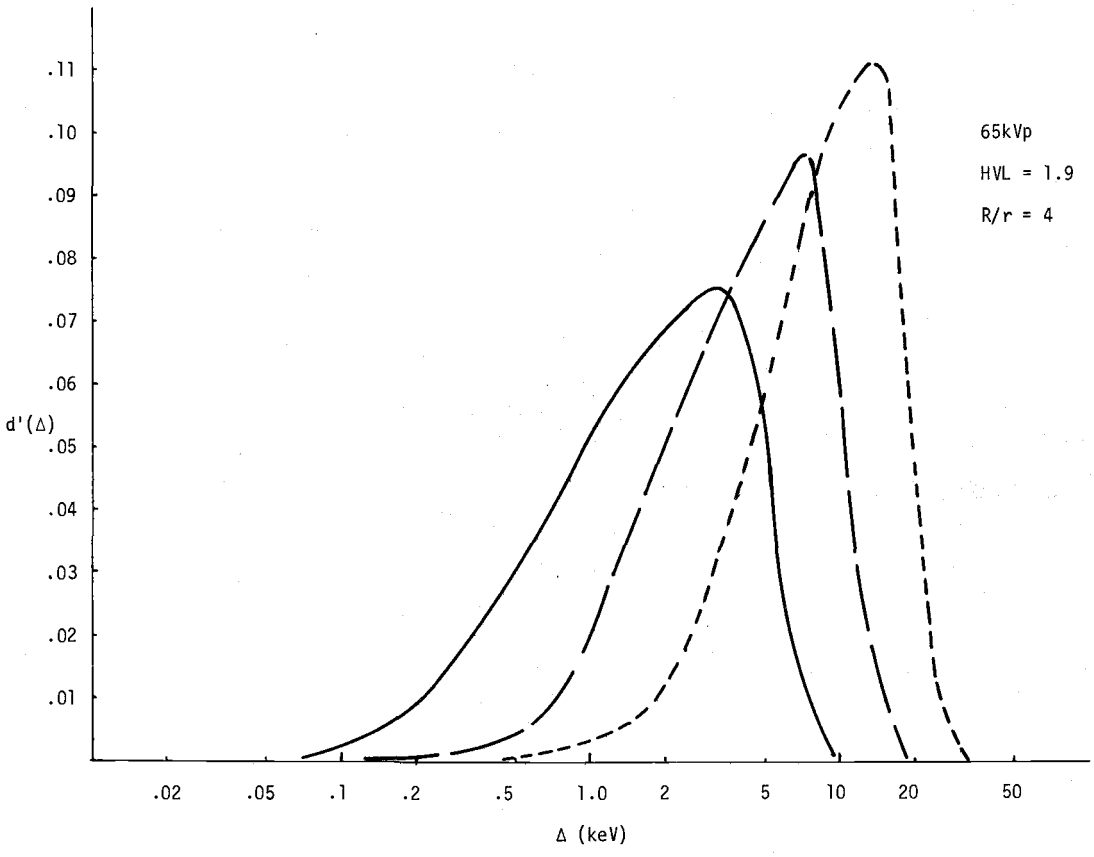

Figure 7.1.5 Effect of site size on d'(Δ); 52 μg cm^{-2} ———, 185 μg cm^{-2} — —, 555 μg cm^{-2} - - - - .

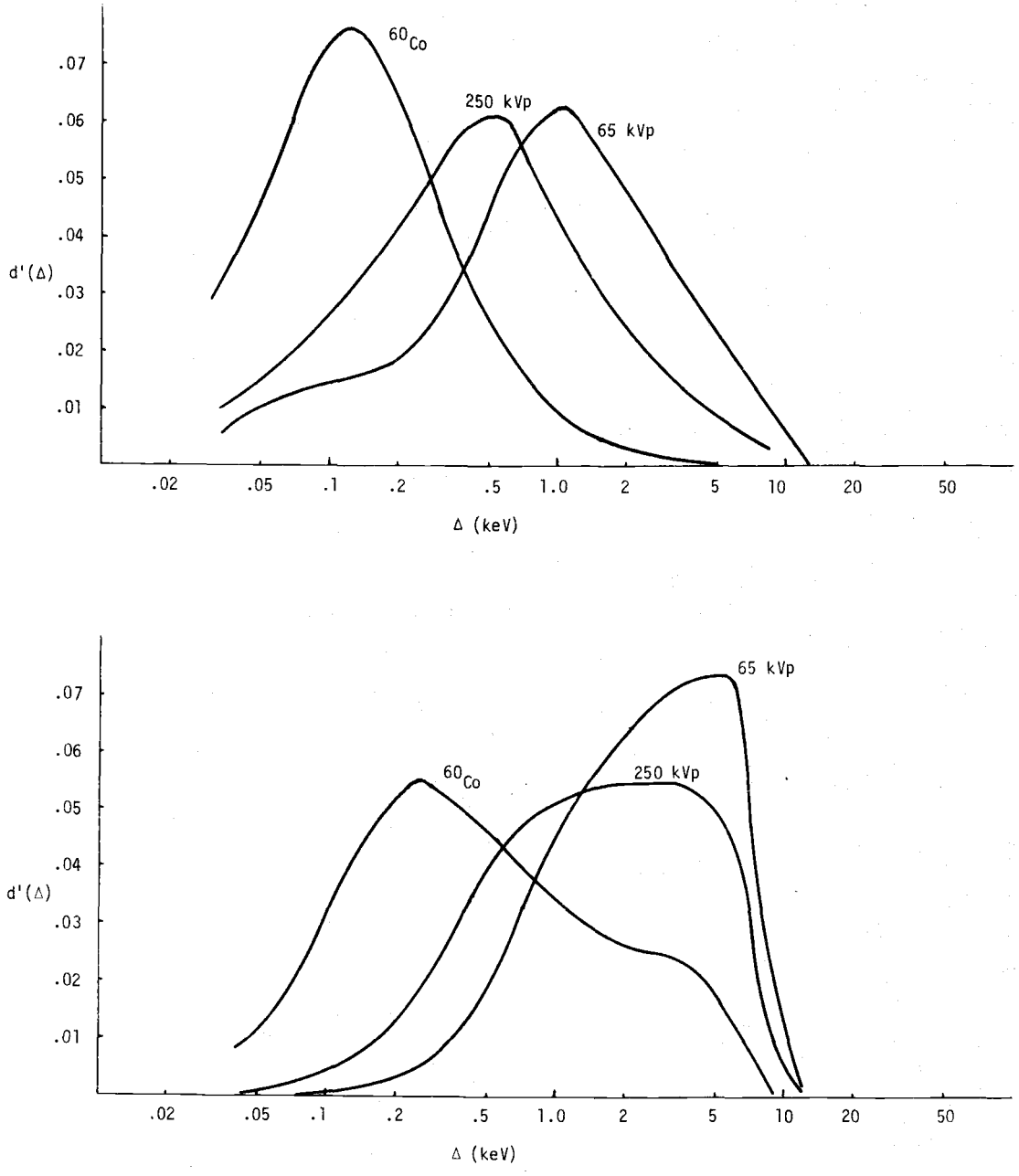

Figure 7.2.1 Comparison of ^{60}Co, filtered 250 kVp, and unfiltered 65 kVp x-rays in terms of f'(Δ) and d'(Δ) for a 92 μg cm^{-2} site

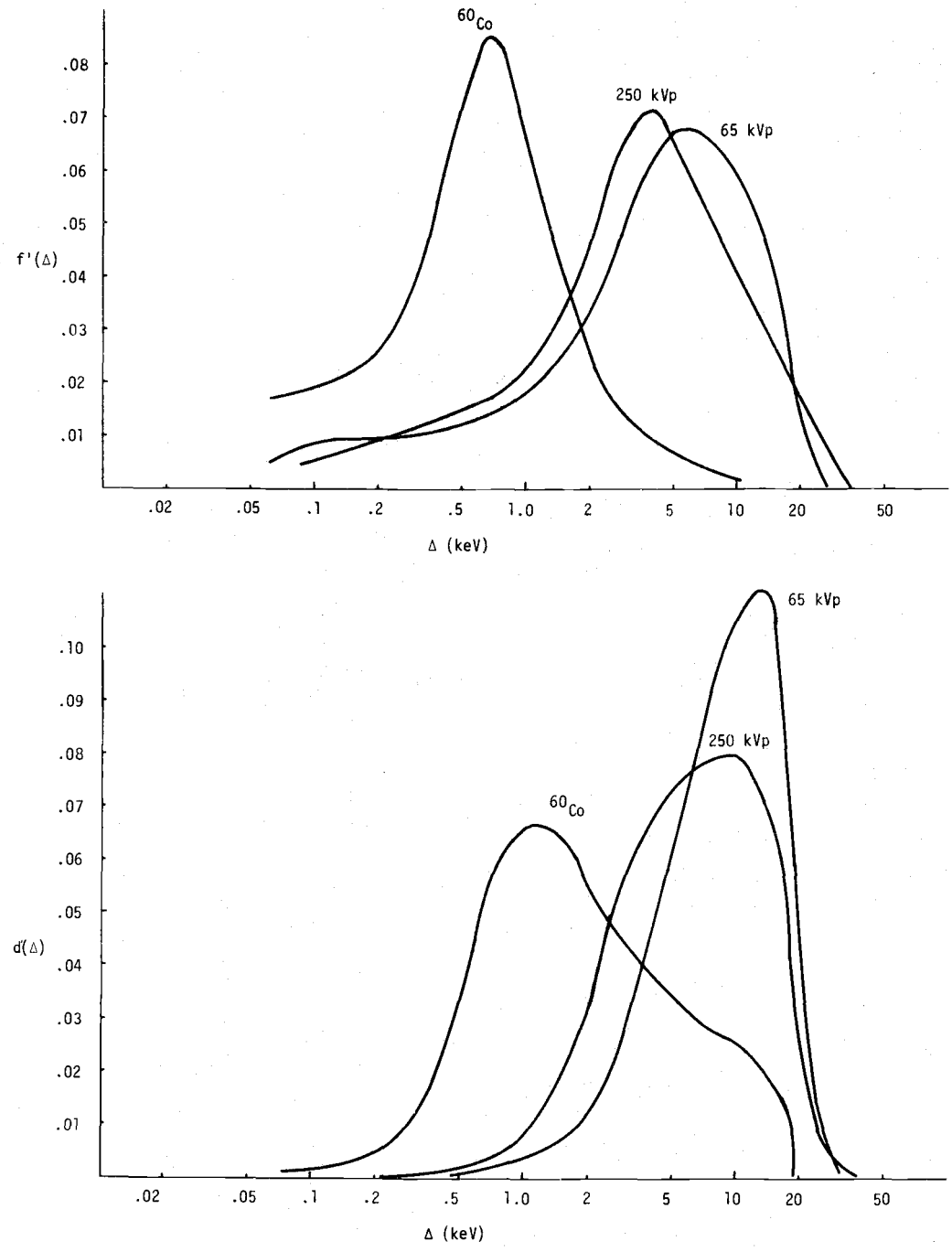

Figure 7.2.2 Comparison of ^{60}Co, filtered 250 kVp, and unfiltered 65 kVp x-rays in terms of f'(Δ) and d'(Δ) for a 555 μg cm^{-2} site

Table 7.2.1

COMPARISON OF $\overline{Y}_p$ OF X-RAYS TO ^{60}Co GAMMA RAYS AS A FUNCTION OF SITE SIZE

b ($\mu g\ cm^{-2}$)	^{60}Co $\overline{Y}_p$ (keV/micron)	250 kVp filtered $\overline{Y}_p$ (keV/micron)	$\overline{Y}_p/\overline{Y}_p\ ^{60}Co$	250 kVp unfiltered $\overline{Y}_p$ (keV/micron)	$\overline{Y}_p/\overline{Y}_p\ ^{60}Co$	65 kVp $\overline{Y}_p$ (kev/micron)	$\overline{Y}_p/\overline{Y}_p\ ^{60}Co$
58	.319	.904	2.84	1.285	4.05	1.68	5.29
92	.253	.815	3.22	1.232	4.88	1.462	5.78
185	.221	.799	3.61	1.159	5.24	1.353	6.14
278	.197	.739	3.76	1.094	5.55	1.235	6.27
555	.183	.678	3.70	.928	5.07		

data indicate that even for relatively large changes in site size the difference between the various radiations is relatively constant.

In simple hit theory models (i.e. where the effect of successive events is not cumulative) the number of events greater than Δ as a function of Δ, $\Phi(\Delta)$, is of interest. Curves showing the $\Phi(\Delta)$ distributions are given in Figures 7.2.3, 7.2.4 and 7.2.5; numerical data can be found in Appendix I. If one distribution has more small events per unit dose than the other, it must have fewer events in some other range and, therefore, $\Phi(\Delta)$ curves for any pair of radiations, at one site size, must cross. An interesting point in comparing two radiations is the value of Δ at this crossing. For example, it can be seen from Figure 7.2.3 that, for a 92 $\mu g/cm^2$ site, if only events above 0.33 keV are considered, filtered 250 kVp x-rays produce a larger number per unit dose, than do ^{60}Co gammas, while if all events above some value less than 0.33 keV are counted, then ^{60}Co has the larger number. Given the assumption that the system being investigated doesn't accumulate damage from single events then if the x-rays are found to be more effective than the ^{60}Co events larger than 0.33 keV must be primarily responsible for the damage. One could then go on to compare various additional radiations for their relative biological effectiveness and their $\Phi(\Delta)$ spectra.

The various functions of T, the total energy imparted to the site by successive events, is of interest if it is assumed that the effects of successive ionizations are accumulated without repair until a damaging level is reached. Figure 7.2.5 illustrates the change in

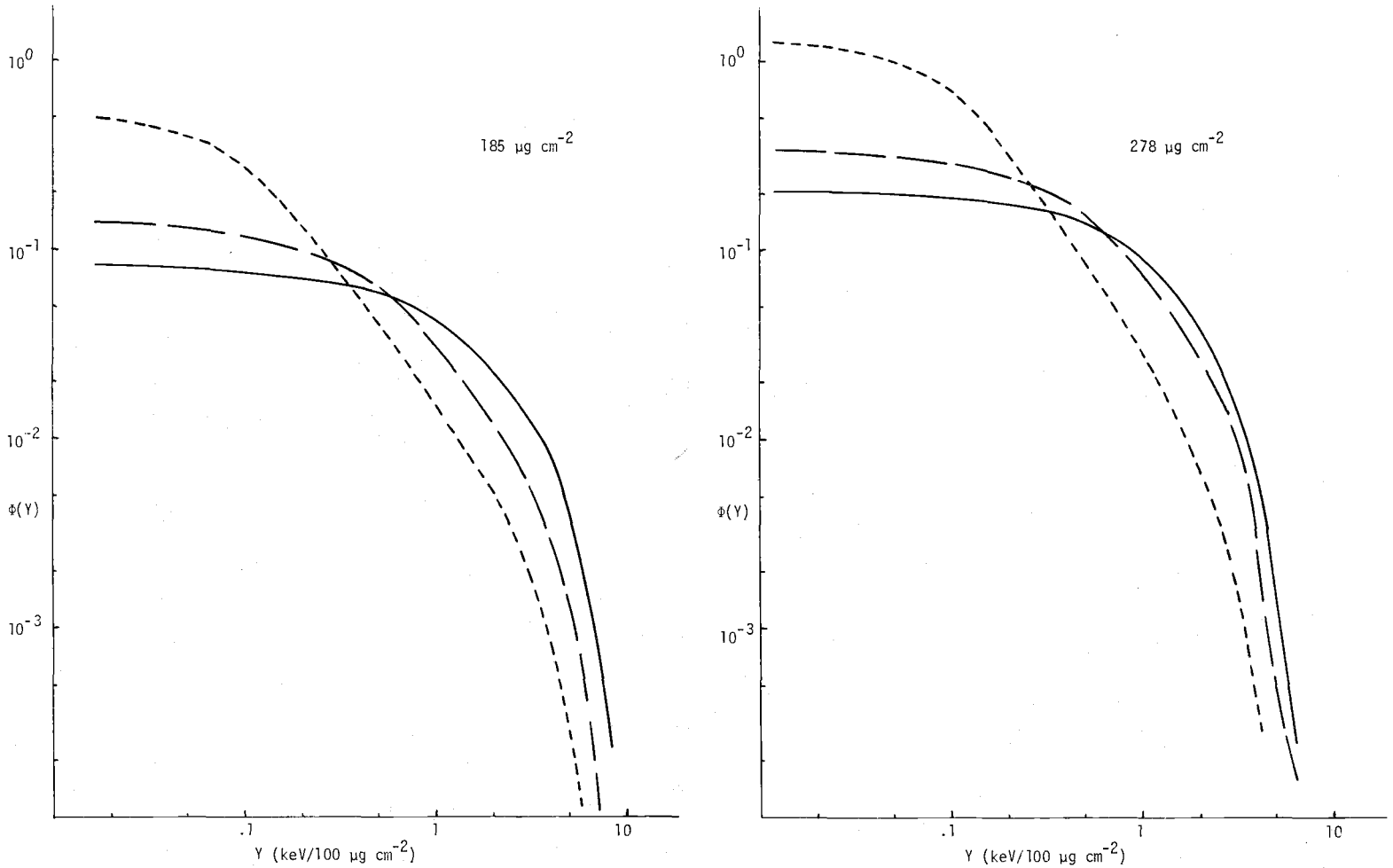

Figure 7.2.3 Comparison of the event frequencies, Φ(Y), for ^{60}Co gamma - - - -, filtered 250 kVp — — and unfiltered 65 kVp x-rays ———.

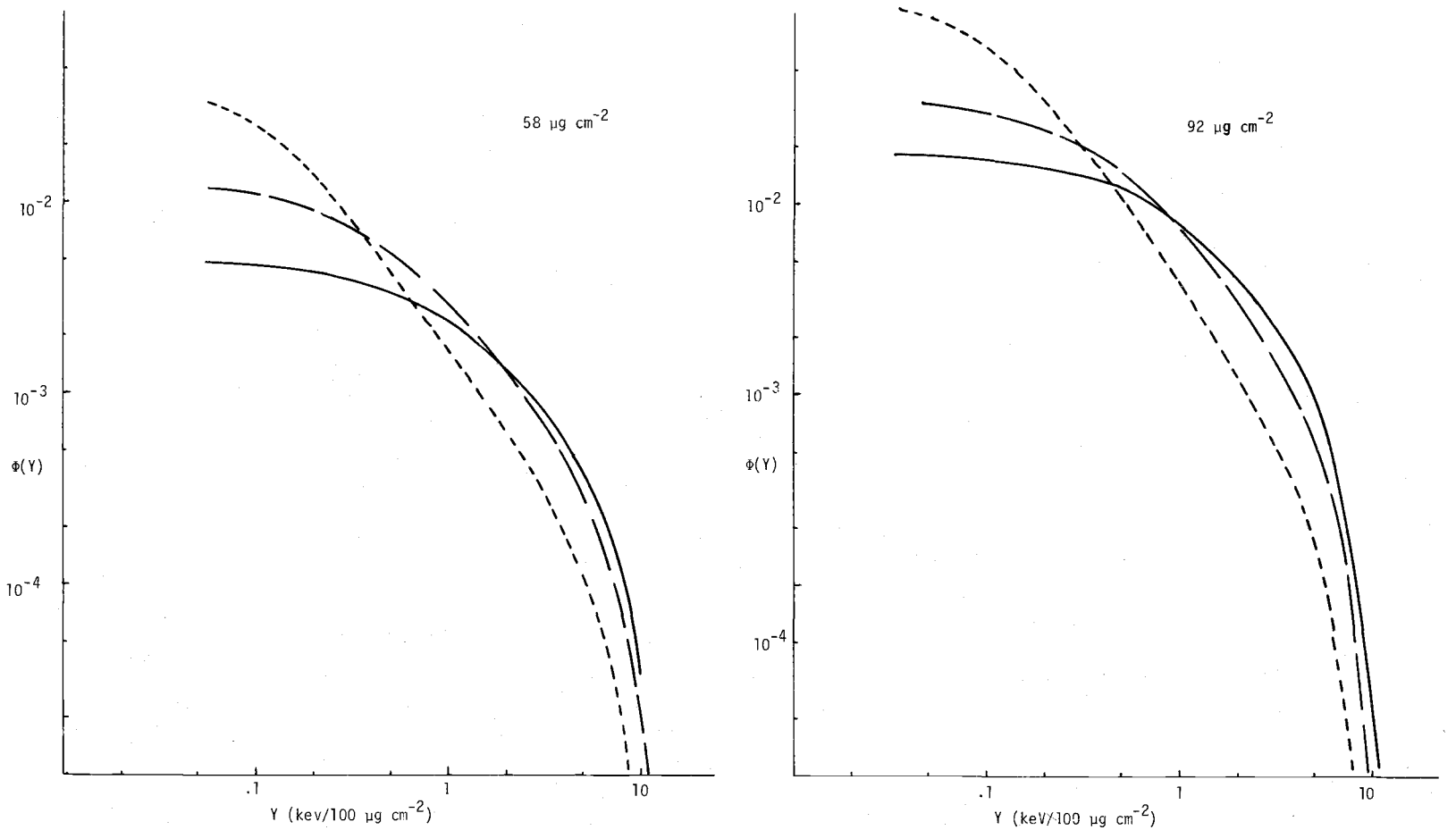

Figure 7.2.4 Comparison of the event frequencies, Φ(Y), for ^{60}Co gamma - - - -, filtered 250 kVp — —, and unfiltered 65 kVp x-rays ———.

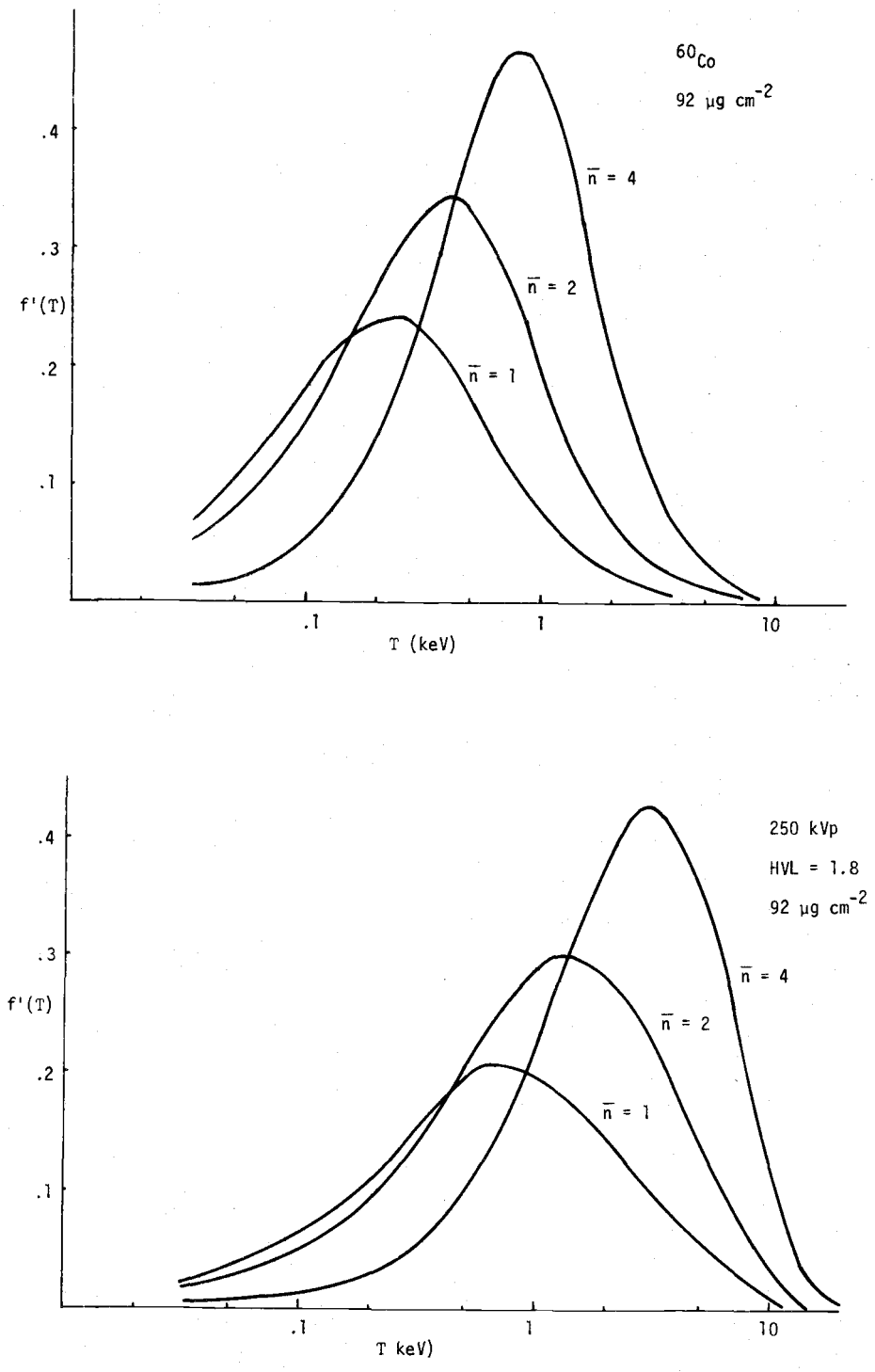

Figure 7.2.5 f'(T) for various mean number of events, $\bar{n}$, for ^{60}Co and 250 kVp x-rays

f(T) with the average number of events in the site. As expected this distribution becomes narrower and more symmetric with increasing numbers of collisions. Various radiations can be compared in terms of T in two ways, one can choose a mean number of events, $\bar{n}$, and compare the probabilities of the radiations producing a given accumulated ionization in that number of events, or one can choose an average energy accumulation (i.e., dose) and compare probabilities of the radiations producing given accumulated ionization at that dose. Figures 7.2.6 and 7.2.7 illustrate these two approaches for the same set of irradiations for a site diameter of 92 μg cm^{-2}. It is clear that these comparisons can be turned around to ask, for example, the mean number of events that would be necessary for the mean energy accumulation, $\bar{T}$, from ^{60}Co gammas to equal $\bar{T}$ from 250 kVp x-rays with a mean number of events equal to two. This is illustrated in Figure 7.2.8.

Again, when investigating most dose effect models it is more useful to know the total number of accumulated ionizations greater than some minimum. The upper part of Figure 7.2.9 compares three irradiations at total doses which result in a mean collision number of two. Notice that at these doses the probability of even a relatively small accumulated ionization (0.1 keV) is less than 0.9 because there is a significant probability of no event at all occurring. When the mean number of events is increased to eight (lower part of Figure 7.2.9) the curves become steeper, but the separation between

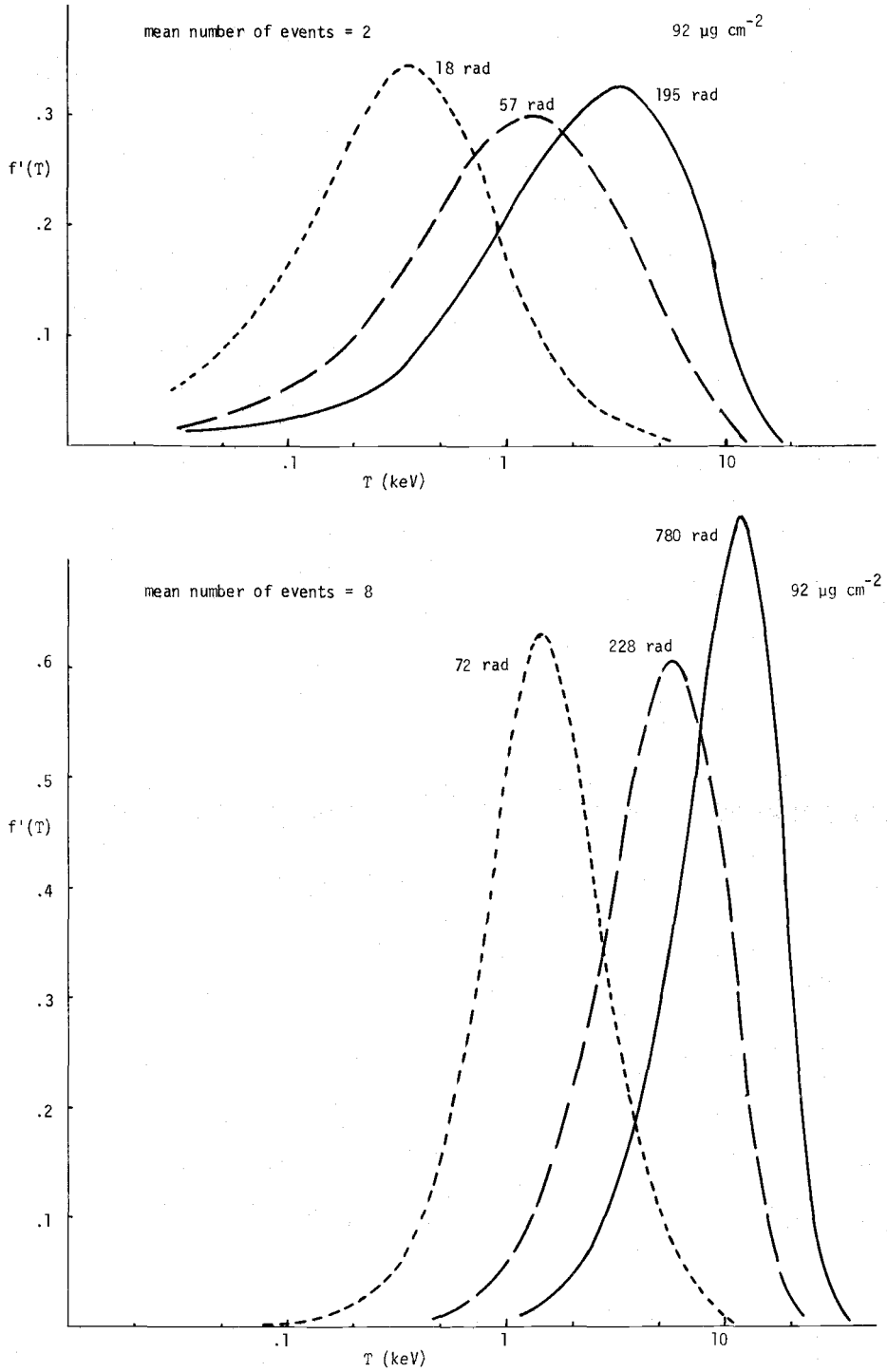

Figure 7.2.6 f'(T) in 92 µg cm^{-2} site for ^{60}Co - - - -, filtered 250 kVp x-ray — —, and unfiltered 65 kVp x-ray ————.

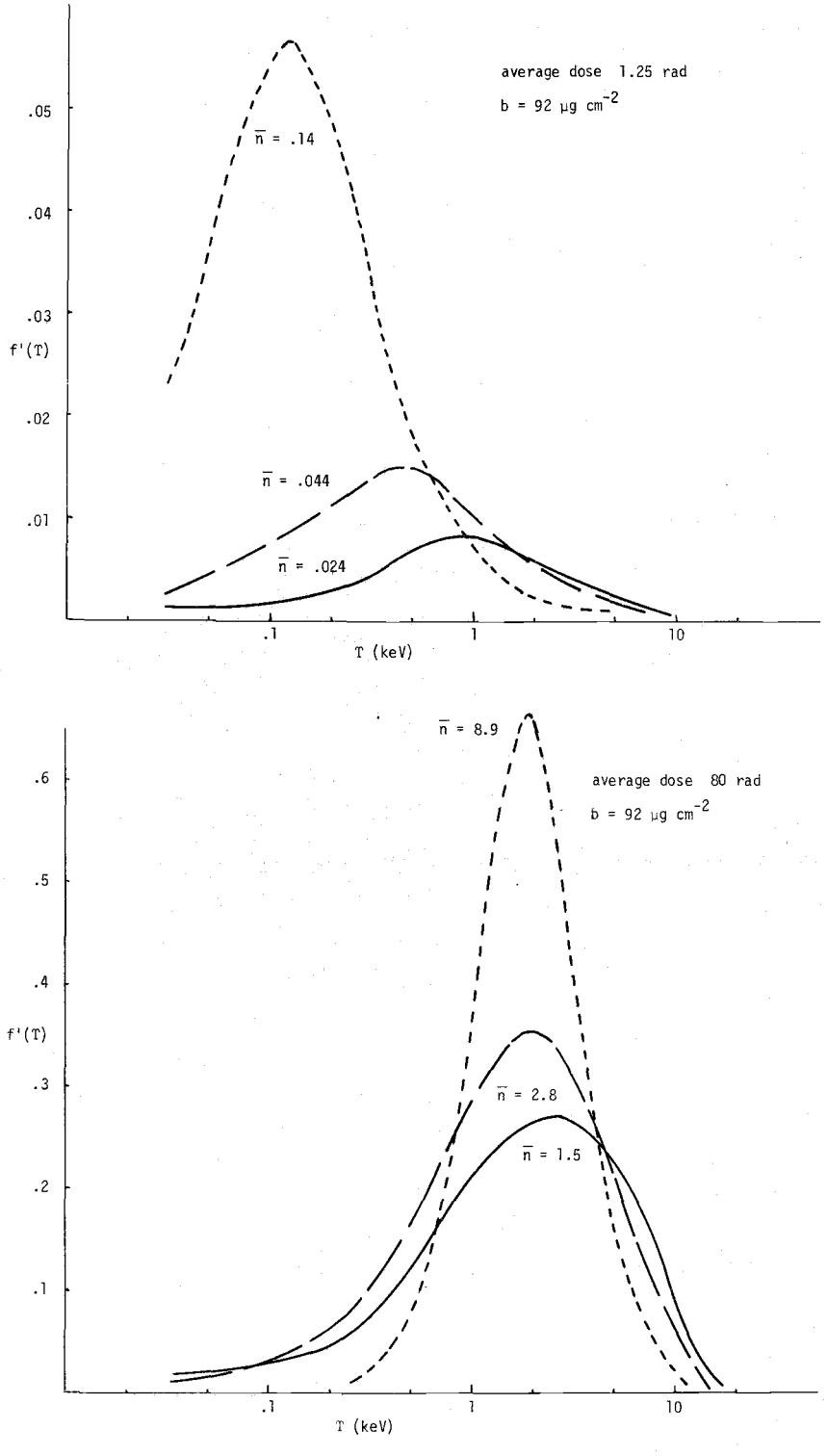

Figure 7.2.7 f'(T) in 92 μg cm^{-2} site for ^{60}Co ----, filtered 250 kVp x-ray —— —, and unfiltered 65 kVp x-ray ——.

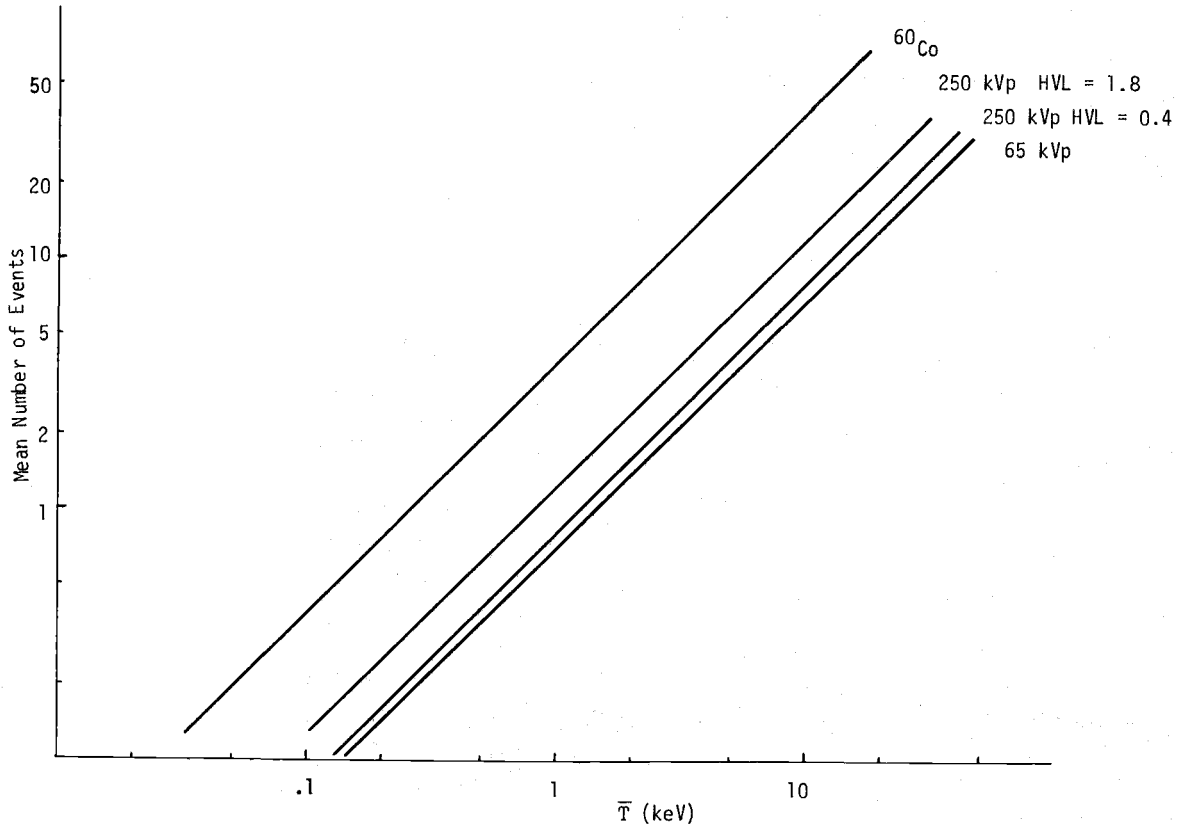

Figure 7.2.8 Mean number of events as a function of $\overline{T}$, the average accumulated energy

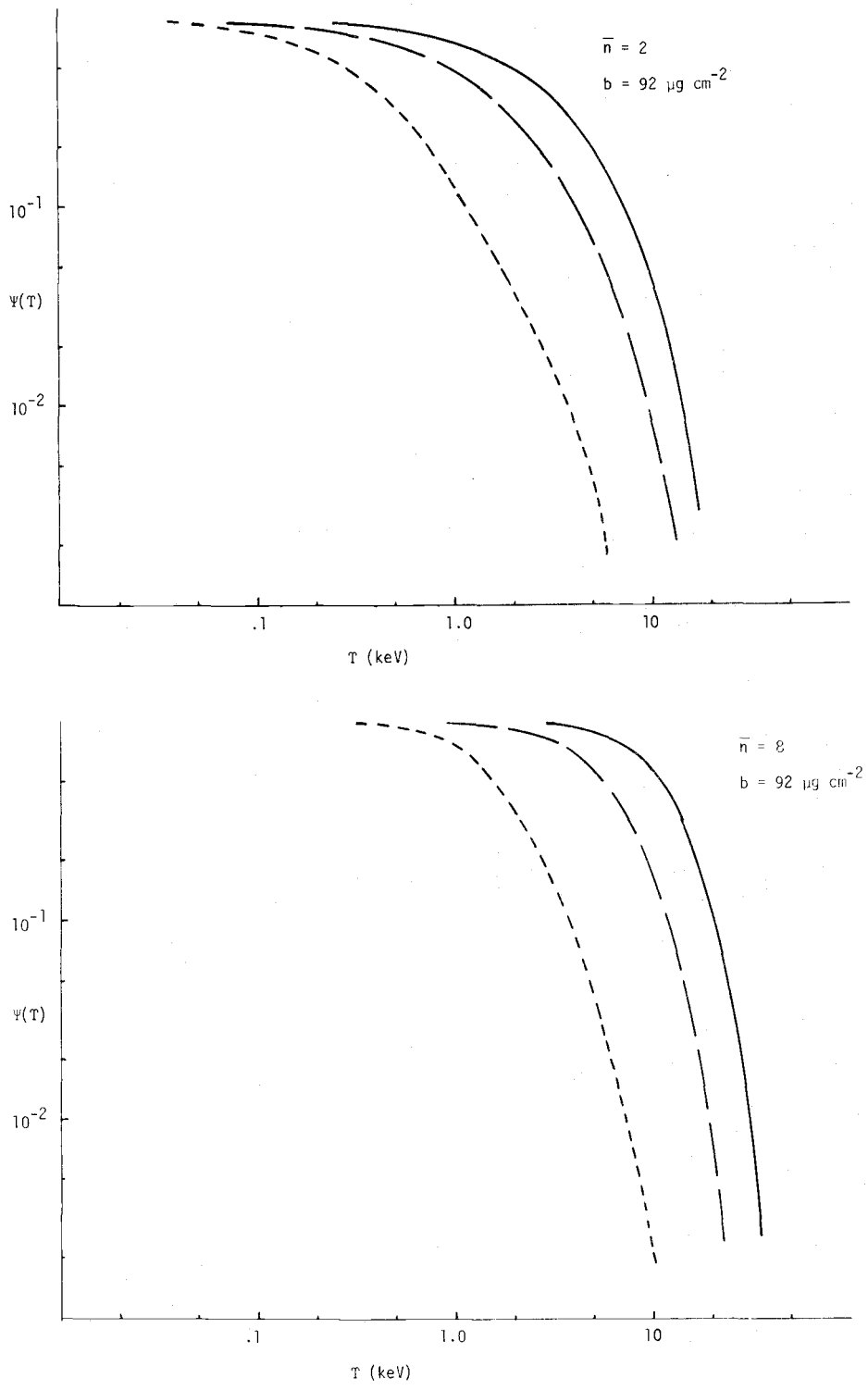

Figure 7.2.9 Ψ(T) for ^{60}Co - - - - , filtered 250 kVp —— ——, and unfiltered 65 kVp x-rays ——— for mean collision numbers ($\bar{n}$) of 2 and 8

them remains relatively constant. This is a result of the difference between the $\overline{Y}_p$'s of the various radiations, $\overline{T}$ is just $\overline{n}\,\overline{Y}_p$. However, when $\Psi(T)$ is plotted for equal doses, Figure 7.2.10, the curves become more similar with increasing dose. This is a reflection of the fact that all of the f(T) distributions tend toward narrow gaussian curves, with increasing numbers of events.

7.3 Effects of Scattered Radiation

Since most biological irradiations are made with significant back-scattering material and at various depths in an absorbing medium, the effects of these situations on the event spectra were checked. Lead is a common scattering material when ^{60}Co irradiators are used so 1/2 cm of lead was placed immediately behind the detector (outside the sphere). No difference could be seen in N(Y) spectra for ^{60}Co taken with and without the lead back scatterer. To further test for the effects of scattered radiation a 5 cm layer of tissue equivalent rubber was placed in the beam just in front of the detector and it was exposed to 250 kVp filtered x-rays; for ^{60}Co gammas a 7.5 cm layer was used. These thicknesses reduce the unscattered beams to approximately 1/3 of their original intensity. Little difference could be seen in the resulting distributions, as illustrated in Figures 7.3.1 and 7.3.2.

These conditions are not exact representations of the conditions for cells irradiated in a ^{60}Co unit or inside a large body of absorbing material, but are close enough that the lack of noticeable effect indicates that major changes in energy deposition spectra due

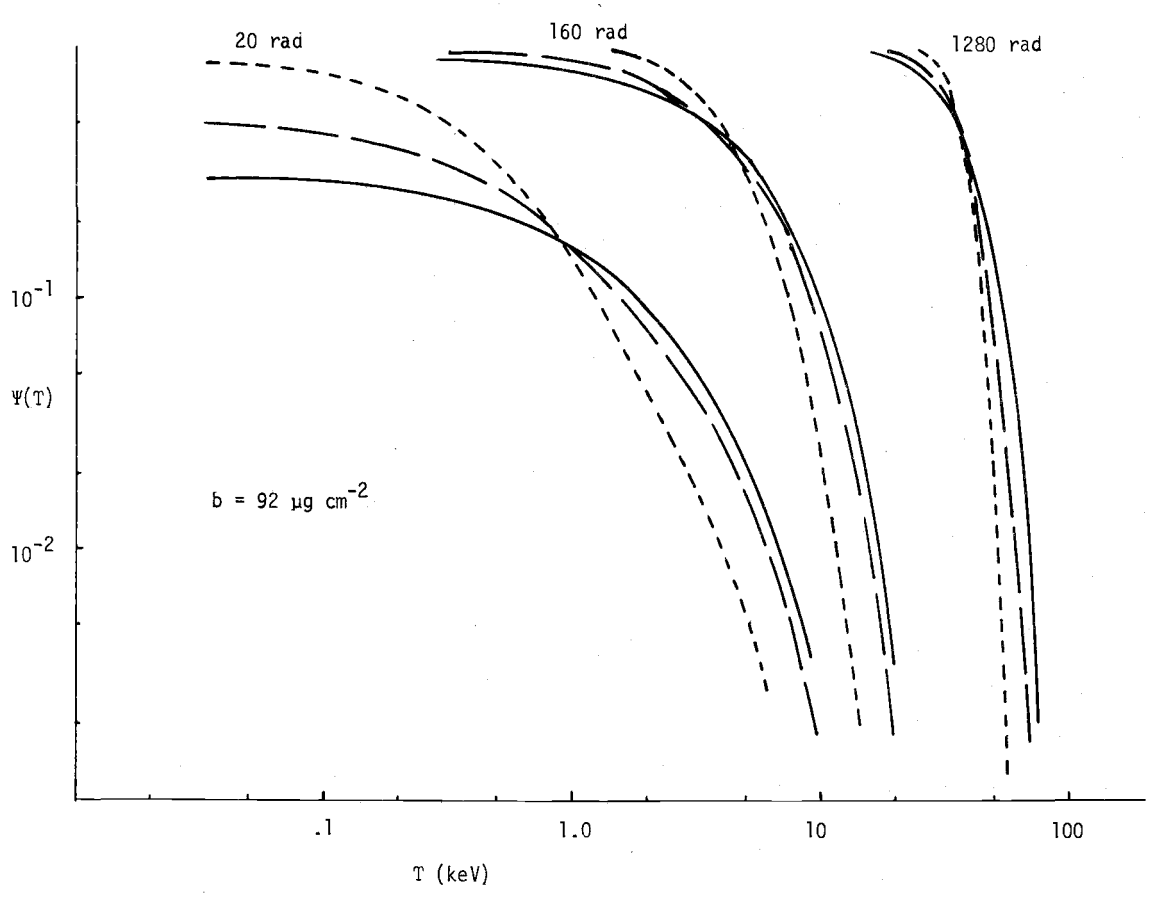

Figure 7.2.10 Ψ(T) for ^{60}Co - - - - , filtered 250 kVp — —, and unfiltered 65 kVp x-rays ———for three different dose levels.

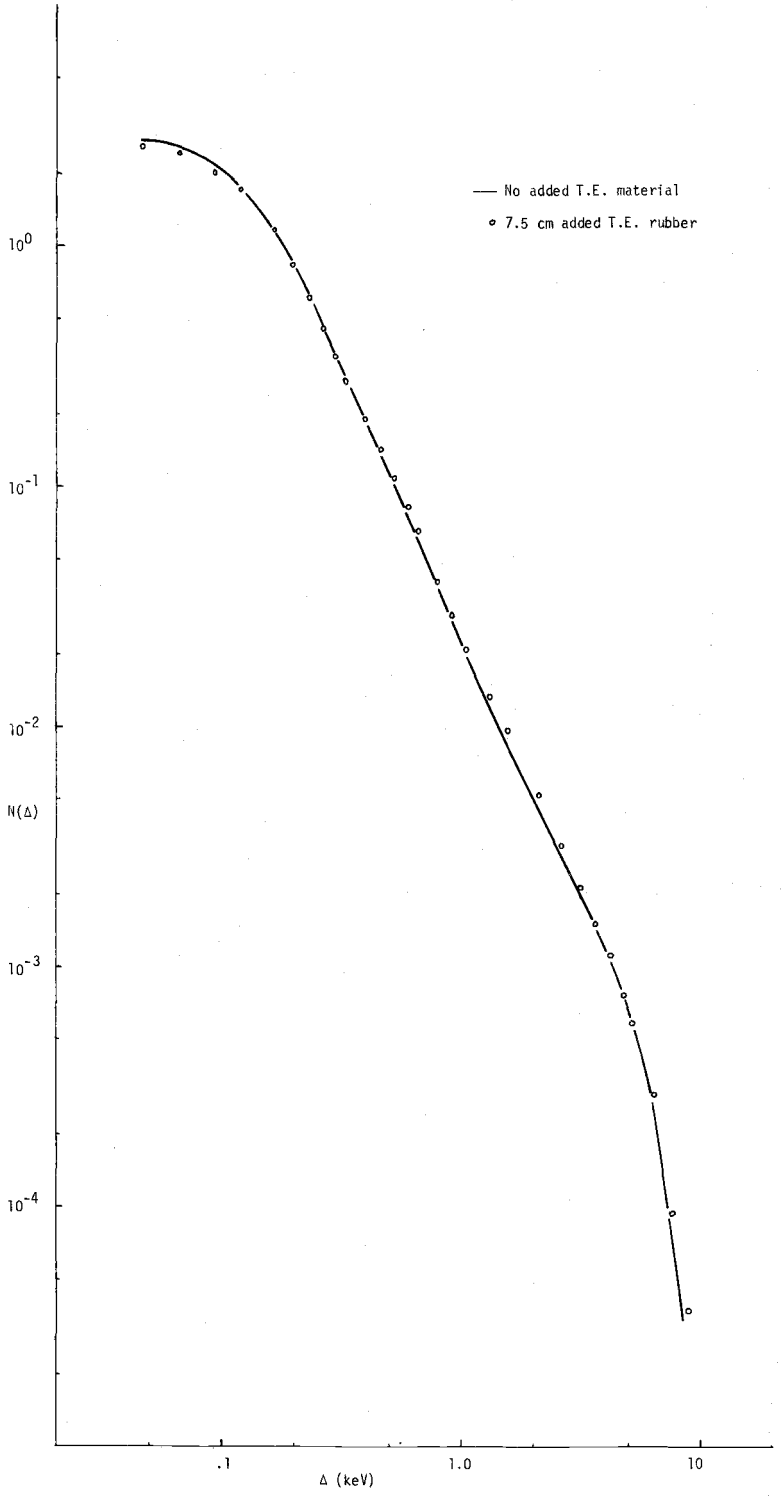

Figure 7.3.1 Effect of 7.5 cm of T.E. scattering material on N(Δ) for ^{60}Co gamma irradiation

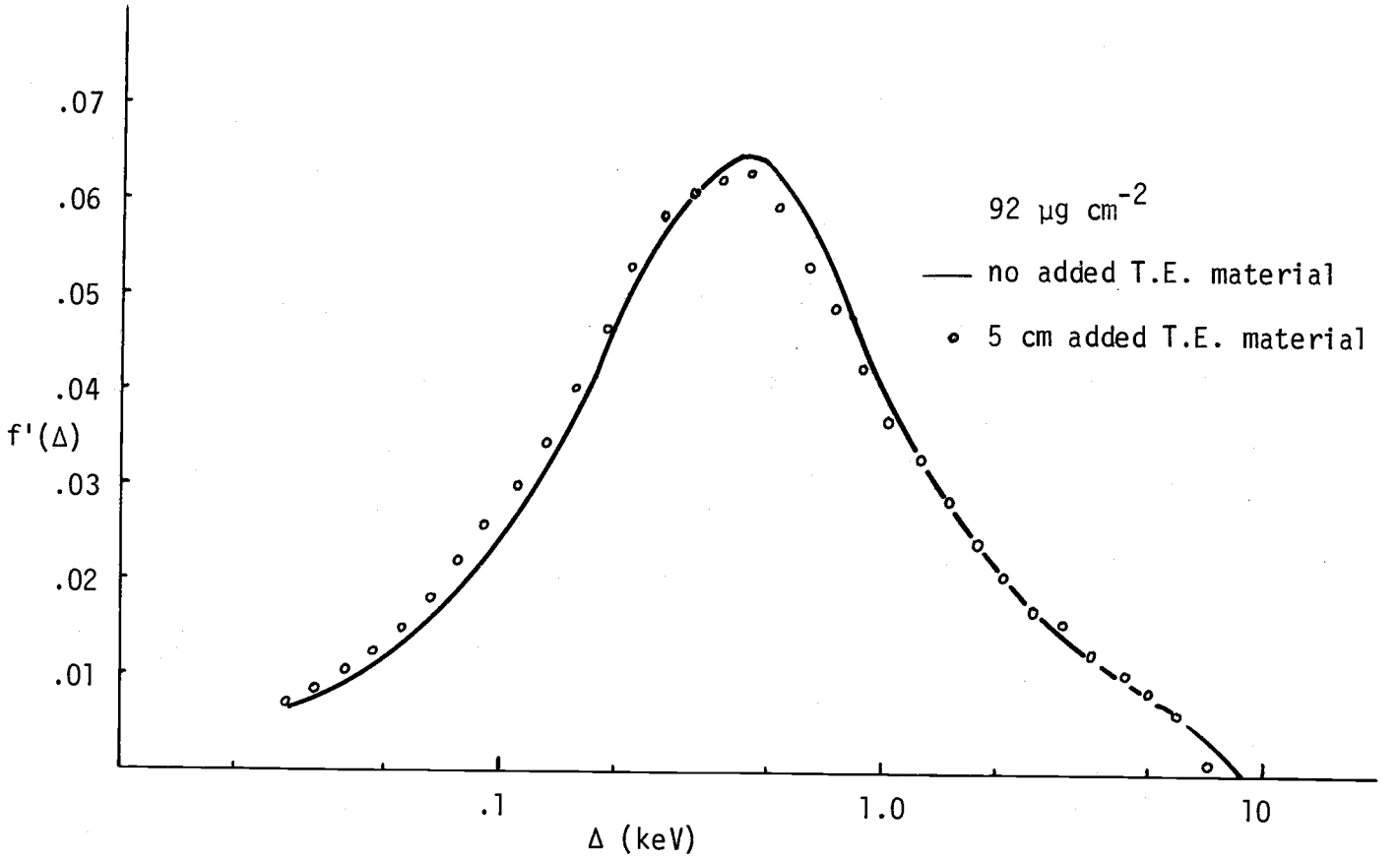

Figure 7.3.2 Effect of 5 cm of scattering material on f(Δ) for filtered 250 kVp x-rays.

to scattered radiation are quite unlikely. One aspect which is not covered in this experiment is the possibility of spectral changes within the first few mm of depth in an absorber. Such changes might result from changes in the electron spectrum with depth, but this cannot be investigated with the present equipment because of the need for a relatively thick plastic vacuum container.

7.4 Discussion

The distributions described above behave in about the way one would expect. Microdosimetry distributions are sometimes thought of as an extension of LET theory which has been well developed (Bruce, Pearson and Freedhoff, 1963; ICRU, 1970; for example). That is, Δ for an event is LET averaged over the path length for that event (with possibly a small correction for entrance and exit of delta rays). Thus the decrease in Y with increasing b which was described in Section 7.1 was easily anticipated.

The shape of the f(Y) distribution is more difficult to predict because it includes the straggling of the energy transfer rate and also the path length distribution. However, it is possible to make useful qualitative comparisons of the differences between various radiations. For example, the maximum Y value for any electron spectrum in a given size site should be about the same since the events of maximum Y are those which include the ends of tracks. The frequency with which these large events occur will depend on the fraction of the path length which is at the end of tracks. Thus radiations

such as ^{60}Co which produce many high energy electrons will have relatively few large events, while large events will be relatively more frequent for x-rays. As the x-ray energy decreases the resulting electron energies and path lengths decrease with a consequent increase in the frequency of large events. Similarly small events result from electrons at minimum LET (high energy electrons) and will occur in proportion to the fraction of the total track which is at high energy. Thus ^{60}Co would be expected to produce a skewed distribution with a peak at low values of Y and a long tail to the maximum for that site size. Much of the electron tracks resulting from x-ray irradiation fall in the intermediate range of LET, and more or less symmetric f(Y) distributions would be expected. As x-ray energy decreases the most likely event size shifts toward larger Y values as observed in Chapter 7.

Converting from $f(\Delta)$ to $d(\Delta)$, of course, adds no information to the data, but does change the emphasis. An $f(\Delta)$ distribution emphasizes the number of sites receiving events of a given size, whereas $d(\Delta)$ shows the fraction of the dose delivered by events of a given size. There is also a difference in normalization. The $f(\Delta)$ distributions represent the same number of events, while $d(\Delta)$ curves represent equal doses (absorbed energy). If one is interested in the number of events per unit dose this can be obtained from the $\Phi(Y)$ distributions tabulated in the appendix.

The above observations refer to single event distributions; the energy imparted by a single charged particle track. At doses commonly

encountered, most sites may be crossed by a significant number of charged particle tracks. The total ionization which the site receives in these multiple crossings is calculated by a compound Poisson folding process giving the $\Psi(T)$ distributions described in Section 7.2. Of course, such distributions may be no more representative of the damage that will be done in the site than is $\Phi(\Delta)$. There are a number of time dependent de-excitation, recombination and possibly repair events which modify damage and prevent the effects of successive tracks from adding directly. A more detailed treatment of the data would require a knowledge of the time factors mentioned above which is not yet available. In the meantime $\Psi(T)$ distributions may be useful in the analysis of systems which do not show repair.

Chapter 8

SUMMARY AND CONCLUSIONS

This study has been concerned with the measurement of energy deposition distributions which may be useful in the study of damage in microscopic sites exposed to ionizing radiation. Theories of damage to individual living cells generally involve the amount of energy deposited in cellular or sub-cellular sites (targets). Ionization in small sites can be measured by using a low pressure gas proportional counter to simulate the sites. However, proportional counters with solid walls surrounding the detector volume are subject to an error called the wall effect (Chapter 2).

The wall effect can be greatly reduced by building a nearly wall-less detector and operating it in a solid-walled container several times the detector's dimensions. The design and testing of a grid-walled detector for this purpose is described in Chapter 3. This detector, which has only 17% of its surface composed of solid material, is shown to be very nearly spherical and to have uniform gain for ions formed throughout its volume. Ions formed outside the spherical region are prevented from drifting into it by an electric field which draws them to auxillary collecting electrodes.

This detector was used both to determine the details of the wall effect, and to measure energy deposition distributions for

typical site sizes and photon irradiations. Two characteristics of the wall effect are of particular interest; its variation with type of irradiation and the way it is effected by changing the distance between the solid wall and detector. Variation of the wall effect with type or irradiation can be seen in Figures 6.1.1 and 6.1.2 of Chapter 6. It is generally believed that the wall effect for photon irradiation is due almost exclusively to the back scatter of electrons. A solid wall, therefore, should produce a decrease in the number of events in the detector in proportion to the albedo for electrons. The absence of a measureable wall effect for photon spectra which produce a large fraction of very low energy electrons (such as 65 kVp or unfiltered 250 kVp x-rays) is most likely the result of electrons being scattered back into the detector by the gas around the wall-less detector. Other factors which may diminish the wall effect are discussed in Section 6.3.

The observed difference between the wall effect for filtered x-rays and ^{60}Co is larger than one would expect on the basis of albedo calculations. This may be related to the fact that the wall effect does not decrease as fast with increasing distance between container wall and detector for ^{60}Co as for filtered x-rays. In fact, for ^{60}Co, the decrease with increasing container size is significantly less than predicted for back-scattered electrons (Section 7.3). This tends to imply that there is more to the wall effect for ^{60}Co gamma rays than has as yet been considered in the available theoretical treatments.

The similarities and differences between the energy absorption distributions of various radiations, when compared to the biological effectiveness of these radiations, may provide basic information on the nature of the biological damage. These energy absorption distributions for ^{60}Co gamma rays and typical x-ray irradiations are presented in Chapter 7. The variation of the single event distributions with site size is shown in Figures 7.1.1 and 7.1.2. The single event distribution is of interest because it is the starting point for determining multiple event distributions, and because certain types of damage may be the result of single hits, without accumulation of damage from successive interactions. When this is the case, the $\Phi(Y)$ values from Figures 7.2.4 and 7.2.5 can be used to determine site size and threshold for damage. The multiple event functions ($f(T)$ and $\Psi(T)$) are useful in cases where all damage is accumulated until an effective level is reached. These functions can be compared; as discussed in Section 7.2, either in terms of equal average numbers of interactions or in terms of average dose. Figure 7.2.10 compares $\Psi(T)$ distributions for ^{60}Co gamma rays and typical x-rays at three dose levels. Data of this type would be useful in conjunction with dose-effect relationships for damage which were known to be completely cummulative--where no recovery or repair occurs.

One goal of this work was to determine for which, if any, irradiation conditions a wall-less detector would be necessary. Due to the unexpected behavior of the wall effect this cannot be completely answered, but it appears that for photon spectra with a large

low energy component a solid-wall detector is completely satisfactory. For ^{60}Co irradiation the errors appear to be about ten percent which may be acceptable for many purposes. However, for filtered 250 kVp x-rays, and probably for other common filtered x-ray energies, the use of a wall-less detector is clearly indicated, at least until more details of the nature of the wall effect can be worked out.

BIBLIOGRAPHY

Berger, Martin J. 1970. Spectrum of Energy Deposited by Electrons in Spherical Regions. *Second Symposium on Microdosimetry*, ed. by H. G. Ebert, Commission of the European Communities, Brussels. p. 541-559.

Berger, Martin J. and Stephen M. Seltzer. 1964. *Tables of Energy Losses and Ranges of Electrons and Positrons*. National Aeronautics and Space Administration. NASA sp-3012, Washington, D.C.

Biavati, G. J. and M. H. Biavati. 1964. Computer Applications - Evaluation of P(Z). *Annual Report on Research Project*. Radiological Research Laboratory, Columbia University, NYO-2740-1, New York. p. 49-51.

Biavati, B. J., W. Gross, H. H. Rossi and A. Kellerer. 1968. Wall-less Proportional Counters. *Annual Report on Research Project*. Columbia University, NYO-2740-5, New York. p. 61-68.

Biavati, M. H., H. H. Rossi, and E. Boer. 1965. Monoenergetic Neutrons 14.7, 5.7 and 3.7 MeV. *Annual Report on Research Project*. Radiological Research Laboratory, Columbia University, NYO-2740-2, New York. p. 41-76

Bichsel, H. 1968. Charged-Particle Interactions. *Radiation Dosimetry*. Second Ed. Vol. I. ed. by Frank H. Attix and William C. Roesch. Academic Press, New York. p. 157-228.

Braby, L. A. 1968. Microdosimeter Development. *Pacific Northwest Laboratory Annual Report for 1967 Volume II, Physical Sciences Part 2, Radiological Sciences*. Battelle-Northwest. BNWL-715. Richland, Washington. p. 204-207.

Braby, L. A., W. C. Roesch, and W. A. Glass. 1970. Energy Deposition Spectra of ^{14}C Beta Radiation in a Uniform Medium. *Radiation Research*, 43;499-503.

Bruce, W. R., M. L. Pearson and Helen S. Freedhoff. 1963. The Linear Energy Transfer Distributions Resulting from Primary and Scattered X-ray and Gamma Rays with Primary HVL's from 1.25 mm Cu to 11 mm Pb. *Radiation Research*, 19;606-620.

Casarett, Alison P. 1968. *Radiation Biology*. Prentice-Hall Inc., Englewood Cliffs, New Jersey. 368p.

Cole, Arthur. 1969. Absorption of 20 eV to 50,000 eV Electron Beams in Air and Plastic. *Radiation Research*. 38;7-33.

Fairstein, E. and J. Hahn. 1965. Nuclear Pulse Amplifiers - Fundamentals and Design Practice. *Nucleonics*. 23;56-61. July 1965.

Fano, U. 1954. Note on the Bragg-Gray Cavity Principle for Measuring Energy Dissipation. *Radiation Research*. 1;237-240.

Glass, W. A., W. C. Roesch, and L. A. Braby. 1970. Energy Deposition in Microscopic Volumes. *Charged Particle Tracks in Solids and Liquids*. ed. by G. E. Adams, D. K. Bewley and J. W. Boag. The Institute of Physics and the Physical Society. London. p. 56-61.

Glass, W. A. and D. N. Samsky. 1967. Ionization in Thin Tissue-like Gas Layers by Monoenergetic Protons. *Radiation Research*. 32;138-148.

Gross, William, B. J. Biavati, and H. H. Rossi. 1969. Microdosimetry of Directly Ionizing Particles with Wall-less Proportional Counters. *Second Symposium on Microdosimetry*, ed. by H. G. Ebert, Commission of the European Communities, Brussels. p. 249-263.

Gross, W., R. Rodgers, H. H. Rossi and J. Kitzman. 1970. Wall-less Proportional Counters. *Annual Report on Research Project*. Columbia University, NYO-2740-7, New York. p. 53-72.

Hall, E. J. 1961. The Relative Biological Efficiency of X-rays Generated by 220 kVp and Gamma Radiation from a Cobalt 60 Therapy Unit. *British Journal of Radiology*. 34;313-317.

Humphrey, R. M. and W. K. Sinclair. 1963. The Relative Biological Effectiveness of 22 MeVp x-rays Co-60 Gamma Rays, and 200 kVcp X-rays VIII. Determined by the Growth Capacity of Tumor Cells in Vitro. *Radiation Research*. 20;593-599.

ICRU. 1954. Recommendations of the International Commission on Radiological Units, Copenhagen, 1953. *Radiology*. 62;106-109.

ICRU. 1968. *Radiation Quantities and Units*. International Commission on Radiation Units and Measurements, Washington, D.C. 8 p.

ICRU. 1970. *Linear Energy Transfer*. International Commission on Radiation Units and Measurements. Washington, D.C. 51 p.

Kellerer, A. M. 1968. *Mikrodosimetrie Grundlagen einer Theroie die Strahlenqualitat*. Institut fur Biologie der GSF and Strahlengiologisches. Institut der Universitat Munchen, Munchen. 157 p.

Kellerer, Albrecht M. 1970. Analysis of Patterns of Energy Deposition. *Second Symposium on Microdosimetry*. ed, by H. G. Ebert. Commission of the European Communities, Brussels. p. 107-134.

Kellerer, Albrecht M. 1971a. Theory of Wall Effects in Microdosimetric Measurements. *Biophysical Aspects of Radiation Quality, Third Panel Report*. To be published.

Kellerer, Albrecht M. 1971b. Event Simultaneity in Cavities. To be published.

Loeb, Leonard B. 1955. *Basic Processes of Gaseous Electronics*. University of California Press, Berkeley. 1012 p.

Radeka, Valjko. 1968. *State of the Art of Low Noise Amplifiers for Semiconductor Radiation Detectors*. Brookhaven National Laboratory, BNL 12798, Upton, New York.

Raether, H. 1964. *Electron Avalanches and Breakdown in Gases*. Butterworths, Washington. 191 p.

Roesch, W. C. 1969. Folding of Distributions. *Pacific Northwest Laboratory Annual Report for 1968 to the USAEG Division of Biology and Medicine Volume II: Physical Science Part 2, Radiological Sciences*. Battelle-Northwest, BNWL-1051, Richland, Washington. p. 173-176.

Roesch, William C. and Frank H. Attix. 1968. Basic Concepts of Dosimetry. *Radiation Dosimetry*. Second Ed. Vol I. ed. by Frank H. Attix and William C. Roesch. p. 1-41.

Roesch, W. C. and W. A. Glass. 1969. Energy Absorption Straggling. *Pacific Northwest Laboratory Annual Report for 1968 to the USAEC Division of Biology and Medicine, Volume II, Physical Sciences, Part II, Radiological Sciences*. Battelle Northwest, BNWL-1051, Richland, Washington. p. 176-183.

Rosenzweig, W. and H. H. Rossi, 1959. Determination of the Absorbed Dose Delivered by Monoenergetic Neutrons. *Radiation Research*. 10;532-544.

Rossi, Harald H. 1967. Energy Distribution in the Absorption of Radiation. *Advances in Biological and Medical Physics*. ed. by John H. Lawrence and John W. Gofman, Vol. II, Academic Press, New York. p. 27-85.

Rossi, Harald H. 1968. Microscopic Energy Distribution. *Irradiated Matter Radiation Dosimetry*. Second Edition, Vol. I. ed. by Frank H. Attix and William C. Roesch. Academic Press, New York. p 43-92.

Rossi, H. H. 1968b. Role of Associated Absorption Events in Lenticular Radiation Injury. *Biophysical Aspects of Radiation Quality, Second Panel Report.* International Atomic Energy Agency, Vienna. p. 161-170.

Rossi, Harald H. 1969. Interpretation of Biological Response in Terms of Microdosimetry. *Annals New York Academy of Science.* 161;260-271.

Rossi, Harald H. 1970a. Experimental Limitations of Microdosimetry. *Second Symposium on Microdosimetry.* ed. by H. G. Ebert. Commission of the European Communities, Brussels. p. 303-326.

Rossi, Harald H. 1970b. The Effects of Small Doses of Ionizing Radiation. *Physics in Medicine and Biology.* 15;255-262.

Rossi, Harald H. and Walter Rosenzweig. 1955. A Device for the Measurement of Dose as a Function of Specific Ionization. *Radiology.* 64;404-411.

Shonka, Francis R., John E. Rose and G. Failla. 1958. Conducting Plastic Equivalent to Tissue, Air and Polystyrene. *Proceedings of the United Nations International Conference on the Peaceful Uses of Atomic Energy.* Vol. 21. United Nations. Geneva. p. 184-187.

Sinclair, W. K., S. E. Bunter and A. Cole. 1959. The Relative Biological Effectiveness of 200 kVp X-rays, Cobalt 60, Gamma Rays, and 22 MeVp X-rays, Determined from the Dose Survival Curve of Saccharomyces cerevisiae. *Radiation Research.* 10;418-432.

Srdoc, Dusan. 1970a. Experimental Technique of Measurement of Microscopic Energy Distribution in Irradiated Matter Using Rossi Counters. *Radiation Research.* 43;302-319.

Srdoc, D. 1970b. An Attempt to Measure the Wall Effect in the Tissue Equivalent Proportional Counter. *Annual Report on Research Project.* Columbia University, NYO-2740-7, New York. p. 96-101.

Toburen, L. H. and W. A. Glass. 1971. Energy Transfer to Electrons in Fast Proton Collisions. 19th Annual Meeting, Radiation Research Society, Boston, Massachusetts. May 9-13, 1971.

Wilson, K. S. J. 1970. Preliminary Measurements with a Cylindrical Wall-less Counter. *Second Symposium on Microdosimetry.* ed. by H. G. Ebert. Commission of the European Communities, Brussels. p. 235-246.

APPENDIX

Included herein are the computer printouts for the single event distributions obtained with the grid-walled detector. It is hoped that these distributions will provide adequate information so that others can compare this experimental work with mathematical models which may be developed in the future.

^{60}Co

Site Size 58 μg cm^{-2} R/r = 6

$\bar{Y}_p$ = 0.319 keV/μ Relative Variance = 3.517

$\bar{Y}_d$ = 1.443 keV/μ Relative Variance = 1.971

Y	N(Y)	f'(Y)	d'(Y)	1-D(Y)	Φ(Y)
.0514	340.0000	.0425896	.0068511	.9931	3.317E-02
.0611	340.0000	.0506435	.0096873	.9835	3.141E-02
.0727	340.0000	.0602220	.0136983	.9698	2.933E-02
.0864	340.0000	.0716300	.0193796	.9504	2.685E-02
.1028	340.0000	.0851791	.0274045	.9230	2.389E-02
.1222	300.0000	.0893708	.0341904	.8888	2.080E-02
.1454	250.0000	.0885617	.0402890	.8485	1.773E-02
.1729	200.0000	.0842706	.0455991	.8029	1.481E-02
.2056	155.0000	.0776633	.0499729	.7529	1.212E-02
.2445	110.0000	.0655386	.0501459	.7028	9.850E-03
.2907	80.0000	.0566795	.0515699	.6512	7.887E-03
.3458	54.0000	.0455061	.0492470	.6020	6.310E-03
.4112	35.0000	.0350738	.0451368	.5568	5.095E-03
.4890	23.5000	.0280029	.0428520	.5140	4.125E-03
.5814	16.5000	.0233803	.0425452	.4714	3.315E-03
.6916	11.8000	.0198879	.0430456	.4284	2.626E-03
.8224	8.0000	.0160337	.0412679	.3871	2.071E-03
.9779	5.1000	.0121544	.0371992	.3499	1.649E-03
1.1629	3.4000	.0096355	.0350675	.3149	1.316E-03
1.3832	2.4500	.0082585	.0357497	.2791	1.030E-03
1.6448	1.7000	.0068143	.0350777	.2440	7.935E-04
1.9558	1.1000	.0052431	.0320934	.2119	6.118E-04
2.3258	.7500	.0042510	.0309419	.1810	4.646E-04
2.7663	.5300	.0035731	.0309344	.1501	3.408E-04
3.2896	.3500	.0028059	.0288875	.1212	2.436E-04
3.9117	.2300	.0021926	.0268418	.0943	1.676E-04
4.6515	.1350	.0015303	.0222782	.0720	1.146E-04
5.5327	.0900	.0012135	.0210121	.0510	7.255E-05
6.5792	.0600	.0009620	.0198086	.0312	3.923E-05
7.8234	.0330	.0006292	.0154048	.0158	1.743E-05
9.3030	.0150	.0003401	.0099014	.0059	5.648E-06
11.0653	.0045	.0001213	.0042024	.0017	1.444E-06
13.1584	.0013	.0000417	.0017167	0	-1.008E-12

Site Size 92 μg cm^{-2} R/r = 6

$\bar{Y}_p$ = 0.253 keV/μ Relative Variance = 3.360

$\bar{Y}_d$ = 1.103 keV/μ Relative Variance = 1.947

Y	N(Y)	f'(Y)	d'(Y)	1-D(Y)	Φ(Y)
.0306	195.0000	.0296248	.0035789	.9964	1.073E-01
.0363	195.0000	.0352280	.0050607	.9914	1.034E-01
.0432	195.0000	.0419013	.0071597	.9842	9.874E-02
.0514	195.0000	.0498271	.0101244	.9741	9.323E-02
.0611	195.0000	.0592497	.0143156	.9598	8.668E-02
.0727	184.0000	.0664815	.0191010	.9407	7.933E-02
.0864	167.0000	.0717694	.0245265	.9161	7.140E-02
.1028	145.0000	.0741019	.0301137	.8860	6.321E-02
.1222	127.0000	.0771765	.0372941	.8487	5.468E-02
.1454	105.0000	.0758756	.0436002	.8051	4.629E-02
.1729	80.0000	.0687611	.0469969	.7581	3.869E-02
.2056	62.0000	.0633699	.0515047	.7066	3.168E-02
.2445	47.0000	.0571228	.0552070	.6514	2.537E-02
.2907	33.0000	.0476932	.0548117	.5966	2.010E-02
.3458	21.5000	.0369591	.0505217	.5461	1.601E-02
.4112	15.0000	.0306628	.0498433	.4962	1.262E-02
.4890	10.0000	.0243076	.0469846	.4493	9.936E-03
.5814	6.8000	.0196554	.0451781	.4041	7.763E-03
.6916	4.6000	.0158151	.0432371	.3608	6.015E-03
.8224	3.0500	.0124696	.0405392	.3203	4.637E-03
.9779	1.9300	.0093827	.0362721	.2840	3.600E-03
1.1629	1.2500	.0072262	.0332192	.2508	2.801E-03
1.3832	.8300	.0057072	.0312059	.2196	2.170E-03
1.6448	.5600	.0045790	.0297731	.1898	1.664E-03
1.9558	.3700	.0035975	.0278149	.1620	1.266E-03
2.3258	.2500	.0028905	.0265754	.1354	9.467E-04
2.7663	.1700	.0023379	.0255663	.1099	6.883E-04
3.2896	.1200	.0019624	.0255198	.0844	4.714E-04
3.9117	.0800	.0015557	.0240561	.0603	2.994E-04
4.6515	.0490	.0011331	.0208351	.0395	1.742E-04
5.5327	.0300	.0008251	.0180468	.0214	8.295E-05
6.5792	.0140	.0004579	.0119092	.0095	3.233E-05
7.8234	.0055	.0002139	.0066154	.0029	8.691E-06
9.3030	.0017	.0000786	.0028914	0	0E 00

^{60}Co

Site Size 185 μg cm^{-2} R/r = 6

$\bar{Y}_p$ = 0.221 keV/μ Relative Variance = 3.304

$\bar{Y}_d$ = 0.949 keV/μ Relative Variance = 1.747

Y	N(Y)	f'(Y)	d'(Y)	1-D(Y)	Φ(Y)
.0153	119.0000	.0151205	.0010477	.9990	4.995E-01
.0182	119.0000	.0179803	.0014815	.9975	4.904E-01
.0216	119.0000	.0213864	.0020959	.9954	4.795E-01
.0257	119.0000	.0254317	.0029638	.9924	4.666E-01
.0306	119.0000	.0302409	.0041907	.9882	4.513E-01
.0363	117.0000	.0353562	.0058262	.9824	4.334E-01
.0432	113.0000	.0406161	.0079609	.9744	4.128E-01
.0514	109.0000	.0465891	.0108589	.9636	3.891E-01
.0611	105.0000	.0533663	.0147907	.9488	3.621E-01
.0727	101.0000	.0610423	.0201179	.9287	3.311E-01
.0864	94.0000	.0675737	.0264892	.9022	2.968E-01
.1028	84.0000	.0718071	.0334732	.8687	2.604E-01
.1222	72.0000	.0731881	.0405687	.8281	2.233E-01
.1454	59.0000	.0713168	.0470082	.7811	1.871E-01
.1729	46.0000	.0661359	.0518512	.7293	1.536E-01
.2056	34.0000	.0581295	.0541947	.6751	1.241E-01
.2445	24.0000	.0487921	.0540915	.6210	9.937E-02
.2907	16.5000	.0398890	.0525854	.5684	7.914E-02
.3458	11.5000	.0330680	.0518512	.5166	6.237E-02
.4112	7.9000	.0270131	.0503692	.4662	4.867E-02
.4890	5.3000	.0215498	.0477809	.4184	3.774E-02
.5814	3.5000	.0169226	.0446179	.3738	2.915E-02
.6916	2.1000	.0120770	.0378740	.3359	2.303E-02
.8224	1.4300	.0097794	.0364698	.2994	1.807E-02
.9779	.9300	.0075628	.0335368	.2659	1.423E-02
1.1629	.6400	.0061888	.0326348	.2333	1.110E-02
1.3832	.4300	.0049458	.0310206	.2022	8.587E-03
1.6448	.3000	.0041033	.0306041	.1716	6.506E-03
1.9558	.2000	.0032528	.0288488	.1428	4.856E-03
2.3258	.1400	.0027076	.0285555	.1142	3.483E-03
2.7663	.0960	.0022084	.0277021	.0865	2.363E-03
3.2896	.0650	.0017781	.0265235	.0600	1.461E-03
3.9117	.0420	.0013662	.0242330	.0358	7.680E-04
4.6515	.0210	.0008123	.0171333	.0186	3.560E-04
5.5327	.0105	.0004831	.0121197	.0065	1.110E-04
6.5792	.0040	.0002188	.0065289	0	0E 00

Site Size 278 μg cm^{-2} R/r = 6

$\bar{Y}_p$ = 0.197 keV/μ Relative Variance = 2.338

$\bar{Y}_d$ = 0.660 keV/μ Relative Variance = 1.425

Y	N(Y)	f'(Y)	d'(Y)	1-D(Y)	Φ(Y)
.0108	135.0000	.0093675	.0005118	.9995	1.270E 00
.0129	135.0000	.0111395	.0007238	.9988	1.255E 00
.0153	135.0000	.0132460	.0010234	.9977	1.238E 00
.0182	135.0000	.0157513	.0014471	.9963	1.218E 00
.0216	135.0000	.0187351	.0020473	.9942	1.194E 00
.0257	135.0000	.0222789	.0028951	.9914	1.166E 00
.0306	135.0000	.0264920	.0040935	.9873	1.132E 00
.0363	135.0000	.0315025	.0057884	.9815	1.091E 00
.0432	135.0000	.0374702	.0081892	.9733	1.043E 00
.0514	133.0000	.0438977	.0114087	.9619	9.870E-01
.0611	131.0000	.0514140	.0158890	.9460	9.211E-01
.0727	131.0000	.0611383	.0224677	.9235	8.428E-01
.0864	125.0000	.0693892	.0303303	.8932	7.538E-01
.1028	115.0000	.0759133	.0394586	.8537	6.565E-01
.1222	100.0000	.0784947	.0485159	.8052	5.559E-01
.1454	82.0000	.0765395	.0562550	.7490	4.578E-01
.1729	62.0000	.0688341	.0601754	.6888	3.696E-01
.2056	45.0000	.0594104	.0617612	.6270	2.935E-01
.2445	32.0000	.0502366	.0621003	.5649	2.291E-01
.2907	22.0000	.0410700	.0603712	.5045	1.765E-01
.3458	13.8000	.0306423	.0535755	.4510	1.372E-01
.4112	8.8000	.0232361	.0483110	.4027	1.074E-01
.4890	5.8000	.0182108	.0450227	.3576	8.406E-02
.5814	4.1000	.0153079	.0450040	.3126	6.444E-02
.6916	2.6500	.0117684	.0411522	.2715	4.936E-02
.8224	1.7500	.0092416	.0384292	.2331	3.752E-02
.9779	1.1500	.0072215	.0357077	.1973	2.826E-02
1.1629	.7500	.0056005	.0329297	.1644	2.108E-02
1.3832	.5400	.0047962	.0335429	.1309	1.494E-02
1.6448	.3600	.0038023	.0316218	.0993	1.006E-02
1.9558	.2200	.0027630	.0273241	.0719	6.522E-03
2.3258	.1400	.0020908	.0245875	.0473	3.842E-03
2.7663	.0850	.0015099	.0211196	.0262	1.907E-03
3.2896	.0500	.0010562	.0175676	.0087	5.534E-04
3.9117	.0160	.0004019	.0079488	.0007	3.828E-05
4.6515	.0010	.0000299	.0007025	0	0E 00

^{60}Co

Site Size 555 μg cm^{-2} R/r = 6

$\bar{Y}_p$ = 0.183 keV/μ Relative Variance = 1.890

$\bar{Y}_d$ = 0.528 keV/μ Relative Variance = 1.278

Y	N(Y)	f'(Y)	d'(Y)	1-D(Y)	Φ(Y)
.0108	110.0000	.0161161	.0009528	.9990	5.419E 00
.0129	110.0000	.0191646	.0013473	.9977	5.313E 00
.0153	92.0000	.0190596	.0015933	.9961	5.208E 00
.0182	80.0000	.0197083	.0019592	.9941	5.099E 00
.0216	70.0000	.0205114	.0024253	.9917	4.986E 00
.0257	61.0000	.0212552	.0029886	.9887	4.869E 00
.0306	55.0000	.0227887	.0038102	.9849	4.744E 00
.0363	52.0000	.0256207	.0050939	.9798	4.603E 00
.0432	51.0000	.0298881	.0070680	.9728	4.438E 00
.0514	52.0000	.0362385	.0101907	.9626	4.239E 00
.0611	55.0000	.0455774	.0152406	.9473	3.988E 00
.0727	58.0000	.0571539	.0227265	.9246	3.673E 00
.0864	59.0000	.0691529	.0327066	.8919	3.292E 00
.1028	57.0000	.0794458	.0446822	.8472	2.855E 00
.1222	52.0000	.0861826	.0576373	.7896	2.380E 00
.1454	42.0000	.0827747	.0658284	.7237	1.924E 00
.1729	31.0000	.0726691	.0687394	.6550	1.524E 00
.2056	21.0000	.0585390	.0658475	.5892	1.201E 00
.2445	15.5000	.0513781	.0687214	.5204	9.185E-01
.2907	10.5000	.0413873	.0658284	.4546	6.905E-01
.3458	6.5000	.0304741	.0576524	.3970	5.227E-01
.4112	4.1000	.0228581	.0514238	.3455	3.968E-01
.4890	2.6000	.0172365	.0461099	.2994	3.019E-01
.5814	1.7000	.0134016	.0426317	.2568	2.281E-01
.6916	1.1500	.0107832	.0408001	.2160	1.687E-01
.8224	.7300	.0081397	.0366238	.1794	1.239E-01
.9779	.4500	.0059665	.0319222	.1474	9.102E-02
1.1629	.3000	.0047300	.0300930	.1174	6.498E-02
1.3832	.2000	.0037507	.0283827	.0890	4.432E-02
1.6448	.1400	.0031221	.0280949	.0609	2.713E-02
1.9558	.0850	.0022540	.0241190	.0368	1.471E-02
2.3258	.0500	.0015767	.0200620	.0167	6.029E-03
2.7663	.0280	.0010502	.0158943	.0008	2.456E-04
3.2896	.0010	.0000446	.0008027	0	0E 00

250 kVp HVL 1.8

Site Size 58 μg cm^{-2} R/r = 6

$\bar{Y}_p$ = 0.904 keV/μ Relative Variance = 2.283

$\bar{Y}_d$ = 2.966 keV/μ Relative Variance = 0.906

Y	N(Y)	f'(Y)	d'(Y)	1-D(Y)	Φ(Y)
.0514	147.0000	.0155187	.0008828	.9991	1.206E-02
.0611	147.0000	.0184534	.0012483	.9979	1.183E-02
.0727	147.0000	.0219436	.0017651	.9961	1.157E-02
.0864	147.0000	.0261005	.0024972	.9936	1.125E-02
.1028	147.0000	.0310375	.0035313	.9901	1.087E-02
.1222	140.0000	.0351494	.0047554	.9853	1.044E-02
.1454	130.0000	.0388118	.0062440	.9791	9.960E-03
.1729	121.0000	.0429681	.0082221	.9709	9.434E-03
.2056	115.0000	.0485620	.0110502	.9598	8.839E-03
.2445	108.0000	.0542304	.0146737	.9451	8.174E-03
.2907	99.0000	.0591134	.0190201	.9261	7.450E-03
.3458	85.0000	.0603684	.0231035	.9030	6.710E-03
.4112	72.0000	.0608081	.0276737	.8753	5.966E-03
.4890	60.0000	.0602560	.0326081	.8427	5.227E-03
.5814	49.0000	.0585163	.0376560	.8051	4.510E-03
.6916	37.0000	.0525560	.0402272	.7648	3.867E-03
.8224	28.0000	.0472952	.0430479	.7218	3.287E-03
.9779	21.5000	.0431835	.0467383	.6751	2.758E-03
1.1629	16.0000	.0382147	.0491833	.6259	2.290E-03
1.3832	12.0000	.0340904	.0521866	.5737	1.872E-03
1.6448	8.5000	.0287149	.0522725	.5214	1.520E-03
1.9558	5.9000	.0237007	.0513035	.4701	1.230E-03
2.3258	4.1000	.0195851	.0504129	.4197	9.902E-04
2.7663	3.0000	.0170452	.0521866	.3675	7.813E-04
3.2896	2.2000	.0148642	.0541174	.3134	5.992E-04
3.9117	1.6000	.0128546	.0556512	.2577	4.417E-04
4.6515	1.0700	.0102224	.0526262	.2051	3.165E-04
5.5327	.7700	.0087499	.0535783	.1515	2.093E-04
6.5792	.5100	.0068916	.0501816	.1014	1.249E-04
7.8234	.3300	.0053025	.0459123	.0554	5.992E-05
9.3030	.1700	.0032483	.0334447	.0220	2.013E-05
11.0653	.0450	.0010227	.0125248	.0095	7.597E-06
13.1584	.0170	.0004594	.0066909	.0028	1.969E-06
15.6467	.0050	.0001607	.0027826	0	0E 00

Site Size 92 μg cm^{-2} R/r = 6

$\bar{Y}_p$ = 0.815 keV/μ Relative Variance = 2.109

$\bar{Y}_d$ = 2.534 keV/μ Relative Variance = 0.859

Y	N(Y)	f'(Y)	d'(Y)	1-D(Y)	Φ(Y)
.0306	99.0000	.0101265	.0003797	.9996	3.396E-02
.0363	99.0000	.0120418	.0005370	.9991	3.355E-02
.0432	99.0000	.0143229	.0007597	.9983	3.306E-02
.0514	99.0000	.0170322	.0010743	.9972	3.247E-02
.0611	99.0000	.0202530	.0015190	.9957	3.178E-02
.0727	95.0000	.0231105	.0020611	.9937	3.099E-02
.0864	89.0000	.0257523	.0027318	.9909	3.010E-02
.1028	84.0000	.0289031	.0036460	.9873	2.911E-02
.1222	80.0000	.0327322	.0049098	.9824	2.799E-02
.1454	74.0000	.0360038	.0064220	.9760	2.675E-02
.1729	69.0000	.0399306	.0084716	.9675	2.538E-02
.2056	65.0000	.0447309	.0112851	.9562	2.385E-02
.2445	61.0000	.0499166	.0149749	.9412	2.214E-02
.2907	55.0000	.0535191	.0190924	.9221	2.030E-02
.3458	51.0000	.0590278	.0250465	.8971	1.827E-02
.4112	44.0000	.0605588	.0305567	.8665	1.620E-02
.4890	37.0000	.0605545	.0363325	.8302	1.412E-02
.5814	31.0000	.0603307	.0430446	.7872	1.205E-02
.6916	23.5000	.0543982	.0461642	.7410	1.018E-02
.8224	17.5000	.0481718	.0486129	.6924	8.529E-03
.9779	12.8000	.0418972	.0502764	.6421	7.092E-03
1.1629	9.3000	.0361984	.0516535	.5904	5.850E-03
1.3832	6.8000	.0314815	.0534326	.5370	4.769E-03
1.6448	5.0000	.0275267	.0555576	.4815	3.825E-03
1.9558	3.5000	.0229125	.0549898	.4265	3.039E-03
2.3258	2.5000	.0194615	.0555414	.3709	2.371E-03
2.7663	1.7700	.0163889	.0556327	.3153	1.809E-03
3.2896	1.2400	.0136533	.0551131	.2602	1.340E-03
3.9117	.8900	.0116527	.0559325	.2042	9.405E-04
4.6515	.5700	.0088744	.0506538	.1536	6.360E-04
5.5327	.4000	.0074074	.0502895	.1033	3.818E-04
6.5792	.2550	.0056155	.0453350	.0580	1.892E-04
7.8234	.1300	.0034041	.0326796	.0253	7.236E-05
9.3030	.0530	.0016503	.0188397	.0065	1.573E-05
11.0653	.0100	.0003704	.0050289	.0014	3.022E-06
13.1584	.0020	.0000881	.0014223	.0000	-9.986E-13

250 kVp HVL 1.8

Site Size 185 μg cm^{-2} R/r = 6

$\bar{Y}_p$ = 0.799 keV/μ Relative Variance = 1.641

$\bar{Y}_d$ = 2.109 keV/μ Relative Variance = 0.696

Y	N(Y)	f'(Y)	d'(Y)	1-D(Y)	Φ(Y)
.0153	75.0000	.0059769	.0001144	.9999	1.392E-01
.0182	75.0000	.0071074	.0001617	.9997	1.382E-01
.0216	75.0000	.0084537	.0002288	.9995	1.370E-01
.0257	75.0000	.0100528	.0003235	.9992	1.356E-01
.0306	75.0000	.0119538	.0004574	.9987	1.340E-01
.0363	70.0000	.0132671	.0006037	.9981	1.321E-01
.0432	64.0000	.0144277	.0007809	.9973	1.301E-01
.0514	57.0000	.0152802	.0009835	.9963	1.279E-01
.0611	52.0000	.0165760	.0012686	.9951	1.256E-01
.0727	48.0000	.0181948	.0016559	.9934	1.231E-01
.0864	44.0000	.0198381	.0021475	.9913	1.203E-01
.1028	41.0000	.0219821	.0028297	.9884	1.172E-01
.1222	39.0000	.0248639	.0038059	.9846	1.137E-01
.1454	37.0000	.0280504	.0051057	.9795	1.098E-01
.1729	36.0000	.0324623	.0070281	.9725	1.053E-01
.2056	35.5000	.0380665	.0098003	.9627	9.992E-02
.2445	34.0000	.0433525	.0132718	.9494	9.385E-02
.2907	33.0000	.0500358	.0182150	.9312	8.684E-02
.3458	31.0000	.0559073	.0242078	.9070	7.901E-02
.4112	28.5000	.0611209	.0314714	.8755	7.045E-02
.4890	25.0000	.0637537	.0390347	.8365	6.152E-02
.5814	20.5000	.0621657	.0452614	.7912	5.282E-02
.6916	16.0000	.0577108	.0499775	.7413	4.473E-02
.8224	12.3000	.0527570	.0543295	.6869	3.734E-02
.9779	9.4000	.0479428	.0587082	.6282	3.063E-02
1.1629	6.7000	.0406351	.0591710	.5691	2.494E-02
1.3832	5.0000	.0360692	.0624718	.5066	1.989E-02
1.6448	3.5000	.0300243	.0618384	.4447	1.568E-02
1.9558	2.4500	.0249914	.0612064	.3835	1.218E-02
2.3258	1.7000	.0206208	.0600542	.3235	9.294E-03
2.7663	1.2500	.0180346	.0624718	.2610	6.768E-03
3.2896	.9000	.0154411	.0636053	.1974	4.605E-03
3.9117	.6700	.0136688	.0669523	.1305	2.691E-03
4.6515	.3900	.0094613	.0551085	.0753	1.366E-03
5.5327	.2000	.0057711	.0399820	.0354	5.577E-04
6.5792	.0800	.0027451	.0226152	.0128	1.733E-04
7.8234	.0220	.0008977	.0087937	.0040	4.757E-05
9.3030	.0070	.0003396	.0039565	.0000	-4.076E-12

Site Size 278 μg cm^{-2} R/r = 6

$\bar{Y}_p$ = 0.739 keV/μ Relative Variance = 1.354

$\bar{Y}_d$ = 1.740 keV/μ Relative Variance = 0.563

Y	N(Y)	f'(Y)	d'(Y)	1-D(Y)	Φ(Y)
.0108	83.0000	.0033951	.0000496	1.0000	3.418E-01
.0129	83.0000	.0040373	.0000702	.9999	3.404E-01
.0153	83.0000	.0048007	.0000992	.9998	3.387E-01
.0182	83.0000	.0057087	.0001403	.9996	3.368E-01
.0216	83.0000	.0067901	.0001985	.9994	3.345E-01
.0257	83.0000	.0080745	.0002808	.9992	3.317E-01
.0306	83.0000	.0096015	.0003970	.9988	3.284E-01
.0363	83.0000	.0114174	.0005614	.9982	3.245E-01
.0432	83.0000	.0135803	.0007942	.9974	3.198E-01
.0514	76.0000	.0147871	.0010283	.9964	3.147E-01
.0611	70.0000	.0161952	.0013392	.9950	3.092E-01
.0727	66.0000	.0181579	.0017855	.9933	3.030E-01
.0864	62.0000	.0202886	.0023730	.9909	2.960E-01
.1028	58.0000	.0225698	.0031391	.9877	2.883E-01
.1222	56.0000	.0259124	.0042855	.9835	2.794E-01
.1454	53.5000	.0294378	.0057894	.9777	2.693E-01
.1729	52.0000	.0340325	.0079609	.9697	2.576E-01
.2056	51.5000	.0400808	.0111492	.9586	2.439E-01
.2445	50.5000	.0467348	.0154585	.9431	2.278E-01
.2907	48.0000	.0528229	.0207769	.9223	2.097E-01
.3458	45.0000	.0589025	.0275571	.8948	1.895E-01
.4112	40.0000	.0622614	.0346383	.8601	1.682E-01
.4890	34.0000	.0629301	.0416309	.8185	1.466E-01
.5814	27.5000	.0605262	.0476138	.7709	1.258E-01
.6916	21.5000	.0562846	.0526646	.7182	1.065E-01
.8224	16.7000	.0519883	.0578460	.6604	8.871E-02
.9779	12.4000	.0459019	.0607322	.5996	7.297E-02
1.1629	9.2000	.0404975	.0637160	.5359	5.908E-02
1.3832	7.0000	.0366504	.0685865	.4673	4.651E-02
1.6448	5.0000	.0311307	.0692767	.3981	3.584E-02
1.9558	3.6000	.0266527	.0705277	.3275	2.670E-02
2.3258	2.6000	.0228899	.0720268	.2555	1.885E-02
2.7663	1.9000	.0198959	.0744653	.1810	1.202E-02
3.2896	1.4000	.0174332	.0775898	.1035	6.046E-03
3.9117	.7500	.0111053	.0587731	.0447	2.237E-03
4.6515	.2400	.0042258	.0265945	.0181	7.881E-04
5.5327	.0800	.0016754	.0125415	.0055	2.135E-04
6.5792	.0250	.0006226	.0055421	0	0E 00

250 kVp HVL 1.8

Site Size 555 μg cm^{-2} R/r = 6

$\bar{Y}_p$ = 0.678 keV/μ Relative Variance = 1.030

$\bar{Y}_d$ = 1.364 keV/μ Relative Variance = 0.486

Y	N(Y)	f'(Y)	d'(Y)	1-D(Y)	Φ(Y)
.0108	34.0000	.0047666	.0000767	.9999	1.492E 00
.0129	34.0000	.0056683	.0001085	.9998	1.484E 00
.0153	34.0000	.0067402	.0001534	.9997	1.474E 00
.0182	31.0000	.0073078	.0001978	.9995	1.463E 00
.0216	29.5000	.0082715	.0002663	.9992	1.450E 00
.0257	26.5000	.0088358	.0003382	.9989	1.437E 00
.0306	25.0000	.0099120	.0004512	.9984	1.422E 00
.0363	23.7000	.0111738	.0006048	.9978	1.405E 00
.0432	22.0000	.0123372	.0007943	.9970	1.387E 00
.0514	20.0000	.0133371	.0010211	.9960	1.367E 00
.0611	18.0000	.0142733	.0012994	.9947	1.345E 00
.0727	16.5000	.0155585	.0016843	.9930	1.322E 00
.0864	15.0000	.0168234	.0021662	.9908	1.297E 00
.1028	13.8000	.0184052	.0028182	.9880	1.269E 00
.1222	13.3000	.0210928	.0038405	.9842	1.238E 00
.1454	13.3000	.0250822	.0054306	.9787	1.200E 00
.1729	13.4000	.0300579	.0077407	.9710	1.155E 00
.2056	13.5000	.0360102	.0110278	.9600	1.101E 00
.2445	13.7000	.0434543	.0158239	.9442	1.036E 00
.2907	13.8000	.0520502	.0225391	.9216	9.578E-01
.3458	13.8000	.0619102	.0318872	.8897	8.650E-01
.4112	12.8000	.0682860	.0418238	.8479	7.626E-01
.4890	11.2000	.0710493	.0517454	.7962	6.561E-01
.5814	9.2000	.0694003	.0601042	.7361	5.521E-01
.6916	7.2000	.0646020	.0665472	.6695	4.552E-01
.8224	5.5000	.0586833	.0718846	.5976	3.672E-01
.9779	4.0000	.0507495	.0739220	.5237	2.911E-01
1.1629	3.0000	.0452610	.0783968	.4453	2.233E-01
1.3832	2.2000	.0394790	.0813354	.3640	1.641E-01
1.6448	1.5500	.0330760	.0810336	.2829	1.145E-01
1.9558	1.0400	.0263897	.0768789	.2061	7.490E-02
2.3258	.7400	.0223288	.0773515	.1287	4.142E-02
2.7663	.4300	.0154327	.0635895	.0651	1.828E-02
3.2896	.1850	.0078956	.0386870	.0264	6.445E-03
3.9117	.0650	.0032987	.0192197	.0072	1.499E-03
4.6515	.0130	.0007845	.0054355	.0018	3.229E-04
5.5327	.0030	.0002153	.0017746	0	-4.364E-11

250 kVp HVL 0.44

Site Size 58 μg cm^{-2} R/r = 6

$\bar{Y}_p$ = 1.285 keV/μ Relative Variance = 1.697

$\bar{Y}_d$ = 3.466 keV/μ Relative Variance = 0.696

Y	N(Y)	f'(Y)	d'(Y)	1-D(Y)	Φ(Y)
.0514	150.0000	.0097761	.0003911	.9996	8.530E-03
.0611	150.0000	.0116248	.0005529	.9991	8.430E-03
.0727	140.0000	.0129020	.0007298	.9983	8.319E-03
.0864	136.0000	.0149076	.0010029	.9973	8.191E-03
.1028	135.0000	.0175970	.0014078	.9959	8.039E-03
.1222	133.0000	.0206147	.0019611	.9940	7.861E-03
.1454	130.0000	.0239608	.0027105	.9912	7.655E-03
.1729	128.0000	.0280613	.0037757	.9875	7.413E-03
.2056	125.0000	.0325871	.0052141	.9823	7.133E-03
.2445	122.0000	.0378195	.0071956	.9751	6.807E-03
.2907	118.0000	.0434980	.0098413	.9652	6.432E-03
.3458	113.0000	.0495457	.0133331	.9519	6.005E-03
.4112	108.0000	.0563105	.0180199	.9339	5.520E-03
.4890	99.0000	.0613792	.0233562	.9105	4.991E-03
.5814	82.0000	.0604549	.0273555	.8832	4.471E-03
.6916	68.0000	.0596302	.0320937	.8511	3.957E-03
.8224	54.0000	.0563105	.0360397	.8150	3.472E-03
.9779	43.0000	.0533193	.0405785	.7744	3.013E-03
1.1629	35.0000	.0516078	.0467045	.7277	2.568E-03
1.3832	27.0000	.0473534	.0509724	.6768	2.160E-03
1.6448	20.5000	.0427543	.0547270	.6220	1.792E-03
1.9558	15.0000	.0371995	.0566212	.5654	1.471E-03
2.3258	11.3000	.0333239	.0603156	.5051	1.184E-03
2.7663	8.4000	.0294643	.0634323	.4417	9.304E-04
3.2896	6.3000	.0262782	.0672741	.3744	7.040E-04
3.9117	4.2000	.0208317	.0634158	.3110	5.245E-04
4.6515	2.8000	.0165145	.0597818	.2512	3.823E-04
5.5327	2.0500	.0143814	.0619220	.1893	2.584E-04
6.5792	1.3500	.0112621	.0576635	.1316	1.613E-04
7.8234	.8700	.0086303	.0525445	.0791	8.700E-05
9.3030	.5600	.0066058	.0478254	.0312	3.009E-05
11.0653	.2000	.0028061	.0241647	.0071	5.920E-06
13.1584	.0400	.0006674	.0068342	.0002	1.709E-07
15.6467	.0010	.0000198	.0002416	0	2.507E-13

Site Size 92 μg cm^{-2} R/r = 6

$\bar{Y}_p$ = 1.232 keV/μ Relative Variance = 1.558

$\bar{Y}_d$ = 3.150 keV/μ Relative Variance = 0.668

Y	N(Y)	f'(Y)	d'(Y)	1-D(Y)	Φ(Y)
.0306	127.0000	.0074814	.0001856	.9998	2.253E-02
.0363	127.0000	.0088964	.0002625	.9996	2.233E-02
.0432	127.0000	.0105817	.0003714	.9992	2.209E-02
.0514	102.0000	.0101063	.0004218	.9988	2.186E-02
.0611	94.0000	.0110749	.0005496	.9982	2.161E-02
.0727	91.0000	.0127492	.0007524	.9975	2.132E-02
.0864	87.0000	.0144978	.0010177	.9964	2.099E-02
.1028	84.0000	.0166456	.0013894	.9950	2.061E-02
.1222	80.0000	.0188509	.0018711	.9932	2.019E-02
.1454	76.0000	.0212954	.0025135	.9907	1.970E-02
.1729	74.0000	.0246629	.0034624	.9872	1.914E-02
.2056	72.0000	.0285354	.0047638	.9824	1.850E-02
.2445	70.0000	.0329890	.0065488	.9759	1.775E-02
.2907	69.0000	.0386680	.0091280	.9668	1.687E-02
.3458	68.0000	.0453264	.0127267	.9540	1.584E-02
.4112	65.0000	.0515222	.0172027	.9368	1.467E-02
.4890	60.0000	.0565526	.0224530	.9144	1.339E-02
.5814	54.0000	.0605238	.0285746	.8858	1.201E-02
.6916	47.0000	.0626571	.0351856	.8506	1.059E-02
.8224	38.0000	.0602413	.0402279	.8104	9.221E-03
.9779	30.0000	.0565526	.0449061	.7655	7.937E-03
1.1629	23.7000	.0531265	.0501644	.7153	6.731E-03
1.3832	18.5000	.0493258	.0553986	.6599	5.611E-03
1.6448	14.0000	.0443883	.0592832	.6006	4.603E-03
1.9558	10.5000	.0395868	.0628685	.5378	3.704E-03
2.3258	7.5000	.0336244	.0634992	.4743	2.941E-03
2.7663	5.4000	.0287956	.0646816	.4096	2.287E-03
3.2896	4.0000	.0253648	.0677522	.3418	1.711E-03
3.9117	2.7500	.0207359	.0658622	.2760	1.241E-03
4.6515	1.8300	.0164087	.0619752	.2140	8.680E-04
5.5327	1.3500	.0143978	.0646816	.1493	5.411E-04
6.5792	.9300	.0117946	.0630095	.0863	2.734E-04
7.8234	.4400	.0066355	.0421518	.0442	1.227E-04
9.3030	.2000	.0035866	.0270930	.0171	4.127E-05
11.0653	.0650	.0013865	.0124572	.0046	9.790E-06
13.1584	.0170	.0004312	.0046071	.0000	0E 00

250 kVp HVL 0.44

Site Size 185 μg cm^{-2} R/r = 6

$\bar{Y}_p$ = 1.159 keV/μ Relative Variance = 1.149

$\bar{Y}_d$ = 2.493 keV/μ Relative Variance = 0.519

Y	N(Y)	f'(Y)	d'(Y)	1-D(Y)	Φ(Y)
.0153	74.0000	.0037058	.0000488	1.0000	9.608E-02
.0182	74.0000	.0044067	.0000690	.9999	9.566E-02
.0216	74.0000	.0052415	.0000977	.9998	9.515E-02
.0257	74.0000	.0062329	.0001381	.9996	9.455E-02
.0306	67.0000	.0067105	.0001768	.9995	9.390E-02
.0363	63.0000	.0075033	.0002351	.9992	9.318E-02
.0432	58.0000	.0082163	.0003062	.9989	9.239E-02
.0514	54.0000	.0090967	.0004032	.9985	9.151E-02
.0611	49.0000	.0098153	.0005173	.9980	9.057E-02
.0727	46.0000	.0109572	.0006367	.9973	8.951E-02
.0864	42.0000	.0113995	.0007870	.9964	8.836E-02
.1028	37.5000	.0126342	.0011199	.9953	8.714E-02
.1222	36.5000	.0146228	.0015413	.9938	8.573E-02
.1454	35.0000	.0166739	.0020899	.9917	8.412E-02
.1729	34.0000	.0192659	.0028722	.9888	8.227E-02
.2056	34.5000	.0232470	.0041213	.9847	8.002E-02
.2445	34.5000	.0276431	.0058273	.9789	7.736E-02
.2907	35.0000	.0333479	.0083596	.9705	7.414E-02
.3458	35.5000	.0402317	.0119956	.9585	7.026E-02
.4112	36.0000	.0485155	.0172018	.9413	6.558E-02
.4890	36.0000	.0576900	.0243283	.9170	6.002E-02
.5814	33.0000	.0628345	.0315275	.8855	5.395E-02
.6916	29.5000	.0663639	.0398728	.8456	4.751E-02
.8224	25.0000	.0673327	.0477828	.7978	4.101E-02
.9779	20.2000	.0647410	.0545913	.7432	3.476E-02
1.1629	15.8000	.0602167	.0603798	.6828	2.896E-02
1.3832	12.0000	.0543973	.0648778	.6180	2.371E-02
1.6448	9.0000	.0485155	.0688072	.5491	1.903E-02
1.9558	6.5000	.0416650	.0702660	.4739	1.501E-02
2.3258	4.5000	.0343007	.0687372	.4101	1.171E-02
2.7663	3.4500	.0312737	.0746095	.3355	8.689E-03
3.2896	2.7000	.0291033	.0825636	.2529	5.882E-03
3.9117	1.9500	.0249990	.0843192	.1686	3.471E-03
4.6515	1.1300	.0172266	.0690929	.0995	1.809E-03
5.5327	.6800	.0112422	.0536323	.0459	7.251E-04
6.5792	.2400	.0051750	.0293577	.0165	2.260E-04
7.8234	.0700	.0017948	.0121074	.0044	5.293E-05
9.3039	.0130	.0005438	.0044024	.0000	0E 00

Site Size 278 μg cm^{-2} R/r = 6

$\bar{Y}_p$ = 1.094 keV/μ Relative Variance = 0.966

$\bar{Y}_d$ = 2.150 keV/μ Relative Variance = 0.454

Y	N(Y)	f'(Y)	d'(Y)	1-D(Y)	Φ(Y)
.0108	110.0000	.0019074	.0000188	1.0000	2.314E-01
.0129	110.0000	.0022682	.0000267	1.0000	2.308E-01
.0153	110.0000	.0026972	.0000377	.9999	2.302E-01
.0182	110.0000	.0032073	.0000533	.9999	2.295E-01
.0216	110.0000	.0038148	.0000754	.9998	2.286E-01
.0257	110.0000	.0045364	.0001066	.9997	2.275E-01
.0306	110.0000	.0053943	.0001508	.9995	2.263E-01
.0363	110.0000	.0064146	.0002132	.9993	2.248E-01
.0432	110.0000	.0076297	.0003016	.9990	2.230E-01
.0514	97.0000	.0080006	.0003761	.9986	2.212E-01
.0611	89.0000	.0087290	.0004879	.9982	2.191E-01
.0727	84.0000	.0097968	.0006511	.9975	2.169E-01
.0864	80.0000	.0110977	.0008773	.9966	2.143E-01
.1028	77.0000	.0127020	.0011941	.9954	2.114E-01
.1222	73.0000	.0143194	.0016007	.9938	2.080E-01
.1454	72.0000	.0167945	.0022325	.9916	2.041E-01
.1729	71.0000	.0196985	.0031146	.9885	1.996E-01
.2056	72.0000	.0237544	.0044663	.9840	1.941E-01
.2445	73.0000	.0286388	.0064029	.9776	1.874E-01
.2907	74.0000	.0345220	.0091780	.9684	1.794E-01
.3458	76.0000	.0421714	.0133356	.9551	1.697E-01
.4112	77.0000	.0508081	.0191058	.9360	1.579E-01
.4890	74.0000	.0580623	.0259625	.9100	1.444E-01
.5814	68.0000	.0634458	.0337355	.8763	1.297E-01
.6916	61.0000	.0676962	.0428142	.8335	1.140E-01
.8224	51.0000	.0673043	.0506179	.7829	9.842E-02
.9779	42.0000	.0659086	.0589419	.7239	8.314E-02
1.1629	32.0000	.0597137	.0635021	.6604	6.930E-02
1.3832	25.5000	.0565984	.0715909	.5888	5.618E-02
1.6448	19.0000	.0501483	.0754306	.5134	4.456E-02
1.9558	14.5000	.0455083	.0813959	.4320	3.401E-02
2.3258	11.0000	.0410532	.0873153	.3447	2.449E-02
2.7663	8.0000	.0355127	.0898396	.2548	1.626E-02
3.2896	5.8000	.0306168	.0921048	.1627	9.162E-03
3.9117	3.5000	.0219695	.0785892	.0842	4.070E-03
4.6515	1.3000	.0097035	.0412763	.0429	1.821E-03
5.5327	.6000	.0053269	.0269519	.0159	5.860E-04
6.5792	.1800	.0019004	.0114337	.0045	1.455E-04
7.8234	.0500	.0006277	.0044908	0	0E 00

250 kVp HVL 0.44

Site Size 555 μg cm^{-2} R/r = 6

$\bar{Y}_p$ = 0.928 keV/μ Relative Variance = 0.688

$\bar{Y}_d$ = 1.567 keV/μ Relative Variance = 0.358

Y	N(Y)	f'(Y)	d'(Y)	1-D(Y)	Φ(Y)
.0108	40.0000	.0030762	.0000358	1.0000	1.081E 00
.0129	40.0000	.0036580	.0000506	.9999	1.077E 00
.0153	40.0000	.0043498	.0000716	.9998	1.072E 00
.0182	33.0000	.0042673	.0000835	.9998	1.068E 00
.0216	29.0000	.0044604	.0001039	.9997	1.063E 00
.0257	26.5000	.0048469	.0001342	.9995	1.058E 00
.0306	25.0000	.0054372	.0001790	.9993	1.052E 00
.0363	23.5000	.0060777	.0002379	.9991	1.045E 00
.0432	21.5000	.0066137	.0003080	.9988	1.038E 00
.0514	19.0000	.0069503	.0003849	.9984	1.031E 00
.0611	17.0000	.0073946	.0004869	.9979	1.023E 00
.0727	15.5000	.0080174	.0006278	.9973	1.014E 00
.0864	14.0000	.0086133	.0008022	.9965	1.004E 00
.1028	13.3000	.0097304	.0010776	.9954	9.939E-01
.1222	12.7000	.0110485	.0014550	.9940	9.819E-01
.1454	12.1000	.0125174	.0019602	.9920	9.684E-01
.1729	12.2000	.0150117	.0027962	.9892	9.521E-01
.2056	12.9000	.0188754	.0041809	.9850	9.316E-01
.2445	14.2000	.0247068	.0065074	.9785	9.048E-01
.2907	16.0000	.0331039	.0103683	.9681	8.689E-01
.3458	17.7000	.0435585	.0162270	.9519	8.217E-01
.4112	19.3000	.0564800	.0250207	.9269	7.604E-01
.4890	20.0000	.0695965	.0366617	.8902	6.850E-01
.5814	19.3000	.0798632	.0500268	.8402	5.983E-01
.6916	16.4000	.0807185	.0601408	.7801	5.108E-01
.8224	13.3000	.0778429	.0689689	.7111	4.264E-01
.9779	10.7000	.0744683	.0784560	.6326	3.456E-01
1.1629	8.1000	.0670354	.0839828	.5487	2.729E-01
1.3832	6.3000	.0620154	.0924115	.4563	2.057E-01
1.6448	4.8000	.0561874	.0995642	.3567	1.448E-01
1.9558	3.4000	.0473257	.0997198	.2570	9.343E-02
2.3258	2.3000	.0380695	.0953879	.1616	5.214E-02
2.7663	1.3500	.0265780	.0792099	.0824	2.332E-02
3.2896	.6100	.0142810	.0506118	.0318	7.833E-03
3.9117	.2000	.0055677	.0234635	.0083	1.795E-03
4.6515	.0500	.0016552	.0082946	0	0E 00

65 kVp HVL 1.9

Site Size 52 μg cm^{-2} R/r = 4

$\bar{Y}_p$ = 1.776 keV/μ Relative Variance = 1.409

$\bar{Y}_d$ = 4.280 keV/μ Relative Variance = 0.571

Y	N(Y)	f'(Y)	d'(Y)	1-D(Y)	Φ(Y)
.0514	89.0000	.0059613	.0001725	.9998	4.907E-03
.0611	89.0000	.0070886	.0002439	.9996	4.872E-03
.0727	89.0000	.0084293	.0003449	.9992	4.830E-03
.0864	89.0000	.0100260	.0004879	.9988	4.781E-03
.1028	89.0000	.0119225	.0006900	.9981	4.722E-03
.1222	89.0000	.0141771	.0009756	.9971	4.652E-03
.1454	89.0000	.0168585	.0013795	.9957	4.569E-03
.1729	89.0000	.0200521	.0019517	.9938	4.470E-03
.2056	89.0000	.0238450	.0027598	.9910	4.352E-03
.2445	85.0000	.0270799	.0037269	.9873	4.218E-03
.2907	82.0000	.0310651	.0050841	.9822	4.065E-03
.3458	80.0000	.0360487	.0070173	.9752	3.887E-03
.4112	78.0000	.0417957	.0096749	.9655	3.681E-03
.4890	74.0000	.0471508	.0129785	.9525	3.448E-03
.5814	70.0000	.0530380	.0173602	.9352	3.186E-03
.6916	62.0000	.0558754	.0217535	.9134	2.910E-03
.8224	53.0000	.0567993	.0262960	.8871	2.630E-03
.9779	46.0000	.0586200	.0322710	.8548	2.341E-03
1.1629	38.0000	.0575841	.0376965	.8171	2.056E-03
1.3832	31.0000	.0558754	.0435070	.7736	1.781E-03
1.6448	24.0000	.0514409	.0476305	.7260	1.527E-03
1.9558	18.5000	.0471508	.0519142	.6741	1.294E-03
2.3258	14.0000	.0424304	.0555527	.6185	1.084E-03
2.7663	11.0000	.0396535	.0617519	.5568	8.887E-04
3.2896	9.5000	.0407241	.0754150	.4814	6.877E-04
3.9117	6.2000	.0316038	.0695931	.4118	5.317E-04
4.6515	4.4000	.0266705	.0698377	.3419	4.000E-04
5.5327	3.3000	.0237921	.0741023	.2678	2.826E-04
6.5792	2.4000	.0205764	.0762088	.1916	1.810E-04
7.8234	1.6000	.0163116	.0718380	.1198	1.005E-04
9.3030	.9700	.0117593	.0615842	.0582	4.242E-05
11.0653	.3800	.0054794	.0341320	.0241	1.537E-05
13.1584	.1400	.0024006	.0177821	.0063	3.523E-06
15.6467	.0350	.0007136	.0062858	0	1.437E-13

Site Size 91 μg cm^{-2} R/r = 4

$\bar{Y}_p$ = 1.462 keV/μ Relative Variance = 1.347

$\bar{Y}_d$ = 3.430 keV/μ Relative Variance = 0.561

Y	N(Y)	f'(Y)	d'(Y)	1-D(Y)	Φ(Y)
.0306	88.0000	.0068834	.0001439	.9999	1.855E-02
.0363	88.0000	.0081853	.0002035	.9997	1.840E-02
.0432	88.0000	.0097358	.0002879	.9994	1.822E-02
.0514	88.0000	.0115774	.0004072	.9990	1.800E-02
.0611	88.0000	.0137668	.0005757	.9984	1.774E-02
.0727	75.0000	.0139522	.0006938	.9977	1.748E-02
.0864	63.0000	.0139400	.0008245	.9969	1.722E-02
.1028	55.0000	.0144718	.0010179	.9958	1.695E-02
.1222	49.0000	.0153312	.0012822	.9946	1.666E-02
.1454	44.0000	.0163706	.0016281	.9929	1.636E-02
.1729	40.0000	.0177015	.0020940	.9908	1.603E-02
.2056	39.0000	.0205236	.0028871	.9880	1.564E-02
.2445	39.0000	.0244047	.0040822	.9839	1.519E-02
.2907	39.0000	.0290205	.0057725	.9781	1.465E-02
.3458	38.0000	.0336329	.0079572	.9701	1.402E-02
.4112	38.0000	.0399947	.0112522	.9589	1.327E-02
.4890	38.0000	.0475579	.0159102	.9430	1.238E-02
.5814	37.0000	.0550646	.0219057	.9211	1.135E-02
.6916	33.0000	.0584151	.0276408	.8934	1.026E-02
.8224	29.0000	.0610446	.0343487	.8591	9.123E-03
.9779	25.0000	.0625762	.0418690	.8172	7.954E-03
1.1629	20.0000	.0595293	.0473638	.7699	6.842E-03
1.3832	16.3000	.0577070	.0546115	.7152	5.765E-03
1.6448	12.5000	.0526246	.0592219	.6560	4.782E-03
1.9558	9.2000	.0460561	.0616312	.5944	3.921E-03
2.3258	6.7000	.0398846	.0634674	.5309	3.176E-03
2.7663	5.0000	.0354031	.0670079	.4639	2.515E-03
3.2896	3.8000	.0319958	.0720139	.3919	1.917E-03
3.9117	2.7500	.0275335	.0736895	.3182	1.403E-03
4.6515	1.9000	.0226211	.0719929	.2462	9.805E-04
5.5327	1.4000	.0198257	.0750489	.1712	6.102E-04
6.5792	.9500	.0159979	.0720139	.0992	3.114E-04
7.8234	.4800	.0096117	.0514487	.0477	1.319E-04
9.3030	.2200	.0052386	.0333441	.0144	3.400E-05
11.0653	.0500	.0014161	.0107213	.0036	7.549E-06
13.1584	.0120	.0004042	.0036386	0	5.436E-13

65 kVp HVL 1.9

Site Size 187 μg cm^{-2} R/r = 4

$\bar{Y}_p$ = 1.353 keV/μ Relative Variance = 1.001

$\bar{Y}_d$ = 2.717 keV/μ Relative Variance = 0.439

Y	N(Y)	f'(Y)	d'(Y)	1-D(Y)	Φ(Y)
.0153	91.0000	.0045964	.0000519	.9999	8.405E-02
.0182	91.0000	.0054658	.0000734	.9999	8.359E-02
.0216	91.0000	.0065012	.0001038	.9998	8.304E-02
.0257	91.0000	.0077309	.0001468	.9996	8.239E-02
.0306	91.0000	.0091929	.0002076	.9994	8.161E-02
.0363	75.0000	.0090096	.0002419	.9992	8.085E-02
.0432	64.0000	.0091445	.0002921	.9989	8.008E-02
.0514	55.0000	.0093451	.0003549	.9985	7.929E-02
.0611	46.0000	.0092939	.0004197	.9981	7.850E-02
.0727	41.0000	.0098504	.0005290	.9976	7.767E-02
.0864	35.5000	.0101447	.0006480	.9969	7.681E-02
.1028	32.0000	.0108743	.0008260	.9961	7.590E-02
.1222	29.5000	.0119204	.0010767	.9950	7.489E-02
.1454	27.3000	.0131179	.0014089	.9936	7.378E-02
.1729	26.0000	.0148599	.0018983	.9917	7.253E-02
.2056	25.3000	.0171949	.0026121	.9891	7.108E-02
.2445	25.5000	.0206082	.0037227	.9854	6.934E-02
.2907	26.0000	.0249865	.0053672	.9800	6.723E-02
.3458	27.0000	.0308628	.0078854	.9721	6.462E-02
.4112	28.0000	.0380600	.0115636	.9606	6.141E-02
.4890	28.0000	.0452573	.0163505	.9442	5.758E-02
.5814	27.5000	.0528561	.0227075	.9215	5.312E-02
.6916	26.3000	.0601254	.0307237	.8908	4.804E-02
.8224	24.0000	.0652456	.0396465	.8511	4.254E-02
.9779	20.0000	.0646533	.0467158	.8044	3.708E-02
1.1629	16.5000	.0634273	.0544981	.7499	3.172E-02
1.3832	13.3000	.0608112	.0621483	.6878	2.659E-02
1.6448	10.5000	.0570899	.0693814	.6184	2.177E-02
1.9558	7.8000	.0504295	.0728767	.5455	1.751E-02
2.3258	6.0000	.0461289	.0792699	.4663	1.361E-02
2.7663	4.6000	.0420649	.0859795	.3803	1.006E-02
3.2896	3.5000	.0380600	.0925085	.2878	6.847E-03
3.9117	2.6000	.0336197	.0971689	.1906	4.008E-03
4.6515	1.5000	.0230645	.0792699	.1113	2.061E-03
5.5327	.8000	.0146313	.0598119	.0515	8.253E-04
6.5792	.3000	.0065246	.0317172	.0198	2.744E-04
7.8234	.0900	.0023275	.0134542	.0063	7.790E-05
9.3030	.0300	.0009226	.0063416	0	0E 00

Site Size 278 μg cm^{-2} R/r = 4

$\bar{Y}_p$ = 1.235 keV/μ Relative Variance = 0.817

$\bar{Y}_d$ = 2.244 keV/μ Relative Variance = 0.384

Y	N(Y)	f'(Y)	d'(Y)	1-D(Y)	Φ(Y)
.0108	320.0000	.0014522	.0000127	1.0000	2.042E-01
.0129	320.0000	.0017269	.0000180	1.0000	2.039E-01
.0153	320.0000	.0020534	.0000254	.9999	2.035E-01
.0182	320.0000	.0024418	.0000359	.9999	2.030E-01
.0216	320.0000	.0029044	.0000508	.9999	2.024E-01
.0257	320.0000	.0034537	.0000719	.9998	2.017E-01
.0306	320.0000	.0041069	.0001016	.9997	2.008E-01
.0363	320.0000	.0048836	.0001437	.9995	1.998E-01
.0432	320.0000	.0058087	.0002033	.9993	1.986E-01
.0514	320.0000	.0069075	.0002875	.9990	1.972E-01
.0611	320.0000	.0082137	.0004066	.9986	1.955E-01
.0727	320.0000	.0097672	.0005749	.9981	1.935E-01
.0864	280.0000	.0101653	.0007117	.9974	1.915E-01
.1028	260.0000	.0112247	.0009345	.9964	1.892E-01
.1222	240.0000	.0123206	.0012197	.9952	1.867E-01
.1454	230.0000	.0140404	.0016528	.9935	1.838E-01
.1729	220.0000	.0159740	.0022367	.9913	1.805E-01
.2056	220.0000	.0189956	.0031629	.9881	1.766E-01
.2445	220.0000	.0225878	.0044722	.9837	1.720E-01
.2907	225.0000	.0274704	.0064676	.9772	1.664E-01
.3458	230.0000	.0334003	.0093534	.9679	1.596E-01
.4112	240.0000	.0414449	.0138016	.9541	1.511E-01
.4890	250.0000	.0513358	.0203282	.9337	1.406E-01
.5814	240.0000	.0586034	.0275951	.9061	1.286E-01
.6916	220.0000	.0638961	.0357869	.8703	1.155E-01
.8224	195.0000	.0673480	.0448551	.8255	1.018E-01
.9779	170.0000	.0698167	.0552926	.7702	8.747E-02
1.1629	140.0000	.0683707	.0643886	.7058	7.349E-02
1.3832	110.0000	.0638961	.0715738	.6342	6.042E-02
1.6448	88.0000	.0607859	.0809693	.5533	4.799E-02
1.9558	65.0000	.0533892	.0845652	.4687	3.707E-02
2.3258	51.0000	.0498129	.0938235	.3749	2.688E-02
2.7663	39.0000	.0453082	.1015046	.2734	1.761E-02
3.2896	28.0000	.0386819	.1030518	.1703	9.697E-03
3.9117	16.5000	.0271053	.0858662	.0845	4.153E-03
4.6515	6.3000	.0123067	.0463598	.0381	1.636E-03
5.5327	2.5000	.0058087	.0260268	.0121	4.480E-04
6.5792	.6500	.0017959	.0095691	.0025	8.064E-05
7.8234	.1200	.0003943	.0024979-	.0000	-5.953E-12

65 kVp HVL 1.9

Site Size 555 μg cm^{-2} R/r = 4

$\overline{Y}_p$ = 1.004 keV/μ Relative Variance = 0.776

$\overline{Y}_d$ = 1.784 keV/μ Relative Variance = 0.307

Y	N(Y)	f'(Y)	d'(Y)	1-D(Y)	Φ(Y)
.0108	320.0000	.0055621	.0000598	.9999	9.967E-01
.0129	320.0000	.0066141	.0000846	.9999	9.900E-01
.0153	320.0000	.0078649	.0001197	.9997	9.822E-01
.0182	320.0000	.0093525	.0001692	.9996	9.728E-01
.0216	265.0000	.0092122	.0001982	.9994	9.635E-01
.0257	220.0000	.0090944	.0002327	.9991	9.544E-01
.0306	185.0000	.0090938	.0002767	.9989	9.453E-01
.0363	160.0000	.0093525	.0003384	.9985	9.359E-01
.0432	140.0000	.0097336	.0004189	.9981	9.262E-01
.0514	125.0000	.0103346	.0005289	.9976	9.158E-01
.0611	110.0000	.0108143	.0006581	.9969	9.050E-01
.0727	100.0000	.0116906	.0008460	.9961	8.933E-01
.0864	87.0000	.0120975	.0010413	.9950	8.811E-01
.1028	80.0000	.0132283	.0013539	.9937	8.679E-01
.1222	74.0000	.0145501	.0017709	.9919	8.533E-01
.1454	68.0000	.0158992	.0023010	.9896	8.374E-01
.1729	65.0000	.0180767	.0031118	.9865	8.193E-01
.2056	62.0000	.0205038	.0041972	.9823	7.987E-01
.2445	61.0000	.0239880	.0058391	.9765	7.747E-01
.2907	60.0000	.0280574	.0081213	.9683	7.465E-01
.3458	60.0000	.0333723	.0114897	.9568	7.131E-01
.4112	60.0000	.0396849	.0162474	.9406	6.733E-01
.4890	60.0000	.0471895	.0229733	.9176	6.260E-01
.5814	59.0000	.0551795	.0319439	.8857	5.707E-01
.6916	55.0000	.0611826	.0421288	.8435	5.094E-01
.8224	50.0000	.0661414	.0541580	.7894	4.431E-01
.9779	43.0000	.0676382	.0658569	.7235	3.753E-01
1.1629	36.0000	.0673376	.0779648	.6456	3.078E-01
1.3832	30.0000	.0667447	.0919173	.5537	2.409E-01
1.6448	23.5000	.0621730	.1018170	.4518	1.786E-01
1.9558	17.5000	.0550544	.1072089	.3446	1.235E-01
2.3258	13.0000	.0486327	.1126158	.2320	7.472E-02
2.7663	9.0000	.0400468	.1103008	.1217	3.458E-02
3.2896	4.5000	.0238109	.0779875	.0437	1.071E-02
3.9117	1.3000	.0081795	.0318564	.0119	2.517E-03
4.6515	.3000	.0022446	.0103953	.0015	2.676E-04
5.5327	.0300	.0002670	.0014707	.0000	0E 00